Master's Thesis

Channel Coding for THz Communication Systems

Viktoria Schram

Lehrstuhl für Digitale Übertragung
Prof. Dr.-Ing. Robert Schober
Universität Erlangen-Nürnberg

Betreuer: Prof. Dr.-Ing. Wolfgang Gerstacker

February 27, 2018

Contents

Abstract

The unprecedented growth in mobile data consumption leads to the necessity for future information networks to operate at higher frequencies than they do today. Terahertz (THz) communication is a new emerging technology comprising a bandwidth of $0.1 - 10\,\text{THz}$. It is able to address the increasing demands of the society for high data rates and for ever-improving high speed transmission by offering a wider bandwidth than current existing networks. To meet certain reliability requirements a combination with channel coding is indispensable. One important area of application comprises data intensive technology concepts with delay critical services, which rely on fast transmission with short packets. The recently proposed approach of finite blocklength coding by Polyanskiy, Poor and Verdú (PPV) provides a powerful tool to approximate the maximum achievable rate for short blocklength coding, referred to as the normal approximation. In this thesis, their method is used to analyze theoretical bounds for a transmission over the THz channel assuming a point-to-point Single Carrier (SC) system. Therefore, these bounds are developed for a transmission with Bit Interleaved Coded Modulation (BICM) and compared to Coded Modulation (CM). Their performance is shown for higher order modulations considering Phase Shift Keying (PSK) and Quadrature Amplitude Modulation (QAM) for various SNR values and different blocklengths. Moreover, the maximum achievable rate in Gbps is obtained. Theoretical results are verified by simulations, considering convolutional coding with various coding rates, Minimum Mean Squared Error Linear Equalization (MMSE-LE) and soft decision decoding. The deviation to the theoretical bounds is analyzed and the maximum achievable rate is derived based on the simulation results. As the THz channel is highly frequency-selective the performance of Coded Orthogonal Frequency Devision Multiplexing (COFDM) in terms of maximum achievable rate is also analyzed and compared to SC systems considering MMSE-LE, Zero Forcing Decision Feedback Equalization (ZF-DFE) or Minimum Mean Squared Error Decision Feedback Equalization (MMSE-DFE). Theoretical bounds are developed for the case that one codeword is transmitted over various OFDM subchannels, causing each symbol to experience different fading. It is shown that an SC approach with MMSE-LE performs worse than the OFDM system. An SC system with ZF-DFE achieves the OFDM performance in the limit of high SNR values. An SC system with MMSE-DFE performs as good as the OFDM system.

Glossary

Abbreviations

AWGN	Additive White Gaussian Noise
BEC	Binary Erasure Channel
BER	Bit Error Rate
BICM	Bit Interleaved Coded Modulation
BSC	Binary Symmetric Channel
CIR	Channel Impulse Response
CM	Coded Modulation
COFDM	Coded Orthogonal Frequency Devision Multiplexing
CTF	Channel Transfer Function
DFE	Decision Feedback Equalizer
DFT	Discrete Fourier Transformation
DMC	Discrete Memoryless Channel
FPGA	Field Programmable Gate Array
HARQ	Hybrid Automatic Repeat Request
i.i.d.	independent identically distributed
ICI	Intercarrier Interference
IDFT	Inverse Discrete Fourier Transformation
IFFT	Inverse Fast Fourier Transformation
IoT	Internet-of-Things
ISI	Intersymbol Interference
LLR	Log Likelihood Ratios
LOS	Line-Of-Sight
MC	Multi Carrier
MMSE	Minimum Mean Squared Error
MMSE-DFE	Minimum Mean Squared Error Decision Feedback Equalization
MMSE-LE	Minimum Mean Squared Error Linear Equalization
NLOS	Non-Line-Of-Sight
OFDM	Orthogonal Frequency Devision Multiplexing
PAPR	Peak to Average Power Ratio
PPV	Polyanskiy, Poor and Verdú
PSK	Phase Shift Keying
QAM	Quadrature Amplitude Modulation
RRC	Root Raised Cosine
Rx	Receiver
SC	Single Carrier
SNR	Signal to Noise Ratio
THz	Terahertz

Tx   Transmitter
WLAN   Wireless Local Area Network
ZF-DFE   Zero Forcing Decision Feedback Equalization

Operators

$||\cdot||$ Euclidean Norm
$(\cdot)^H$ Hermitian Matrix
$*$ Convolution
x^* Complex Conjugated
$\mathbb{E}\{\cdot\}$ Average Operator
$\mathbb{V}\{\cdot\}$ Variance Operator
$\mathcal{M}$ Bit Mapping
$\mathcal{M}^{-1}$ Bit Demapping
Π Interleaver
Π^{-1} Deinterleaver

Symbols

A Random Input Variable
α Roll-Off Factor
α_{QAM} Normalization Constant
$a[\kappa]$ Source Sequence for $\kappa = 1, ..., m$
$\hat{a}[\kappa]$ Decoded Source Sequence for $\kappa = 1, ..., m$
B_{coh} Coherence Bandwidth [Hz]
B_{s} Subcarrier Bandwidth [Hz]
BW Bandwidth [Hz]
$\mathcal{B}$ Set of Codewords after Interleaving
C Capacity [bit/channeluse]
$c[\kappa_c]$ Coded Sequence for $\kappa_c = 1, ..., n'$
$\hat{c}[\kappa_c]$ Deinterleaved Demapped Sequence $\kappa_c = 1, ..., n'$
$\tilde{c}[\kappa_c]$ Coded and Interleaved Sequence for $\kappa_c = 1, ..., n'$
$\hat{\tilde{c}}[\kappa_c]$ Demapped Sequence $\kappa_c = 1, ..., n'$
$\mathcal{C}$ Set of Codewords
d_{min} Hamming Distance
Δf Subcarrier Spacing [Hz]
$\Delta \tau$ Excess Delay [s]
ϵ Error Probability
η Fraction
$\mathbf{f}_{\mathrm{opt}}$ Optimal Equalization Filter
$\mathcal{F}$ Feasible Set
$g[\kappa_n]$ Discrete Time Channel Output Sequence (before Equalization) for
                    $\kappa_n = 1, ..., n$
$g(t)$ Continuous Time Channel Output Sequence (before Equalization)
$h(\tau, r, \zeta)$ Continuous Time Channel Impulse Response

$h_{\mathrm{eq}}(\tau, r, \zeta)$	Equivalent Continuous Time Channel Impulse Response
$h[\kappa_n]$	Discrete Time Channel Impulse Response for $\kappa_n = 1, ..., n$
$h_{\mathrm{overall}}[\kappa_n]$	Discrete Time Channel Impulse Response (after Equalization) $\kappa_n = 1, ..., n$
$h_{\mathrm{T}}(t)$	Transmit Pulse Shape Filter
$h_{\mathrm{W}}(t)$	Whitening Filter
$H_{\mathrm{eq}}(f, r, \zeta)$	Equivalent Channel Transfer Function
$i(X; Y)$	Mutual Information Random Variable, Information Density, Information Spectrum
$i_{\mathrm{BICM}}(X; Y)$	Mutual Information Random Variable for BICM
$\tilde{i}(X; Y)$	Modified Mutual Information Random Variable
$I(X; Y)$	Mutual Information
k	Number of Bits per Symbol
K	Number of OFDM Subcarriers
$l[\kappa_c]$	Deinterleaved Sequence of LLR Values for $\kappa_c = 1, ..., n'$
$\tilde{l}[\kappa_c]$	Sequence of LLR Values for $\kappa_c = 1, ..., n'$
L_c	Constraint Length
$\mathscr{L}$	LLR Calculation
m	Length of Uncoded Word
mse	Mean Squared Error (for Simulation Results)
M	Constellation Size
n	Blocklength of a Codeword (at Channel Input)
n^*	Minimum Blocklength of a Codeword (at Channel Input)
n'	Blocklength of a Codedword (before Mapping)
N	Number of Subchannels
N_{cu}	Number of Channeluses
N_u	Number of Used Subcarriers
P	Power [W]
$P_{Y\mid X}(Y\mid X)$	Channel Transition Probability
$P_X(X)$	Channel Input Distribution
$P_Y(Y)$	Channel Output Distribution
φ	Crosscorrelation Matrix
$\mathbf{\Phi}$	Autocorrelation Matrix
$Q(\cdot)$	Q-Function
Q_Y	Auxiliary Channel Output Distribution
q_b	Length of Feedback Filter
q_f	Length of Feedforward Filter
r	Distance between Rx and Tx [m]
$R^*(n, \epsilon)$	Maximum Achievable Rate [bit/channeluse]
R	Transmission Rate [bit/channeluse]
R_c	Coding Rate
SNR	Signal to Noise Ratio
SNR_k	Signal to Noise Ratio for Subcarrier k
$\mathrm{SNR}_{\mathrm{in}}$	Signal to Noise Ratio at the Input of the Transmission System
$\mathrm{SNR}_{\mathrm{MMSE-LE}}$	Signal to Noise Ratio at the Output of MMSE-LE
$\mathrm{SNR}_{\mathrm{MMSE-DFE}}$	Signal to Noise Ratio at the Output of MMSE-DFE

$\mathrm{SNR_{ZF-DFE}}$	Signal to Noise Ratio at the Output of ZF-DFE
σ_e^2	Minimum Mean Squared Error
σ_x^2	Variance of Amplitude Coefficients
σ_z^2	Noise Variance
T	Symbol Duration of Single Carrier Transmission Scheme [s]
T_{channel}	Duration of Channel Impulse Response [s]
T_G	Duration of Guard Interval [s]
T_{MC}	Duration of Multi Carrier Information Data [s]
T_{OFDM}	Symbol Duration of OFDM Transmission Scheme [s]
τ	Delay Variable [s]
τ_1	Shortest Propagation Path [s]
$\tau_{\max}$	Longest Propagation Path [s]
V	Channel Dispersion [bit^2/channeluse]
W	Number of Messages
$W^*(n, \epsilon)$	Maximum Achievable Code Size
$\mathcal{W}$	Message Set
$x(t)$	Continuous Time Channel Input
$x[\kappa_n]$	Discrete Time Channel Input Sequence for $\kappa_n = 1, ..., n$
x^n	Realization of Random Variable with Dimension n
X	Random Channel Input Variable
$\mathcal{X}^n$	Set of Channel Inputs of Length n
$\mathcal{X}$	Set of Channel Inputs
$\mathcal{X}_b^i$	Set of Channel Inputs for Bit b and at Bit Position i
$y[\kappa_n]$	Sequence of Received Symbols (after Equalization) for $\kappa_n = 1, ..., n$
y^n	Channel Output with Dimension n
Y	Random Channel Output Variable
$\mathcal{Y}$	Set of Channel Outputs
$z(t)$	Continuous Time Additive White Gaussian Noise
$z[\kappa_n]$	Discrete Time Additive White Gaussian Noise for $\kappa_n = 1, ..., n$
$z_c(t)$	Colored Noise
$z_{\mathrm{filtered}}[\kappa_n]$	Colored Noise (after Equalization) for $\kappa_n = 1, ..., n$
z^n	Additive White Gaussian Noise with Dimension n
Z	Random Noise Variable
ζ	Vector of Scattering Properties

Chapter 1

Introduction

Over the past years the rapid development of various mobile technologies led to a great increase of wireless data traffic for creation, sharing and consumption of information, accompanied by rising demands for high speed transmission, with further increasing overall trends [1, 2, 3]. Additionally, the development of 5G and the era of Internet-of-Things (IoT) gives rise to new technology concepts like, e.g., machine-to-machine communication and autonomous systems, where short packets of time sensitive control information have to be communicated with very low latency and high reliability [4]. Also well known and steadily improving applications like interactive voice or video communications rely on these two conditions. Terahertz (THz) communication is a new emerging technology which overcomes the capacity limitations of current existing mobile networks by offering higher operation frequencies and more bandwidth, enabling THz technologies to satisfy the demands for low delay and high speed transmission with ease [1]. In combination with channel coding a powerful tool is created to also ensure high reliability [5].

In 1948 the performance limit of channel coding has been introduced by Shannon in his groundbreaking work in [6] for an asymptotic regime. However, the key for low delay transmission is a finite blocklength approach, i.e., a non-asymptotic analysis. In this area of research, Polyanskiy, Poor and Verdú (PPV) developed new non-asymptotic bounds in [7] which are computationally feasible and which exhibit a great generality. Additionally, the authors provide a tightened and extended expression for the normal approximation, initially introduced by Strassen ([8]) in 1962. It provides the possibility to approximate the minimum blocklength needed to achieve a certain fraction of capacity for a given error probability. By applying this approximation, design guidelines can be provided for a system model that has to fulfill certain reliability criteria.

This chapter is organized as follows. In Subchapter 1.1 an overview is provided over recent developments in THz communications. Next, in Subchapter 1.2 related work

regarding finite blocklength coding and some background information is given. Finally, in Subchapter 1.3 an overview of this thesis and its contribution concludes this chapter.

1.1 Recent Progress in THz Transmission

Results in [9] and [10] demonstrate that data rates in the order of several hundred Gbps or even Tbps can indeed be achieved. In [9] this is verified for a transmission distance of up to 1 m. Furthermore, in [10] different bounds are proposed for the maximum distance, considering various transmission schemes and an efficient power allocation algorithm. These results and those of related work, e.g. [1] and [11], encourage the further development of THz communication systems.

THz communication technologies can be involved in a wide area of future applications. They can for instance enhance approaches which require high data rates like wireless short-range communication between devices, ultra-high-speed data communication in small cells or secure wireless communication for safety applications [1]. Moreover, the development of new nanoscale machine communication concepts and networks is encouraged. Possible applications can for instance be foreseen in the healthcare sector as health monitoring systems, or for the development of new paradigms like the Internet-of-Nano-Things [1]. Further applications for THz transmission can be found in space, with the great advantages that space applications do not suffer from atmospheric attenuation due to the atmosphere free environment [12]. THz wireless communication could be used as an interior Wireless Local Area Network (WLAN) within a spacecraft providing high data rates for the crew and instruments. Furthermore, wireless communication applications on a planet's surface with high data rates might be enabled [12]. Finally, inter-satellite Terahertz communication links providing high-throughput communication with high security and the ability to defeat interference could be established [13].

Since the initial demonstration of THz wireless communications using pulsed and continuous waves almost 17 years ago, great research has been conducted worldwide ([14]) regarding hardware technologies to improve the THz communication approach [15]. Developed hardware technologies are either photonic- and electronic-based or completely electronic-based approaches [15]. An electro-optical approach was followed in [16], where Single Carrier (SC) and Multi Carrier (MC) systems were analyzed for a transmission at around 200 GHz. Data rates of up to 100 Gbps were achieved by using a gain-switched optical comp source. In [17] the authors analyzed an electro-optical approach to realize Orthogonal Frequency Devision Multiplexing (OFDM) transmission over a THz communication link. They demonstrated a transmission around 325 GHz using 64QAM$-$OFDM and achieved a data rate of 59 Gbps for a transmission distance of

5 cm. A completely electrical approach has been considered in [18]. The research group investigated a completely wireless 100 Gbps system at 240 GHz. It is implemented and validated on a Field Programmable Gate Array (FPGA) platform. A Hybrid Automatic Repeat Request (HARQ) type-I method is used, which simplifies system design, while further concepts like frame fragmentation, aggregation and acknowledgment compression are used to decrease the probability of bit errors. The system is able to achieve nearly 120 Gbps with a Bit Error Rate (BER) of up to $2 \cdot 10^{-3}$.

These results and ongoing research show that THz transmission is theoretically and practically realizable, with a wide area of applications available for future wireless THz communication systems. To be able to give practical design guidelines for such systems, in this thesis the theory of finite blocklength coding is applied considering an electrical transmission approach. In this context, the normal approximation is used to approximate theoretical bounds for the maximum achievable rate.

1.2 Related Work

In 1962, a first expression of the normal approximation was provided in [8] considering a Discrete Memoryless Channel (DMC). Recently in 2009, extensions were developed by Hayashi ([19]) for DMCs with cost constraints and additive Markov channels. In 2010, PPV ([7]) developed further tightened expressions for the Additive White Gaussian Noise (AWGN) channel.

Since then, further research was performed to adapt the latest concept ([7]) of finite blocklength coding and an expression of the normal approximation to various channel models. An important parameter that has to be taken into account by using the approach of normal approximation is the *channel dispersion* which is channel dependent. The dispersion for the AWGN channel, the parallel AWGN channel and the Gaussian channel with non-white noise and Intersymbol Interference (ISI) is studied in [20]. For all mentioned cases a continuous channel input is assumed. In [21] channel dispersion was analyzed for memoryless channels with cost constraints.

Additionally, further refinements were given for the normal approximation of various channels. The normal approximation for channels with memory is analyzed closer in [22], where the communication model considers a Gilbert-Elliott channel with and without state knowledge at the receiver. In the work of MolavianJazi ([4]) the finite blocklength coding approach was applied to a transmission over a coded modulation system considering an AWGN channel with discrete channel input and continuous channel output. He provided a deeper analysis and derivation of the bounds given by PPV for his channel model. In [23] a new system model was proposed called 'parallel bit interleaved

coded modulation', which is equal to a binary symmetric channel model. The authors provide a further analysis of their scheme and a development of the channel dispersion with an adjusted expression for the normal approximation. Recently, in the work of Tomaso ([24]) a further refinement of the PPV findings was given. Moreover, he provided unified expressions for the normal approximation and the channel dispersion for parallel AWGN channels, which, although equally designated, are different to the model in [20]. In his work also OFDM transmission is considered assuming individual fading of each coded symbol in one codeblock.

Moreover, various case studies using the normal approximation in different fields were undertaken, e.g., covert communication in [25] or energy harvesting tasks in [26].

1.3 Contribution and Outline

In this thesis, transmission over the THz channel is considered. By the application of interleaving and equalization, difficulties resulting from the frequency selectivity of this channel can be overcome. The overall system model used for simulations is a Bit Interleaved Coded Modulation (BICM) system. This method is different from the approach presented in [23], the model according to [27] is used instead. For transmission higher order modulations assuming Phase Shift Keying (PSK) and Quadrature Amplitude Modulation (QAM) are considered. The simulative finite blocklength performance is shown by using a practical coding scheme, namely convolutional codes.

Based on the approach of MolavianJazi in [4] the normal approximation is adjusted to the implemented BICM system. The bounds and the derivation for Coded Modulation (CM) in [4] are used as a reference. Based on the findings in [4], new bounds for BICM and a transmission over the AWGN channel are proposed.

Simulation results are obtained for a transmission over the equalized THz channel as well as for a transmission over an AWGN channel. As discrete channel input should also be considered the concept of [20] is not applied and the following approach is used instead. Simulative results achieved by considering a transmission over the THz channel are compared to the theoretical bounds for discrete channel input assuming an AWGN channel. The loss that occurs because of colored noise after equalization is observed by a comparison with the simulation results of a transmission over the AWGN channel.

Additionally, an analysis of finite blocklength performance for an OFDM transmission over the THz channel assuming continuous channel input is given. It is compared to SC systems, which consider different equalization strategies.

This thesis is organized as follows. In Chapter 2 the overall system model is presented. Thereby, the transmission scenario will be demonstrated, the BICM system will be intro-

duced and more information will be given about the transmit signal design. In Chapter 3, necessary preliminaries from information theory will be given and the approach of PPV will be introduced and adapted to the BICM system used in this thesis. In Chapter 4 a comparison with simulation results will show the appropriateness of the proposed bounds. Additionally, in Chapter 5 theoretical bounds for an OFDM system are developed and compared to SC systems. Finally, Chapter 6 concludes this work.

Chapter 2

System Model

The transmission chain considered throughout this work consists of a Transmitter (Tx) model, a discrete-time channel model and a Receiver (Rx) model. For the performance analysis the transmission environment from previous work in [9] is used as a sample scenario. This ensures that previous results can be taken as a basis for further development. Throughout this work a point-to-point transmission model is considered.

This chapter provides a comprehensive overview of the developed system model and of the settings around Tx and Rx. It is organized as follows. In Subchapter 2.1 the chosen transmission scenario according to [9] is presented. Thereafter, in Subchapter 2.2 the components of the simulation framework which is based on a Bit Interleaved Coded Modulation (BICM) system are introduced. Finally, in Subchapter 2.3 some requirements for the transmit signal design are explained, which were set to guarantee advantages for future developments.

2.1 Presentation of the Transmission Scenario

The Terahertz (THz) frequency range is defined from $0.1\,$THz to $10\,$THz with wavelengths between $3\,$mm and $30\,\mu$m. The THz channel is characterized by a very high molecular absorption which leads to signal distortion and colored noise, cf. e.g. [9]. Together with the spreading loss the molecular absorption results in a very high and frequency-selective path loss affecting even Line-Of-Sight (LOS) links of THz transmission [9]. Moreover, a high reflection loss depending on the characteristics of the surfaces reflecting the THz waves influences the Non-Line-Of-Sight (NLOS) components [9]. Such difficult transmission characteristics limit THz wave propagation to a few meters ([9]) and lead to the assumption that in the beginning main applications of THz technologies will occur indoors as the channel characteristics can be modeled easily without taking into account difficult weather conditions for instance. Moreover according to [28, 29] and [30] more than $80\,\%$ of mobile traffic originates or terminates in an indoor environment, making

stable and reliable data transmission essential for residents, visitors and workers of a building. This is why throughout this thesis, the focus is set on indoor THz transmission.

To build on previous results, the indoor transmission scenario is set according to [9], where the environment has the following properties. Tx and Rx are in a small rectangular office room of size: length × width × height $= 5\,\mathrm{m} \times 2.75\,\mathrm{m} \times 2.5\,\mathrm{m}$. Both are assumed to be at a height of $1.5\,\mathrm{m}$ and the distance between Tx and Rx is $r = 2.5\,\mathrm{m}$.

The used channel model in this work is taken from [9], where an equivalent continuous-time Channel Impulse Response (CIR) $h_{\mathrm{eq}}(\tau, r, \zeta)$ is developed via a ray tracing approach for the frequency range of $0.1\,\mathrm{THz}$ to $1\,\mathrm{THz}$. In this model multipath propagation is considered characterized by the delay variable τ, and the coordinates of all relevant scattering points of the environment are summarized in vector ζ. The variable r denotes the distance between the Tx and the Rx. As the channel transfer function $H_{\mathrm{eq}}(f, r, \zeta)$ is highly frequency-selective, the total bandwidth BW is divided into $N = 32$ subbands of equal width $\Delta f = \frac{BW}{N}$ such that the dispersion of each subchannel is better controlled. In the following, we assume that one such subband has been selected for the transmission. A subband approach is better realizable, because transmission over the full bandwidth faces significant challenges regarding device technology [10]. Moreover, each subchannel is assumed to be time-invariant during a certain transmission interval (transmit signal burst), i.e., Tx and Rx are stationary and not moving.

The Signal to Noise Ratio (SNR) for transmission highly depends on the distance between Tx and Rx and on the subband chosen for transmission [9]. To build on previous results the Tx and Rx positions are chosen like in [9] and are shown in Figure 2.1. They are indicated by the terms 'Rx' and 'Tx' in each Subfigure. As was depicted in [9], the LOS component of the Channel Transfer Function (CTF) dominates over the NLOS components with a higher path gain (cf. [9, Figure 8]). However, the LOS component is significantly influenced by molecular absorption which increases with higher operation frequency (cf. [9, Figure 3]). These characteristics cause difficult transmission properties. The higher the subband is chosen for transmission and the larger the distance between Tx and Rx is set, the lower the SNR value becomes. Figure 2.1 depicts by different colors the SNR conditions for the office room assuming the Rx to be at any point in the room. The yellow part indicates an SNR of $20\,\mathrm{dB}$ and higher, while an SNR of minus $10\,\mathrm{dB}$ and lower is shown in dark blue. These information are given for the first subband (Figure 2.1 (a)), the sixth subband (Figure 2.1 (b)) and the 32th subband (Figure 2.1 (c)). The subfigures show that the SNR gets worse the higher the operation frequency is taken. The SNR for the considered Tx-Rx position is $7.7\,\mathrm{dB}$ for the first, $0.4\,\mathrm{dB}$ for the sixth and $-14.6\,\mathrm{dB}$ for the last subband. It can also be observed from the subfigures that the SNR degrades significantly when the distance between Rx and Tx gets increased. For

further considerations the first subband is chosen for transmission, as it shows the best transmission properties (cf. Figure 2.1 (a)). More information about the parameters of the first subband are given in Table 2.1.
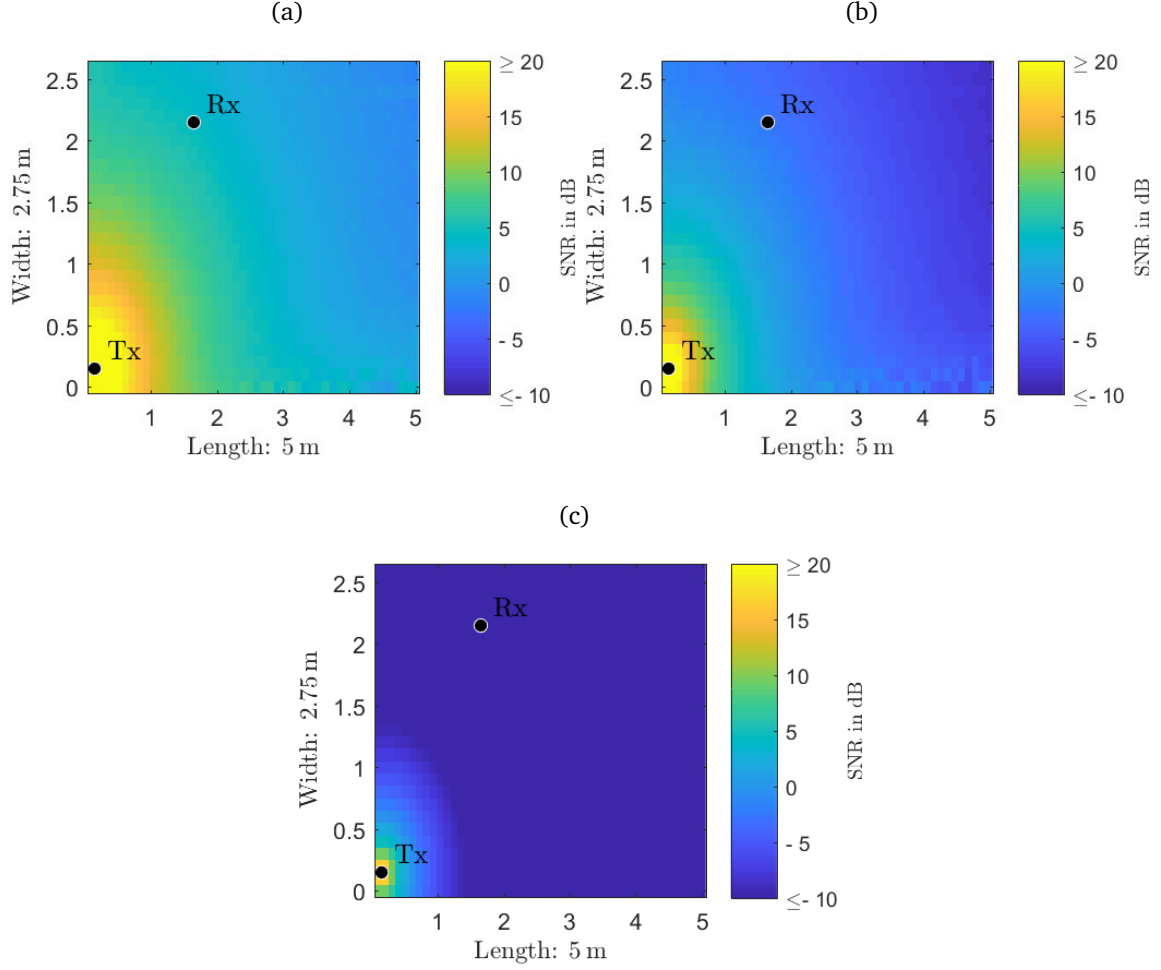

Figure 2.1: SNR conditions in the considered room environment for a transmission over (a) the first subband, (b) the sixth subband and (c) the 32th subband assuming the Rx to be at any point in this room. Additionally, the Rx-Tx scenario considered in [9] is indicated by 'Tx' and 'Rx'.

Table 2.1: Properties of the first THz subband

Frequency range	$0.1 - 0.1281\,\text{THz}$
Bandwidth BW	$0.0281\,\text{THz}$
Symbol duration T	$0.04\,\text{ns}$
Noise variance σ_z^2 for given Rx-Tx position	$0,198$
Channel energy E_h for given Rx-Tx position	1.174
SNR for given Rx-Tx position	$7.7\,\text{dB}$

2.2 Design of a BICM Transmission System

Coded Modulation (CM), i.e., the combination of coding and modulation, is a more bandwidth efficient scheme than uncoded modulation [31]. Over the past years a great variety of extensions to the original CM system, developed in 1974 by Massey ([32]), were introduced in order to cope with different transmission issues. Some breakthroughs were, for example, presented by Ungerboeck who developed trellis coded modulation ([33]) and Imai and Hirakawa who came up with multilevel coding [34]. Moreover, in 1992 it was shown by Zehavi that the reliability of coded modulation over fading channels can be improved significantly by using BICM [27, 35].

While CM concepts consider coding and modulation to be a single entity, BICM separates the actual coding from the modulation through an interleaving operation [34, 36]. As a consequence, encoded bits that are correlated through the coding process are mapped onto temporally separated symbols, i.e., consecutive coded bits, which are presented by different symbols, are affected by independent fades [37]. This is a great benefit for a transmission over fading channels compared to CM systems. Additionally, BICM provides the possibility to choose the modulation format and the encoder schemes independently. This enables an adaptation of the transmission to the channel conditions, making the realization of adaptive modulation and coding structures possible [34, 36, 37].

A good code performance for a transmission over fading channels depends strongly on the minimum Hamming distance $d_{\min}$ of a code, which is also termed 'code diversity' [27]. Two codewords differ in $d_{\min}$ positions [5]. By the application of bit-interleaving the code diversity gets increased [34]. Therefore, BICM is favorable for a transmission over frequency-selective channels. However, if a transmission over Additive White Gaussian Noise (AWGN) channels is considered there occurs a small loss in capacity for BICM schemes compared to a CM system [36]. The reason therefore is, that for a transmission over the AWGN channel a large Euclidean distance of the codewords is more important than code diversity as there are no fades in the channel [27, 31, 37]. It gets decreased by using the bit-interleaved scheme, which instead maximizes the Hamming distance [27, 31, 37]. A large Euclidean distance is important if a Viterbi decoder with soft input is applied [31, 38]. Therefore, CM is better suited for a transmission over an AWGN channel, though for the right choice of mapping a BICM is also considered as a valid option as the loss in capacity is very small compared to the capacity achieved by CM [27]. It was shown in [36] that binary Gray mapping is optimum to achieve the largest BICM capacity for moderate-to-large SNR values [36, 37]. Gray codes are defined as ordered sequences of binary tuples where two adjacent tuples differ only in a single bit [39]. For small values of SNR strictly regular set partitioning labeling is significantly better [37, 40]. Set partitioning is based on partitioning the signal constellation set into
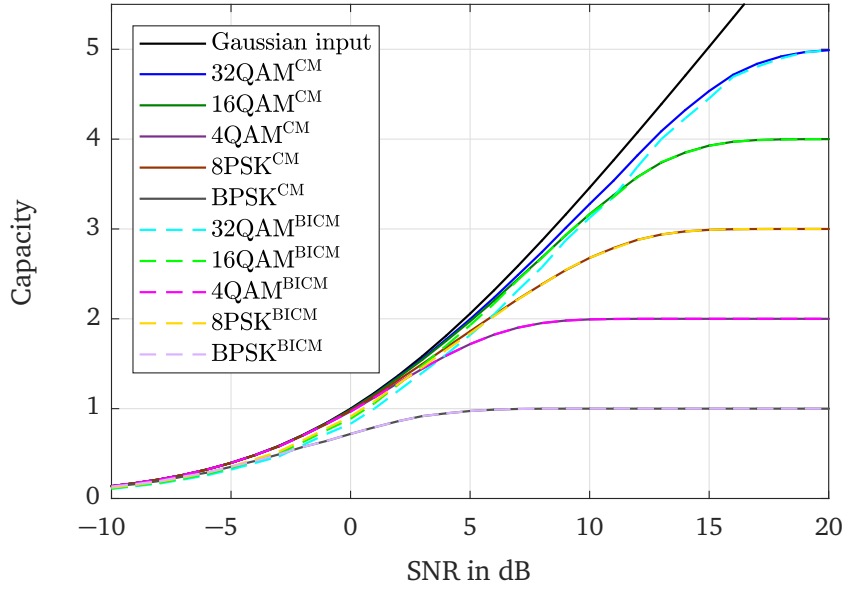
Figure 2.2: Colored solid lines: Capacity for a transmission over a CM system. Dashed lines: Capacity for a transmission over a BICM system. Black line: Reference capacity for continuous Gaussian input. Transmission over an AWGN channel is considered. Figure according to [27, Figure 4].

subsets of equal cardinality in a bisective manner, such that in each step the minimum Euclidean distance of the elements within each subset increases [39]. For means of simplicity only Gray coding is considered throughout this work.

The theoretical achievable capacities for a transmission over an AWGN channel are depicted in Figure 2.2. Solid colored lines indicate the achievable capacity for a transmission with CM and dashed lines show the performance for a BICM system. Additionally, both cases are indicated by superscripts 'CM' and 'BICM'. As a reference the capacity for continuous Gaussian input is shown in black. The deviation of BICM to CM transmission is small for a transmission with 16QAM, 4QAM, BPSK and 8PSK. Moreover, these results confirm the findings in [27, Figure 4]. Transmission with 32QAM shows a larger gap between CM and BICM because there is no real Gray mapping available for this constellation [41]. The performance of BICM can be further improved by using set partitioning and an iterative decoding process in the Rx, which aims to increase the Euclidean distance of the BICM scheme to improve the results of soft-decision feedback based iterative decoding [31, 36].

These fundamental research findings lead to the choice that a BICM transmission system is established for the simulation framework in this thesis. By using BICM, all benefits for a transmission over fading channels can be exploited throughout the simulation. For means of simplicity a BICM without iterative decoding will be used in this work.

This Chapter has the following structure. First, the Tx model is described in Subchapter 2.2.1. Thereafter, a short repetition of the channel model developed in [9] is given in Subchapter 2.2.2. Finally, in Subchapter 2.2.3 the Rx model is introduced.

In this Chapter vectors are denoted by bold lower case letters, (i.e., $\mathbf{x}$,) matrices are given by bold upper case letters (i.e., $\mathbf{X}$) and sequences are indicated as $x[\kappa_n]$ for $\kappa_n = 1, ..., n$. A set is given by a calligraphic letter (i.e., $\mathscr{X}$).

2.2.1 Transmitter Model
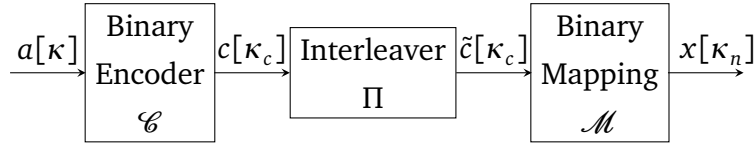
Figure 2.3: Transmitter model

The discrete-time Tx model is depicted in Figure 2.3. An encoder encodes the source sequence $a[\kappa]$ for $\kappa = 1, ..., m$ into a code sequence $c[\kappa_c]$ for $\kappa_c = 1, ..., n'$, with $n' > m$. The variables m and n' define the length of the uncoded and coded word, respectively. The binary code is given by the set of codewords $\mathscr{C}$. The coded sequence is then passed to a bit interleaver Π, which outputs the interleaved sequence $\tilde{c}[\kappa_c]$. This sequence is finally one-to-one mapped on channel symbols $x[\kappa_n]$ for $\kappa_n = 1, ..., n$, with n being the length of the transmitted symbol sequence.

One requirement of this work is to analyze low latency transmission, therefore, a convolutional encoder is applied for the encoding process. It was shown in [42] that for short to moderate codeword length convolutional codes are a competitive alternative to other coding schemes as they cause short delays in terms of structural delay, which comprises data delay and decoding performance. Convolutional codes are characterized by encoders with memory, i.e., each bit in a coded sequence is dependent on the preceding encoder input bits [5]. The process of encoding can be described as a convolution of an encoder input sequence of arbitrary length with the generator polynomial of the encoder [5]. In practice data is processed in a short finite block structure. Therefore, for further considerations, terminated convolutional codes are used in combination with a Viterbi decoder. By terminating each word after n' symbols, it can be guaranteed that each bit does only influence the current codeword it is incorporated in, but no succeeding codewords [5]. This prevents error propagation in the decoding process and

is moreover advantageous if a frame structure should be implemented [5]. The different implemented coding rates, calculated by [4]

$$R_c = \frac{m}{n'},$$ (2.1)

are given in Table 2.2, which also shows the applied generator polynomials in octal form and the puncturing pattern, if puncturing was needed to realize different rates from a mother code. Additionally, the constraint length L_c is given, which is the number of memory elements of the convolutional encoder plus one [5]. Finally, the references are given for more information.

A bit-interleaver Π is applied at the encoder output [27]. Its size is equal to the block-length n'. As interleaving operation a random interleaver according to [27] is applied, where the permutation of the coded bits is random in two dimensions. Firstly, they get permuted over their positions and secondly over time [34]. Interleaving transforms the code $\mathscr{C}$ into code $\mathscr{B}$ [49].

After the interleaving operation, a mapping is performed according to a binary mapping $\mathscr{M}$. In this thesis the performance of BPSK, 4QAM, 16QAM, 32QAM and 8PSK transmission is analyzed. The alphabet size M denotes the number of discrete constellation points, which are in the set $\mathscr{X}$, i.e., $M = |\mathscr{X}|$. The value M gives a constraint to the code word length n, with has to satisfy $n := kN_{\mathrm{cu}}$ with N_{cu} denoting the number of channel uses and $k = \log_2(M)$ being the number of bits per symbol. The mapping gets performed according to [40]

$$\mathscr{M} : \tilde{\mathbf{c}} = [\tilde{c}[1], ..., \tilde{c}[k]] \in \{0,1\}^k \to x \in \mathscr{X} \subseteq \mathbb{C},$$ (2.2)

Table 2.2: The following parameters of realized coding rates R_c are given: the generator polynomial in octal, the puncturing pattern (if it was applied), the constraint length L_c and references.

R_c	Generator polynomial	Puncturing pattern	L_c	Reference
1/7	[35 27 25 27 33 35 37]	–	5	[43]
1/5	[37 27 33 25 35]	–	5	[43]
1/4	[37 35 33 25]	–	5	[44]
1/3	[75 53 47]	–	6	[45]
1/2	[171 133]	–	7	[45]
2/5	[37 27 33 25 35]	[1100011001]	5	n.a.
2/3	[23 35 0; 0 5 13]	–	[5; 4]	[46]
3/4	[171 133]	[110110]	7	[47]
5/6	[171 133]	[1101010101]	7	[48]
7/8	[171 133]	[11011010101010]	7	[48]

where blocks of k bits get mapped to signal constellation symbols according to a Gray mapping. For BPSK transmission $\mathscr{X} \subseteq \mathbb{R}$ is taken.

In [9] it was shown that for a transmit power of $1\,\mathrm{W}$, a transmission with Tbps can be achieved. Therefore, for further considerations the transmit power is assumed to be $P = 1\,\mathrm{W}$.
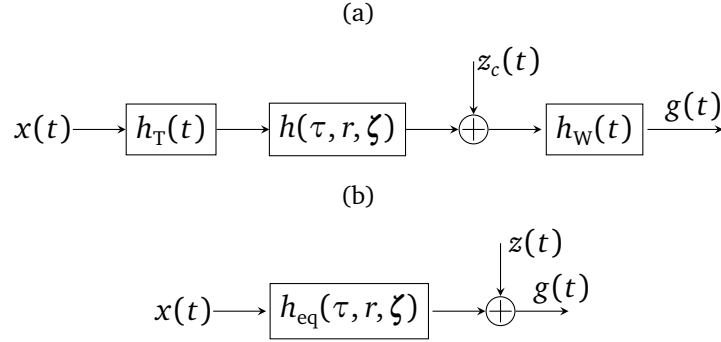
2.2.2 Channel Model

Figure 2.4: (a) Channel model with transmit pulse shape filter $h_{\mathrm{T}}(t)$, colored noise $z_c(t)$ and whitening filter $h_{\mathrm{W}}(t)$.
(b) Equivalent THz channel model with i.i.d additive white Gaussian noise $z(t)$.

Throughout this work, the developed discrete-time channel model from [9] is used. Its derivation is described shortly in the following. The continuous-time system model is shown in Figure 2.4 (a). The variable $g(t)$ denotes the continuous-time received signal before equalization, while $x(t)$ is the continuous-time transmit signal. Furthermore, $h(\tau, r, \zeta)$ is the continuous-time CIR considering multipath propagation characterized by delay variable τ, the scattering properties of the environment with vector ζ and the distance between Tx and Rx by r. For pulse shaping a Root Raised Cosine (RRC) filter $h_{\mathrm{T}}(t)$ is used at the Tx. Transmission over the THz channel is influenced by colored noise $z_{\mathrm{c}}(t)$. For the Rx input filter a band limiting noise whitening filter $h_{\mathrm{W}}(t)$ is used to whiten the received signal and transform $z_{\mathrm{c}}(t)$ to independent identically distributed (i.i.d.) additive white Gaussian noise $z(t)$.

According to [50] the system model in Figure 2.4 (a) can be converted into an equivalent system model by introducing an equivalent continuous-time CIR $h_{\mathrm{eq}}(\tau, r, \zeta)$, which contains the transmit filter $h_{\mathrm{T}}(t)$, the channel and the continuous-time whitening filter $h_{\mathrm{W}}(t)$. In Figure 2.4 (b), the equivalent continuous-time system model containing i.i.d. additive white Gaussian noise $z(t)$ with zero mean and variance σ_z^2 is shown [9, 50].

The equivalent discrete-time THz channel is illustrated in Figure 2.5. It is obtained by sampling the continuous-time received signal $g(t)$ at a rate $\frac{1}{T}$ for a fixed $T = \frac{(1+\alpha)N}{BW}$,
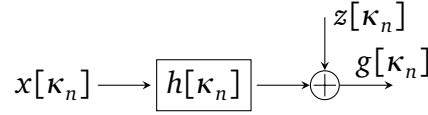
Figure 2.5: Equivalent discrete-time channel model (without equalization).

where $\alpha = 0.25$ is the roll-off factor of the RRC filter [10]. As was already mentioned in Subchapter 2.1, the channel transfer function $H_{eq}(f, r, \zeta)$ is highly frequency-selective and therefore, a subband approach with $N = 32$ is preferred [9]. Moreover, constant scattering is assumed in each subband and N equivalent discrete-time CIRs $h_{eq_N}[\kappa_n]$ can be obtained. As described in Subchapter 2.1, the considered subband for transmission is the first subband ($N = 1$), since it shows the best SNR conditions. For further considerations throughout this work, and for means of simplicity, the equivalent discrete-time channel $h_{eq_1}[\kappa_n]$ will in the following be referred to as $h[\kappa_n]$.
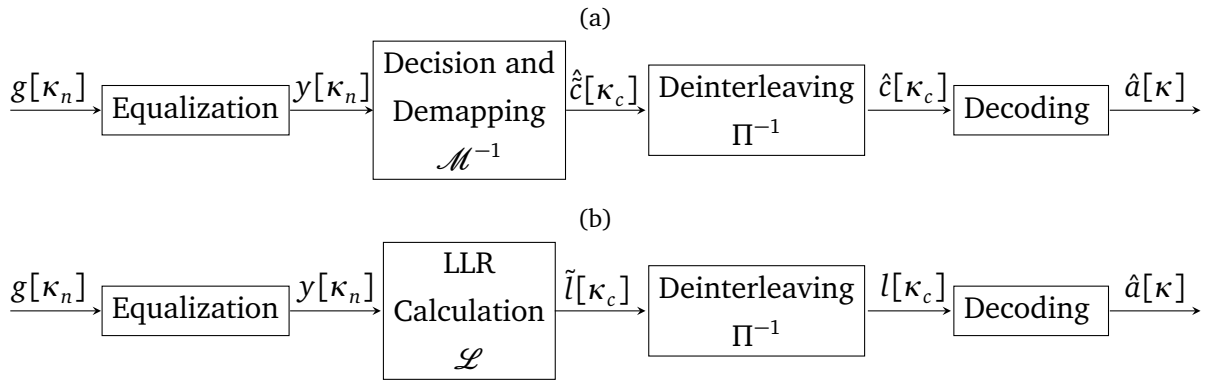
2.2.3 Receiver Model

Figure 2.6: Receiver model for (a) hard and (b) soft-decision decoding.

In Figure 2.6 the Rx-Model is illustrated. Figure 2.6 (a) shows the system model for hard-decision decoding, while the block diagram for soft-decision decoding is given by Figure 2.6 (b). Both are described in the following.

The goal of the Rx is to estimate the source sequence $a[\kappa]$ based on the distorted noisy received sequence $g[\kappa_n]$. Both Rx models start with an equalization part, which is needed, because the subchannel approach leads to subchannels with (controllable) frequency-selectivity, which introduces Intersymbol Interference (ISI), i.e., different transmitted symbols superimpose and influence each other. Equalization is used to account for the ISI effect and to reverse the symbol distortion [50]. In this work Minimum Mean Squared Error Linear Equalization (MMSE-LE) according to [50] is applied. This kind of equalizer is chosen, because it balances a reduction in ISI with noise enhancement [51]. The calculation of its optimum filter coefficients is described in the following.

For further considerations, perfect channel state information (CSI) is assumed. More-over, the signals $g[\kappa_n]$ and $x[\kappa_n]$ are assumed to be weak-sense stationary stochastic processes [50]. The optimal equalizer filter coefficients $\mathbf{f}_{\mathrm{opt}}$ are obtained by minimizing over the mean-squared error (MSE) between the transmitted signal $x[\kappa_n]$ and its estimate $\hat{x}[\kappa_n]$. For a better usability in the next chapters, a slight abuse in usual nomenclature is accepted and for further considerations the estimate of $x[\kappa_n]$ is denoted by $y[\kappa_n]$, i.e., the MSE is given by [50, 51, 52]

$$J(\mathbf{f}) = \mathbb{E}\{|x[\kappa_n] - y[\kappa_n]|^2\} \tag{2.3}$$

$$= \mathbf{f}^H \mathbf{\Phi}_{gg}\mathbf{f} - (\mathbf{f}^H \boldsymbol{\varphi}_{gx} + \boldsymbol{\varphi}_{gx}^H\mathbf{f}) + \sigma_x^2, \tag{2.4}$$

for $(\cdot)^H$ being the Hermitian matrix operation. $\mathbf{\Phi}_{gg} = E\{\mathbf{g}[\kappa_n]\mathbf{g}^H[\kappa_n]\}$ denotes the auto-correlation matrix of the filter input $g[\kappa_n]$, $\boldsymbol{\varphi}_{gx} = E\{\mathbf{g}[\kappa_n]x^*[\kappa_n]\}$ is the crosscorrelation vector between the received symbol $g[\kappa_n]$ and the desired symbol $x[\kappa_n]$. The received vector is defined as $\mathbf{g}[\kappa_n] = [g[\kappa_n]\,g[\kappa_n-1]\ldots g[\kappa_n-q_f]]$, with q_f being the equalizer filter length [50]. To obtain $\mathbf{f}_{\mathrm{opt}}$, the (conjugate) Wirtinger derivative of Equation (2.4) has to be taken. Thereafter, the whole expression can be resolved for $\mathbf{f}_{\mathrm{opt}}$ and the Wiener solution is finally given by [50]

$$\mathbf{f}_{\mathrm{opt}} = \mathbf{\Phi}_{gg}^{-1}\boldsymbol{\varphi}_{gx}. \tag{2.5}$$

To derive theoretical bounds in further chapters, the theoretical output SNR of the equalization, $\mathrm{SNR}_{\mathrm{MMSE-LE}}$, is needed. It is obtained by [50]

$$\mathrm{SNR}_{\mathrm{MMSE-LE}} = \frac{\sigma_x^2}{\sigma_e^2} - 1, \tag{2.6}$$

with σ_x^2 being the variance of the used discrete symbol constellation alphabet $\mathcal{X}$ and σ_e^2 being the Minimum Mean Squared Error (MMSE) calculated by [50]

$$\sigma_e^2 := \min_{\mathbf{f}} J(\mathbf{f}) = \sigma_x^2 - \mathbf{f}_{\mathrm{opt}}^H\boldsymbol{\varphi}_{gx}. \tag{2.7}$$

Equation (2.6) accounts for bias compensation of the error signal by the subtraction of 1. The unbiased $\mathrm{SNR}_{\mathrm{MMSE-LE}}$ is furthermore influenced by noise and residual ISI after equalization. Its deviation from the given input SNR, termed as $\mathrm{SNR}_{\mathrm{in}}$, which is the SNR before equalization, should be as small as possible. $\mathrm{SNR}_{\mathrm{in}}$ is given by

$$\mathrm{SNR}_{\mathrm{in}} = \frac{E_h P}{\sigma_z^2}, \tag{2.8}$$
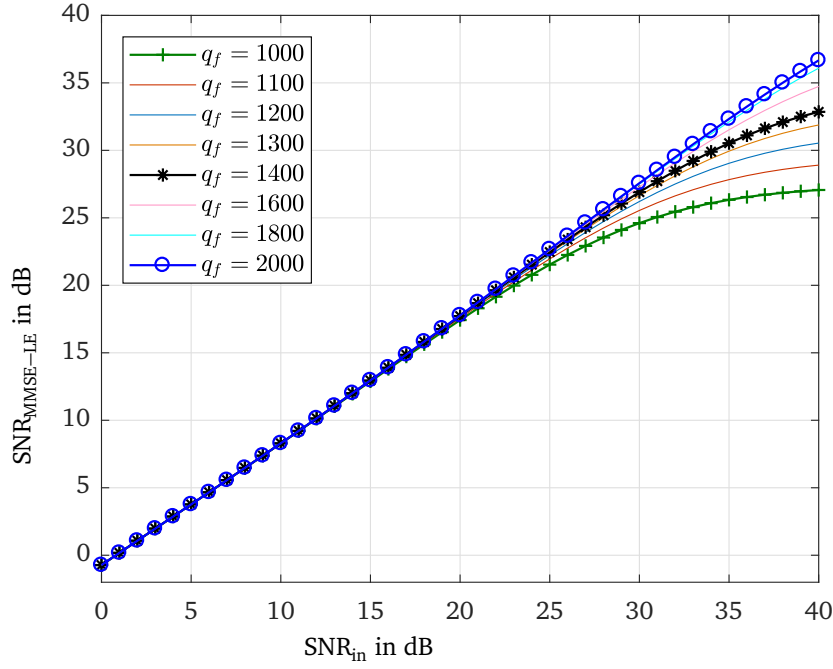
Figure 2.7: $\mathrm{SNR_{MMSE-LE}}$ over $\mathrm{SNR_{in}}$ for a transmission over the first subband of the THz channel

where E_h is the channel energy given in Table 2.1, P is the transmit power and σ_z^2 denoting the noise variance. The deviation can be controlled by the equalizer filter length q_f. The impact of q_f is depicted in Figure 2.7. The loss in $\mathrm{SNR_{in}}$ is in the range of 2 dB for high $\mathrm{SNR_{in}}$ and in the range of 1 dB for low $\mathrm{SNR_{in}}$. The higher q_f is chosen, the more ISI can be mitigated and the less noise enhancement is caused. For applications in reality, q_f should be chosen as the smallest filter length possible which meets given requirements. In the case of the described office scenario in Subchapter 2.1 the $\mathrm{SNR_{in}}$ range of interest is between 0 and 15 dB if the Rx is assumed to be not directly next to the Tx. For further considerations, the filter length is chosen as $q_f = 1000$ as a higher filter length does not significantly improve $\mathrm{SNR_{MMSE-LE}}$ for the given $\mathrm{SNR_{in}}$.

After equalization an equivalent channel model with channel $h_{\mathrm{overall}}[\kappa_n] = f_{\mathrm{opt}}[\kappa_n] * h[\kappa_n]$ and filtered noise $z_{\mathrm{filtered}}[\kappa_n] = f_{\mathrm{opt}}[\kappa_n] * z[\kappa_n]$, i.e., colored noise, can be obtained (cf. Figure 2.8). The equalization results for selected scenarios are depicted in Figure 2.9. It can bee seen that the overall channel $h_{\mathrm{overall}}[\kappa_n]$ is an almost perfectly equalized
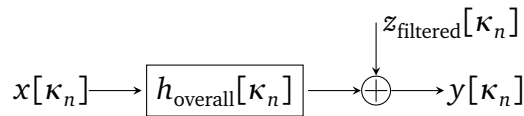

Figure 2.8: Equivalent channel model after equalization

channel with some residual ISI for low SNR_{in} values of $0\,dB$ and $7\,dB$ (cf. Figure 2.9 (a) and Figure 2.9 (b)). In the case of $20\,dB$ it shows indeed a great equalization performance with almost no residual ISI (cf. Figure 2.9 (c)).

For the verification of theoretical results, a simulation framework is used, which uses the equivalent channel model according to Figure 2.8. In this case a bias compensation of the estimation error is performed differently compared to the theoretical approach given in Equation (2.6). It is done by a multiplication of the equalizer filter output signal $y[\kappa_n]$ by a proportionality factor that is the main cursor tap weight coefficient of the total overall system response, i.e., by $\frac{1}{h_{\text{overall}}[0]}$ [50, 53]. The SNR after equalization in the case of simulation is calculated as

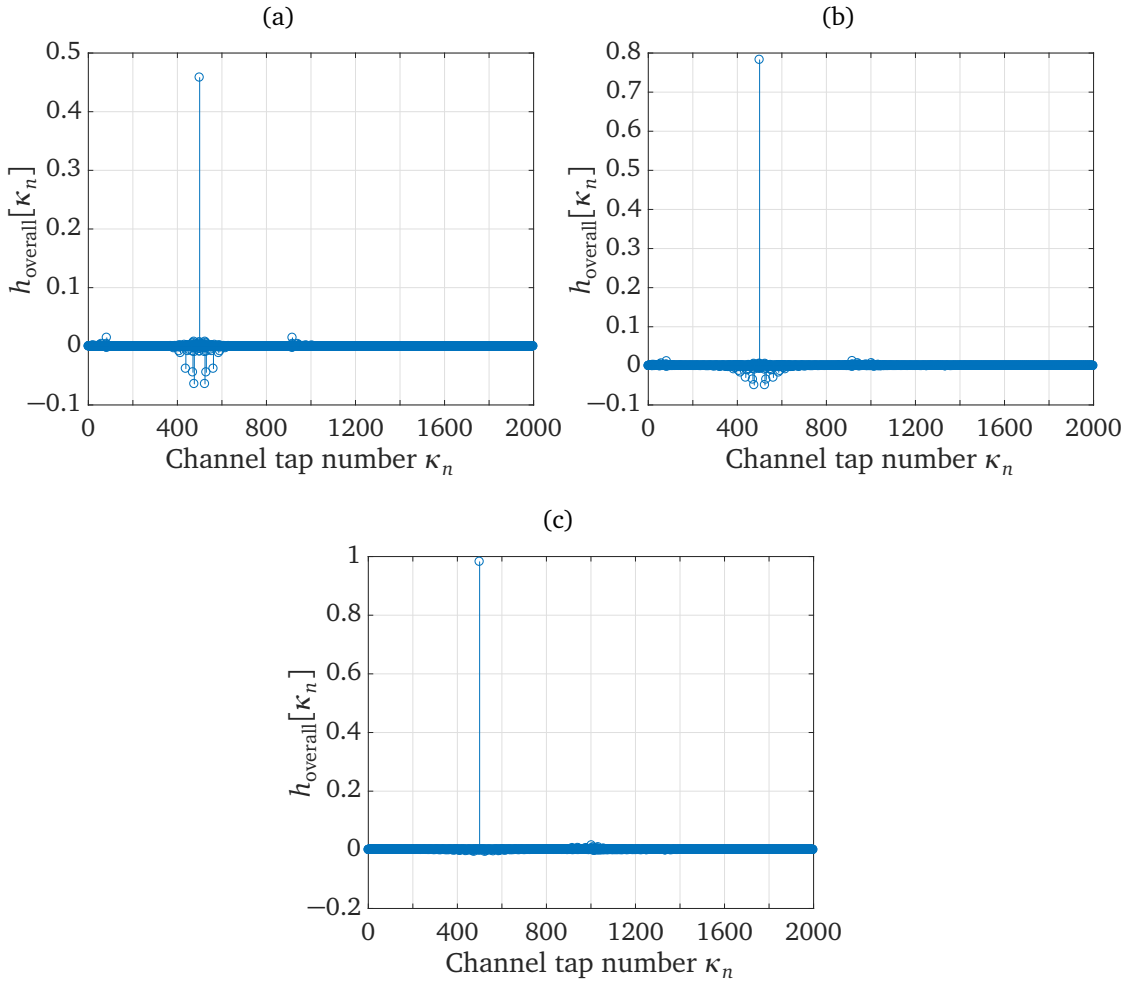$$\text{SNR}_{\text{MMSE-LE}}^{\text{sim}} = \frac{\sigma_x^2}{\text{mse}} \tag{2.9}$$

Figure 2.9: Overall channel after equalization for (a) $SNR_{in} = 0$ dB, (b) $SNR_{in} = 7$ dB and (c) $SNR_{in} = 20$ dB

and mse being the mean squared error (MSE) given by

$$\text{mse} = \mathbb{E}\{|x[\kappa_n] - y[\kappa_n]|^2\}, \tag{2.10}$$

where $x[\kappa_n]$ and $y[\kappa_n]$ are taken according to the equivalent channel model after equalization given in Figure 2.8.

After equalization and bias compensation, two methods for the further processing can be used, named hard-decision decoding and soft-decision decoding. In both cases a Maximum Likelihood Sequence Estimation (MLSE) is performed to determine, from the received distorted data, the sequence $\hat{a}[\kappa]$. This is done by the use of the Viterbi algorithm to find the sequence $\hat{a}[\kappa]$ that was transmitted with the highest likelihood [37].

If the choice is to use hard-decision decoding (Figure 2.6 (a)), first a demapper performs the inverse mapping to the bit sequence $\hat{\hat{c}}[\kappa_c]$ according to [39]

$$\hat{\hat{c}}[\kappa_c] = \mathcal{M}^{-1}\left(\arg\min_{x[\kappa_n]\in\mathcal{X}}\{|y[\kappa_n] - x[\kappa_n]|\}\right), \tag{2.11}$$

where the inner part constitutes a decision devise, which determines the smallest distance of a received signal point to a signal point taken from the discrete constellation alphabet $\mathcal{X}$. Next, a deinterleaver Π^{-1} performs the inverse interleaving operation to get the deinterleaved sequence $\hat{c}[\kappa_c]$. Thereafter a Viterbi decoder is used, which first performs slicing the sequence $\hat{c}[\kappa_c]$ to get 0 and 1 values. Then it finds an all-zero-state-to-all-zero-state path whose (encoder) output sequence is closest to the sliced sequence in terms of Hamming distance [37, 38, 54].

The performance of the BICM system can be improved by using soft-decision decoding instead of hard-decision decoding (cf. Figure 2.6 (b)). To limit the loss of information, arising from separating coding and modulation in a BICM system and to achieve the highest code diversity [27], soft information about the coded bits is propagated to the decoder in the form of Log Likelihood Ratios (LLR) [36, 37]. LLR-values give more information about the reliability of the transmitted bits. For each particular (coded) bit i for $i = 1, ..., k$ in one symbol they are computed by [37]

$$\mathcal{L} : L_i = \ln\left[\frac{P(b_i = +1|y)}{P(b_i = -1|y)}\right] \tag{2.12}$$

$$= \ln\left[\frac{P(y|b_i = +1)}{P(y|b_i = -1)}\right] + \ln\left[\frac{P(b_i = +1)}{P(b_i = -1)}\right], \tag{2.13}$$

i.e., the logarithm of the ratios of the probabilities that bit b_i is $+1$ or -1 conditioned on the fact that the signal y was received [37]. If the constellation points are transmitted

equiprobably and an AWGN channel model is assumed, the LLR value of the ith bit L_i
for $i = 1, ..., k$ can be rewritten as

$$\mathscr{L} : L_i = \ln \left[\frac{\sum\limits_{x \in \mathscr{X}_1^i} \exp(\frac{|y-x|^2}{2\sigma^2})}{\sum\limits_{x \in \mathscr{X}_0^i} \exp(\frac{|y-x|^2}{2\sigma^2})} \right] , \tag{2.14}$$

where $\mathscr{X}_b^i$ is a subset of $\mathscr{X}$ for bit value b and bit position i. In the considered system
model one also has to account for the ISI effects and noise enhancement after equalization.
This is why the unbiased error variance after equalization has to be taken into account,
which is given by Equation (2.10), i.e., in this case $\sigma^2 := \text{mse}$.

   After LLR-calculation, the sequence of soft-estimates $\tilde{l}[\kappa_c]$ is passed to the deinterleaver,
which performs deinterleaving to sequence $l[\kappa_c]$. Thereafter, this sequence is given to
the decoder. For decoding, first the received sequence of LLR-values is quantized to
2^{10} levels. Afterwards, the quantized values are used by the Viterbi algorithm, which
searches the trellis diagram for an all-zero-state-to-all-zero-state path whose (encoder)
output sequence is closest to the sequence of quantized values in terms of Euclidean
distance and takes the encoder input sequence corresponding to the optimal path to be
the most likely message sequence [37, 54].

2.3 Properties of the Transmit Signal

The transmit signal is designed as a burst of variable length containing a predefined
number of codewords, each of the same length. The codeword length can be set accord-
ing to given latency requirements. Terminated convolutional codes ensure that each
codeword can be coded and decoded independently from preceding codewords.

   This first system design aims to establish a basic simulation framework, which is to be
developed further in future work. This approach can be improved for example to transmit
frames which contain several subframes comprising various coded data. This data can
be of different kind for instance information containing symbols, control symbols or
reference signals.

   Furthermore, an approach considering frame fragmentation as in [18] could be realized.
Long frames are more likely to be influenced by the distorting channel [18]. If bit errors
occur in large frames, which cannot be reconstructed at the Rx anymore, a large amount of
data would have to be retransmitted or would be lost, if no retransmission is considered.
Shorter frames are therefore preferred for a transmission over noisy channels [18].
Furthermore, if an error occurs in a short frame, retransmission can be performed faster
than for long frames [18].

Chapter 3

Fundamentals of Finite Blocklength Coding

In 1948, Shannon established the fundamental performance limit for the maximum achievable channel capacity assuming infinite coding delay and complexity [55]. Since then various channels were analyzed regarding channel capacity using approaches based upon probabilistic limit theorems, such as the laws of large numbers, ergodic theory or large deviation [56]. Common assumptions are often asymptotically large blocklength or vanishingly small error probabilities [4]. However, for communication system design with specific quality-of-service requirements like, e.g., strict latency or certain reliability, the main question that arises is:

What is the minimum blocklength n^* which sustains a desired error probability ϵ and guarantees to achieve a fraction η of the channel capacity [55]?

An answer cannot be provided accurately by using conventional information theoretic results based on performance limits, but can be given by using findings from the non-asymptotic regime instead [55].

In early years, non-asymptotic bounds were developed to confirm the asymptotic results and to provide more insight for system design [55]. Classical bounds, like for instance bounds developed by Feinstein, Gallager, Shannon, or Wolfowitz are very general [55]. Unfortunately, they show a bad non-asymptotic performance, except for bounds developed for special cases, e.g., for the AWGN channel or for the Binary Erasure Channel (BEC) [55]. Furthermore, the computation of these classical bounds is very cumbersome [55]. Therefore, approximations of these bounds, i.e., of the achievable coding rates, are needed to provide accurate and tight results not only for large but also for short to moderate blocklength [4, 55].

One option is to use the error exponent, also called reliability function [55]. This concept considers a fixed communication rate and shows the exponential decay of error

probability with respect to the blocklength. However, this method achieves only good finite blocklength estimates for rates far from capacity [55].

Another possibility is to incorporate a quantity called *channel dispersion* into the approximation process. It is related to the second derivative of the error exponent, but is much easier to calculate [4]. This value is part of the normal approximation, which was introduced in 1962 by Strassen ([8]) and which can be used to approximate the maximum achievable rate of a channel. Recently, in 2010 a refined approach was proposed by Polyanskiy, Poor and Verdú (PPV) [7]. In their work they demonstrate a good approximation of tight non-asymptotic bounds for short to moderate blocklength by incorporating this additional knowledge about the channel and their refinements [7]. Therefore, the research findings of PPV in [7] are used to give a tight approximation of theoretical bounds for a transmission over the THz channel with delay critical and specific reliability requirements.

The rest of this chapter is organized as follows. In Subchapter 3.1 important information theoretical background is reviewed, which is required for a better understanding of the main topic. Thereafter, in Subchapter 3.2 an introduction into the theory of finite blocklength coding according to PPV is given.

3.1 Preliminaries from Information Theory

$$A \longrightarrow \boxed{\text{Encoder}} \xrightarrow{X} \overset{P_{Y|X}}{\boxed{\text{Noisy channel}}} \xrightarrow{Y} \boxed{\text{Decoder}} \xrightarrow{\hat{A}}$$
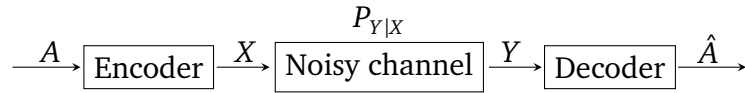
Figure 3.1: General simplified system model

For the notations used in the sequel, random variables will be defined by upper case letters, (e.g., X, Y,) realizations of random variables are given by lower case letters, (e.g., x, y) and a set will be indicated by calligraphic letters (e.g., $\mathscr{X}, \mathscr{Y}$). Moreover, for the case of simplicity a sequence $x[\kappa_n]$ for $\kappa_n = 1, ..., n$ is abbreviated by x^n. Therefore, x^n denotes a realization of a random variable with dimension n and $\mathscr{X}^n$ is the set containing realizations of random variables with dimension n. X^n is a random variable with dimension n.

In this chapter the simplified channel model given in Figure 3.1 is assumed. The random variable A denotes an a priori unknown message, equiprobably taking values in the message set $\mathscr{W} = \{1, ..., W\}$. Hence, the length of the uncoded word is $m = \log_2(W)$ with W being the amount of messages that are to be transmitted, i.e., $W = |\mathscr{W}|$. In Figure 3.1 the channel input is denoted by the random variable $X \in \mathscr{X}$ and the channel

output by the random variable $Y \in \mathcal{Y}$ for $\mathcal{X}$ and $\mathcal{Y}$ being the channel input alphabet and output alphabet, respectively. For reasons of simplicity, the encoder is assumed to perform no mapping, i.e., the uncoded words of length m are just encoded to codewords X of length n. This is the communication model introduced by Shannon [55, 57]. The coding rate is given by Equation (2.1) for $n' = n$. In this case, the transmission rate equals the coding rate, i.e., $R = R_c$ [57].

The codewords are sent over a point-to-point channel. Its description is given in the following by Definition 3.1.

Definition 3.1. A general point-to-point channel consists of an input alphabet $\mathcal{X}$, an output alphabet $\mathcal{Y}$, and an n-letter channel transition probability given by [4]

$$P_{Y^n|X^n}(y^n|x^n) : \mathcal{X}^n \to \mathcal{Y}^n.$$

For any stationary memoryless channel the following holds [4]

$$P_{Y^n|X^n}(y^n|x^n) = \prod_{t=1}^{n} P_{Y|X}(y_t|x_t). \tag{3.1}$$

The channel output y^n is taken by the decoder to estimate the sent message A with a certain error probability ϵ.

A code is clearly defined by a tuple of parameters (n, W, ϵ) ([55]), with a more precise description given in the following.

Definition 3.2. For a general point-to-point channel $P_{Y^n|X^n}(y^n|x^n) : \mathcal{X}^n \to \mathcal{Y}^n$, an (n, W, ϵ) code is composed of a message set $\mathcal{W} = \{1, ..., W\}$ and a corresponding set of codewords $\mathcal{X}^n$ and mutually exclusive, collectively exhaustive decoding regions $\{x^n(i), D_i\}$ with $x^n(i) \in \mathcal{X}^n$ being the ith codeword of the set, $D_i \subseteq \mathcal{Y}^n$ and $i \in \mathcal{W}$, such that a certain error probability is satisfied [4].

One option is to assume an average error probability ϵ_n given by [4]

$$\epsilon_n := \frac{1}{W} \sum_{i=1}^{W} P[Y^n \notin D_i | X^n = x^n(i)] \le \epsilon, \tag{3.2}$$

while another possibility is to assume a maximum error probability $\epsilon_{\max}$ given by

$$\epsilon_{\max} := \max_{x^n(i) \in \mathcal{W}} P[Y^n \notin D_i | X^n = x^n(i)] \le \epsilon. \tag{3.3}$$

For further considerations an average error probability given by Equation (3.2) is assumed. The maximal code size achievable with a given error probability and blocklength is denoted by [7]

$$W^*(n, \epsilon) = \max\{W : \exists (n, W, \epsilon)\, \text{code}\} \tag{3.4}$$

and consequently, Definition 3.3 follows.

Definition 3.3. A rate $R(n, \epsilon)$ is called achievable for the general point-to-point channel $P_{Y^n|X^n}(y^n|x^n)$ with blocklength n and average error probability ϵ_n if an (n, W, ϵ) code exists [4].

Shannon proved in [6] that for any stationary memoryless channel ([4]) there exist sequences of (n, W, ϵ) codes which achieve a positive asymptotic rate R and vanishing error probability $\epsilon \to 0$ for increasing blocklength n

$$R = \lim_{n\to\infty} \frac{1}{n} \log_2(W) > 0. \tag{3.5}$$

However, not all rates are achievable for vanishing error probability, there is a maximum achievable rate given as the channel capacity C, i.e., [6, 7, 55]

$$\lim_{\epsilon\to 0} \liminf_{n\to\infty} \frac{1}{n} \log_2 W^*(n, \epsilon) = C. \tag{3.6}$$

The channel capacity of any stationary and memoryless channel is obtained by [6, 58]

$$C = \max_{P_X} I(X;Y), \tag{3.7}$$

where P_X is the input distribution and $I(X;Y)$ denotes the average mutual information defined as [4, 59]

$$I(X;Y) = \mathbb{E}\{i(X;Y)\} \tag{3.8}$$

$$= \sum_x \sum_y P_{XY}(x,y) \log_2\left(\frac{P_{XY}(x,y)}{P_X(x)P_Y(y)}\right) \tag{3.9}$$

$$= \sum_x \sum_y P_X(x)P_{Y|X}(y|x) \log_2\left(\frac{P_{XY}(x,y)}{P_X(x)P_Y(y)}\right) \tag{3.10}$$

$$= \sum_x \sum_y P_X(x)P_{Y|X}(y|x) \log_2\left(\frac{P_{Y|X}(y|x)}{P_Y(y)}\right), \tag{3.11}$$

$$\tag{3.12}$$

where

$$P_Y(y) = \sum_x P_X(x)P_{Y|X}(y|x) \tag{3.13}$$

is the distribution induced on the channel output by the input P_X and $i(X;Y)$ being the mututal information random variable ([59]), also called information density ([7, 56]) or information spectrum ([23]), given by

$$i(X,Y) = \log_2\left(\frac{P_{X|Y}(x|y)}{P_X(x)}\right) = \log_2\left(\frac{P_{Y|X}(y|x)}{P_Y(y)}\right). \tag{3.14}$$

For finite blocklength n, a quantity called information rate ([56]) or normalized mutual information random variable ([4]) gives more insight about the performance and is given by

$$\frac{1}{n}i(X^n, Y^n) := \frac{1}{n}\log_2\left(\frac{P_{Y^n|X^n}(Y^n|X^n)}{P_{Y^n}(Y^n)}\right). \tag{3.15}$$

For memoryless channels with independent and identically distributed inputs the following holds [56]

$$\frac{1}{n}i(X^n, Y^n) = \sum_{t=1}^{n} i(X_t, Y_t). \tag{3.16}$$

However, Equation (3.16) does not hold for a non-i.i.d. input distribution. A non-i.i.d. input distribution induces a non-i.i.d. output distribution [4]. A non-i.i.d. input distribution can indeed be the impact of channel input power constraints caused on an i.i.d. input distribution [4]. In such cases, when the actual output distribution is not i.i.d., it is desirable for calculation purposes to consider auxiliary distributions on the output alphabet [7]. Then the reference of the mutual information random variable is changed from the actual output distribution P_{Y^n} to an arbitrary product distribution Q_{Y^n}. Hence, a modified normalized mutual information random variable is obtained given by [4, 7]

$$\frac{1}{n}\tilde{i}(X^n, Y^n) := \frac{1}{n}\log_2\left(\frac{P_{Y^n|X^n}(Y^n|X^n)}{Q_{Y^n}(Y^n)}\right). \tag{3.17}$$

The result is, that Equation (3.16) holds for $\frac{1}{n}\tilde{i}(X^n, Y^n)$ although the summands are not independent [4].

Furthermore, Wolfowitz showed that Equation (3.6) holds even for $0 < \epsilon < 1$. This result is known as the strong converse to the channel coding problem and can be described by [7]

$$\limsup_{n\to\infty} \frac{1}{n}\log_2 W^*(n,\epsilon) \le C. \tag{3.18}$$

For any fixed probability of error $0 < \epsilon < 1$ and $n \to \infty$ both, Equation (3.6) and Equation (3.18), lead to the fundamental limit, which satisfies [55]

$$\log_2 W^*(n,\epsilon) = nC + o(n). \tag{3.19}$$

For the proof of the channel coding theorem three tasks have to be performed, namely a proof of the converse, of the achievability and of the asymptotic results. These three terms are described closer in the next definitions.

Definition 3.4. Converse: an upper bound on the size of any code W with given arbitrary blocklength n and error probability ϵ [7].

Definition 3.5. Achievability: a lower bound on the size of a code W that can be guaranteed to exist with given arbitrary blocklength n and error probability ϵ [7].

Definition 3.6. Asymptotics: the bounds on the log size of the code normalized by blocklength, i.e., $\frac{\log_2(W)}{n}$, asymptotically coincide as a result of the law of large numbers (memoryless channels) or another ergodic theorem (for channels with memory) [7].

The asymptotic analysis of the upper bound and of the lower bound of a specific channel model, considering the finite blocklength regime for discrete memoryless channels or for Gaussian channels, leads to final inequalities on which an expansion can be applied. The results of these expansions coincide and correspond to the normal approximation, which can be used to approximate the maximum achievable rate for different blocklengths n [4, 22, 55]. The upper bound and the lower bound are used to verify, that the rate obtained by applying the normal approximation is achievable [4, 22, 55]. It was shown in various examples in the literature (cf. [4, 7, 21, 22, 24, 25, 26, 60, 61] and more) that the normal approximation gives an excellent estimate for the value of $\log_2 W^*(n, \epsilon)$, restricted by upper and lower bounds, for many different channels. It is approximated by [55]

$$\log_2 W^*(n, \epsilon) \approx Cn - \sqrt{Vn} \cdot Q^{-1}(\epsilon), \tag{3.20}$$

where V is the channel specific parameter called channel dispersion and $Q^{-1}(\epsilon)$ is the inverse Q-function for $Q(x) = \int\limits_{x}^{\infty} \frac{1}{\sqrt{2\pi}} e^{-t^2/2} dt$. The maximum achievable rate can be inferred by dividing Equation (3.20) by n.

In the following, the channel models of interest will be analyzed closer regarding capacity calculation with real and complex channel input. Therefore, in Subchapter 3.1.1 the properties of a Gaussian channel are reviewed and in Subchapter 3.1.2 the characteristics of the discrete-input-continuous-output Gaussian channel will be shown. The aim is to review the basic information theoretical background to be able to understand the derivation of the channel dispersion and the introduction of a more precise expression of the maximum achievable rate (compared to Equation (3.20)) for a continuous channel input as well as for a discrete channel input. These calculations are covert in Subchapter 3.2.

3.1.1 Gaussian Channel

For a memoryless real Gaussian channel the channel transition probability density $P_{Y^n|X^n}(y^n|x^n) : \mathbb{R}^n \to \mathbb{R}^n$ is given by [4, 33]

$$P_{Y^n|X^n}(y^n|x^n) = \prod_{t=1}^{n} P_{Y|X}(y_t|x_t) = (2\pi)^{-n/2} e^{\frac{-\|y^n-x^n\|^2}{\sigma_z^2}}. \tag{3.21}$$

For the case of a memoryless complex Gaussian channel it is accordingly given by [33]

$$P_{Y^n|X^n}(y^n|x^n) = \prod_{t=1}^{n} P_{Y|X}(y_t|x_t) = (2\pi)^{-n} e^{\frac{-\|y^n-x^n\|^2}{2\sigma_z^2}}, \tag{3.22}$$

with the channel transition probability density $P_{Y^n|X^n}(y^n|x^n) : \mathbb{C}^n \to \mathbb{C}^n$.

The additive, memoryless Gaussian channel can be written equivalently in the additive form [4]

$$Y^n = X^n + Z^n, \tag{3.23}$$

with Z^n being the zero-mean i.i.d. Gaussian noise with variance σ_z^2 for the real case and $2\sigma_z^2$ for the complex channel [4, 33]. Without further constraints, the capacity of this channel may achieve infinity [4]. The reason therefore is, that on the one hand for $\sigma_z^2 = 0$ error free transmission is possible [4]. On the other hand, for $\sigma_z^2 \neq 0$ one can select codewords arbitrarily far apart such that any number of messages can be communicated with an arbitrarily small probability of error [4]. Therefore, the channel input has to be constrained to some feasible set $\mathscr{F}^n \subset \mathscr{X}^n$. One option is to set a maximal input power constraint, given by [4, 7]

$$\frac{1}{n} \sum_{t=1}^{n} x_t^2 \leq P. \tag{3.24}$$

An alternative option is an average power constraint, averaged over the whole code-book [7]. However, for the combination of an average error probability and average power constraint, the strong converse (cf. Equation (3.18)) does not hold [7]. Therefore, for further considerations, it is assumed, that Definition 3.2 holds for a maximal power constraint, which is an average per codeword power constraint [21].

For asymptotically large blocklength $n \to \infty$, $\mathscr{X}^n = \mathbb{R}^n$ and $\mathscr{Y}^n = \mathbb{R}^n$, the capacity of the real point-to-point Gaussian channel with a cost constraint Gaussian channel input is given by [4, 6, 20]

$$C_{\text{real}}(\text{SNR}) := \max_{P_X \leq P} I(X; Y) = \frac{1}{2} \log_2(1 + \text{SNR}) \tag{3.25}$$

and for a cost constraint complex Gaussian channel input with $\mathcal{X}^n = \mathbb{C}^n$ and $\mathcal{Y}^n = \mathbb{C}^n$, it is known to be [6]

$$C_{\text{complex}}(\text{SNR}) := \max_{P_X \leq P} I(X; Y) = \log_2(1 + \text{SNR}). \tag{3.26}$$

Both expressions hold for equal-power, maximal-power and average-power constraints [7, 20]. The channel capacity can be achieved with an i.i.d. Gaussian channel input distribution [4, 62].

3.1.2 Discrete-Input-Continuous-Output Gaussian Channels

In practical cases, transmission of continuous input symbols requires highly complex transmitters [4]. Moreover, decoding a Gaussian code would require an exhaustive search over the whole codebook for the most likely candidate [36]. Therefore, a discrete channel input is assumed, which is easier to realize. Hence, for the following the assumption is made that the encoder-part in Figure 3.1 performs encoding and mapping to discrete constellation points. The channel input alphabet set $\mathcal{X}$ contains codewords consisting of discrete constellations points, i.e., set $\mathcal{X}^n$ contains codewords of length n composed of discrete constellation points. The channel output is still the entire real line $\mathcal{Y} = \mathbb{R}$ or complex domain $\mathcal{Y} = \mathbb{C}$, respectively. This model results in a transmission rate being [5]

$$R = R_c \cdot \log_2(M). \tag{3.27}$$

Popular modulation schemes, used in practice are MPSK and MQAM. For a complex point-to-point Gaussian channel and a transmit power given by P, the MPSK constellation is defined by [4]

$$x_t \in \sqrt{P} \times \left\{ \cos\left((2k-1)\frac{\pi}{M}\right) + j \sin\left((2k-1)\frac{\pi}{M}\right) \right\}_{k=1}^{M}, \quad t = 1, ..., n \tag{3.28}$$

and the MQAM constellation is given by [4]

$$x_t = x_{t,I} + j x_{t,Q}, \quad t = 1, ..., n \tag{3.29}$$

$$x_{t,I}, x_{t,Q} \in \sqrt{\frac{P}{\alpha_{\text{QAM}}}} \times \{-(\sqrt{M} - 1), ..., -1, +1, ..., +(\sqrt{M} - 1)\}, \tag{3.30}$$

where α_{QAM} is a normalizing constant given by [4]

$$\alpha_{\text{QAM}} = \frac{2(M - 1)}{3}. \tag{3.31}$$

This constant is needed to ensure that the average power of the individual symbols with respect to the probability distribution P_X selecting the symbols is equal to the power constraint P given in Equation (3.24), i.e., [4]

$$\mathbb{E}_{P_X}[\|X\|^2] = \sum_{i=1}^{M} P_X(x(i))\|x(i)\|^2 = P,$$
(3.32)

where $x(i)$ denotes the ith element of the corresponding constellation. Note that a maximum power constraint was set earlier for the channel in Equation (3.24), due to the peak power (amplitude) limitations usually constraining practical amplifiers [63]. However, the MQAM constellation is assumed to satisfy this constraint on average (cf. Equation (3.32)). A peak power constraint could also be assumed for MQAM constellations, leading to a highly complex adaptation of capacity calculation [63]. As this is out of scope of this thesis, in the sequel an average power constraint is assumed for MQAM and the concept of [4] is followed. Later on, it will be accounted for the failure of MQAM not fulfilling the maximum power constraint of the channel, due to a constraint violation probability that has to be considered at finite blocklength [4].

For a uniform distribution, the power requirement for the transmitted symbols simplifies to [4]

$$\frac{1}{M} \sum_{i=1}^{M} \|x(i)\|^2 = P.$$
(3.33)

Capacity for CM

One transmission system that uses a discrete channel input is CM. The performance of CM can be seen as an upper bound for various further modified transmission schemes, because its capacity is the closest to the Shannon bound (cf. Figure 2.2). Therefore, the calculation of the channel capacity for CM will be introduced in the following. For MPSK, symmetry properties of the channel and of the PSK input proves that an i.i.d. discrete uniform input distribution achieves the capacity for any SNR value, assuming the power constraint given by Equation (3.33) (cf. Equation (3.7)) [4, 64]. In the limit of asymptotically large blocklength, the capacity of MPSK assuming an i.i.d. uniform input distribution is given by [4, 33]

$$C_{\text{PSK}}^{\text{CM}}(\text{SNR}) := \log_2(M) - \frac{1}{M} \sum_{i=1}^{M} \mathbb{E}_Z \left[\log_2 \left(\sum_{l=1}^{M} e^{\frac{\|Z\|^2 - \|x(i) + Z - x(l)\|^2}{2\sigma_z^2}} \right) \right].$$
(3.34)

For MQAM in general a non-uniform distribution achieves the capacity and a uniform distribution is capacity-achieving only for very high or very low SNR [4]. Finding the capacity-achieving input distribution is a highly complex task [4]. Uniform inputs,

although not optimal in general, are still more relevant and favorable in practice due to implementation constraints [4]. Therefore, the capacity for MQAM corresponds to [4]

$$C_{\text{QAM}}^{\text{CM}}(\text{SNR}) = C_{\text{PSK}}^{\text{CM}}(\overline{\text{SNR}}), \tag{3.35}$$

for $\overline{\text{SNR}} = \text{SNR} - \delta$ and $\delta > 0$ being an arbitrarily small constant. The decrease in the SNR occurs to account for the fact, that MQAM does fulfill the maximum power constraint of the channel only on average [4]. The variable δ is a small constant or slowly decaying function of n which captures the power margin necessary to ensure that i.i.d-generated codewords barely violate the power constraint [4]. Its exact value is obtained by optimization [4]. According to [4] $\delta = \min(0.05 \cdot \text{SNR}, 0.25)$ can be used for illustration purposes. Equation (3.35) will be used as the practical capacity of the discrete-input Gaussian channel for QAM schemes [4].

The exact derivation of the capacity for CM is given in [4] and [33].

Capacity for BICM

For simulative analysis in this work the BICM system introduced in Chapter 2 is considered. As already mentioned, the capacity deviates slightly from the CM capacity. This is also depicted in Figure 2.2. The BICM scheme according to [27] assumes $k = \log_2(M)$ parallel binary channels. Its capacity is the sum of k individual capacities given by [65]

$$C^{\text{BICM}}(\text{SNR}) = \sum_{j=1}^{k} I(B_j; Y) \tag{3.36}$$

$$= \sum_{j=1}^{k} \mathbb{E} \left\{ \log_2 \frac{\sum\limits_{x' \in \mathscr{X}_b^j} \exp(-|X - x' - Z|^2)}{\frac{1}{2} \sum\limits_{x' \in \mathscr{X}} \exp(-|X - x' - Z|^2)} \right\}, \tag{3.37}$$

where B_j denotes the binary input random variable corresponding to the jth parallel channel. $\mathscr{X}_b^j$ represents the sets of constellation symbols with bit b in the jth position of the binary label. The expectation is performed over all input symbols x in $\mathscr{X}_b^j$ for $b = 0, 1$, and over all possible noise realizations Z. Equation (3.37) can further be simplified to [65]

$$C_{\text{PSK}}^{\text{BICM}}(\text{SNR}) = \sum_{j=1}^{k} \frac{1}{2} \sum_{b=0}^{1} \left(C_{\mathscr{X}}^{\text{CM}}(\text{SNR}) - C_{\mathscr{X}_b^j}^{\text{CM}}(\text{SNR}) \right). \tag{3.38}$$

For an exact derivation of this expression, the interested reader is referred to [65]. For the same reason as explained for CM, Equation (3.38) holds for MPSK transmission, and for MQAM transmission the following is assumed

$$C_{\mathrm{QAM}}^{\mathrm{BICM}}(\mathrm{SNR}) = C_{\mathrm{PSK}}^{\mathrm{BICM}}(\overline{\mathrm{SNR}}), \tag{3.39}$$

with $\overline{\mathrm{SNR}} = \mathrm{SNR} - \delta$ and $\delta > 0$ being an arbitrarily small constant.

3.2 Introduction to Finite-Blocklength-Coding based on the Work of PPV

In 2010 PPV achieved a breakthrough with their paper "Channel coding rate in the finite blocklength regime". By now it was cited over 900 times and used for many research tasks. The paper investigates the performance of finite blocklength codes for general channels, e.g., for the AWGN channel, for the BEC and for the Binary Symmetric Channel (BSC). New and computationally tractable bounds are provided to determine the maximum achievable rate at a particular blocklength n and for certain error probability ϵ [66]. Those bounds are developed with non-asymptotic tightness and generality in mind [55]. As this work is highly important for the non-asymptotic coding regime, a short overview of the findings is given in the following.

New bounds are derived for a non-asymptotic regime, i.e., fixed blocklength and code size are considered. In the beginning, an exact expression for an achievability (Definition 3.1) considering average error probability and using random coding is presented [66]. However, the computation of this bound is still highly complex [66]. Furthermore, a simpler converse (Definition 3.4), called random coding union bound, on the average error probability of a random coding ensemble is presented [66]. This bound may be weakened to earlier achievability results of Gallager and Shannon [66]. Another upper bound on the average error probability that is derived is called the dependence testing bound. It is easier to compute then most previous bounds [66]. Moreover, it can be extended to channels with input constraints [66]. The maximal error probability bound is a general upper bound on the maximal error probability of a random code ensemble. It is shown that this bound is easy to compute for the special cases of a BEC or a BSC [66]. Finally, the last two bounds that are presented in the paper are the $\kappa\beta$ bound, which is another maximal error probability achievability bound and a general converse for average and maximal error probability. Both include a Neyman-Pearson hypothesis testing [66]. It is shown that previous results obtained by Fano's inequality, Wolfowitz's
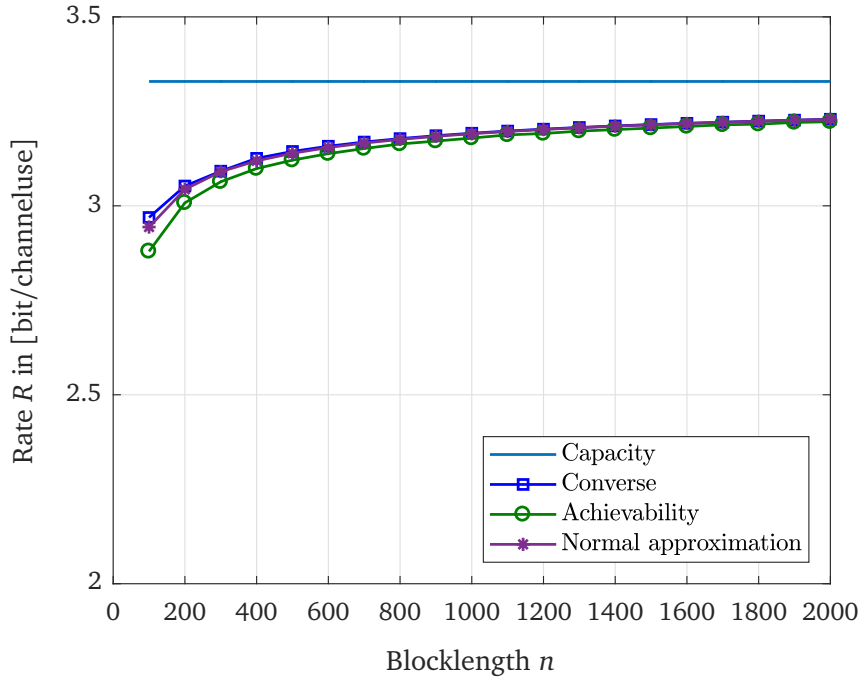
Figure 3.2: Normal approximation, converse and $\kappa\beta$ bound performances for $\epsilon = 10^{-6}$ and SNR $= 20$ dB and a transmission over the AWGN channel. Figure according to [7, Figure 13].

strong converse and the Shannon-Gallager-Berlekamp converse may be obtained as special cases of the general converse [66].

The asymptotic-regime considered in the paper of PPV shows the asymptotic analysis of upper and lower bounds (cf. Definition 3.6) [66]. In this context, a tightened normal approximation is given, which approximates both, converses and achievabilities quite well [24]. Results are shown for the Discrete Memoryless Channel (DMC) and for the Gaussian channel. One example is also depicted in Figure 3.2. The result is shown for $\epsilon = 10^{-6}$ and SNR $= 20$ dB. It can be observed, that indeed the normal approximation approximates upper and lower bound well.

Therefore, the normal approximation is taken to approximate theoretical bounds for a transmission over the THz channel. To introduce this method closer, in the following in Subchapter 3.2.1 the channel dispersion, which is one main component of the normal approximation, will be presented. Thereafter, tightened expressions for the normal approximation will be given in Subchapter 3.2.2.

3.2.1 Channel Dispersion

For channels that satisfy the strong converse (cf. Equation (3.18)), the following approximation for the achievable rate is asymptotically tight in the limit [20]

$$\frac{\log_2 W^*}{n} \approx C. \tag{3.40}$$

However, it was shown for many channels, error rates and block-length ranges of practical interest that Equation (3.40) is too optimistic [20]. There is no information about the dependency of $\log_2 W^*$ on the error probability ϵ incorporated [58]. A much tighter approximation can be obtained by incorporating the second order coding rate given by $\sqrt{V}Q^{-1}(\epsilon)$, which is the definition according to Hayashi ([19]) (cf. Equation (3.20)). It contains a parameter referred to as the channel dispersion V [20]. It measures the stochastic variability of the channel relative to a deterministic channel with the same capacity and gives a possibility to evaluate the backoff from capacity due to finite blocklength coding [7, 22]. Its definition is given in the following.

Definition 3.7. The dispersion V (measured in squared information units per channel use) of a DMC or AWGN channel with capacity C is equal to [7, 20]

$$V = \lim_{\epsilon \to 0} \limsup_{n \to \infty} \frac{1}{n} \left(\frac{nC - \log_2(W^*(n, \epsilon))}{Q^{-1}(\epsilon)} \right)^2 \tag{3.41}$$

$$= \lim_{\epsilon \to 0} \limsup_{n \to \infty} \frac{1}{n} \frac{(nC - \log_2(W^*(n, \epsilon)))^2}{2\log_2\left(\frac{1}{\epsilon}\right)}. \tag{3.42}$$

According to [58] and [23] the channel dispersion V for all memoryless channels is obtained by taking the variance of the information spectrum given by Equation (3.14), i.e.,

$$V_{\text{orig}} = \mathbb{V}_{P_{Y|X}}[i(X;Y)]. \tag{3.43}$$

In the finite blocklength regime, the average mutual information is of more interest, given by Equation (3.15) [4, 56]. To satisfy a given cost constraint, only $x^n \in \mathscr{F}^n$ should be used, where $\mathscr{F}^n$ is the feasible set of codewords according to the input cost constraint (cf. Equation (3.24)) [4]. Therefore, the channel dispersion conditioned on this sequence is given by [4]

$$V = \mathbb{V}_{P_{Y^n|X^n=x^n}}\left[\frac{1}{n}i(x^n;Y^n)\right]. \tag{3.44}$$

Dispersion for the continuous-input-continuous-output Gaussian channel

An i.i.d Gaussian input distribution does not satisfy the cost constraint given in Equation (3.24) [4]. To satisfy the cost constraint, a non-i.i.d. input distribution P_X^n that leads to a zero cost-violation probability $P_{X^n}[X^n \notin \mathscr{F}^n]$ is recommended in [4]. According to [4] the uniform distribution on the n-dimensional power shell, i.e., $\|x^n\|^2 = nP$, can be used. However, this choice induces a non-i.i.d. output distribution P_{Y^n}. This choice is also second-order optimal, i.e., it achieves the smallest dispersion possible [4]. However, it leads to the result, that Equation (3.16) does not hold and an auxiliary product output distribution has to be used to get a modified mutual information random variable according to Equation (3.17). From there, for the finite blocklength regime, the n-letter formulation according to Equation (3.15) is used. For a real Gaussian channel it is given by [4]

$$\frac{1}{n}\tilde{i}(x^n; Y^n) = \frac{1}{n}\log_2\left[\frac{(2\pi)^{-n/2}e^{-\|Y^n-x^n\|^2/(2\sigma_z^2)}}{(2\pi(1+\mathrm{SNR}))^{-n/2}e^{-\|Y^n\|^2/2(1+\mathrm{SNR})}}\right]. \tag{3.45}$$

Finally by using Equation (3.44) and by performing some calculations the channel dispersion is obtained by [4, 55]

$$\mathbb{V}_{Y^n|X^n=x^n}\left[\frac{1}{n}\tilde{i}(x^n; Y^n)\right] = \frac{V^{\mathrm{AWGN}}(\mathrm{SNR})}{n}. \tag{3.46}$$

Extensive derivations are given in [4]. In this thesis, only the main results will be shown.

For $\epsilon < 0.5$ the dispersion for the real AWGN channel for equal, maximal and average power constraints and $x^n \in \mathscr{F}^n$, for $\mathscr{F}^n = \{x^n \in \mathbb{R}^n : \|x^n\|^2 = nP\}$, is given by [4, 7, 20]

$$V_{\mathrm{real}}^{\mathrm{AWGN}}(\mathrm{SNR}) = \frac{1}{2}\frac{\mathrm{SNR}\cdot(\mathrm{SNR}+2)}{(\mathrm{SNR}+1)^2}\log_2^2 e, \tag{3.47}$$

and the dispersion for the complex AWGN channel and adjusted feasible set $\mathscr{F}^n$ is given by [4, 58]

$$V_{\mathrm{complex}}^{\mathrm{AWGN}}(\mathrm{SNR}) = \frac{\mathrm{SNR}\cdot(\mathrm{SNR}+2)}{(\mathrm{SNR}+1)^2}\log_2^2 e. \tag{3.48}$$

It should be noted, that a capacity achieving i.i.d. Gaussian input distribution does not achieve the optimal maximal achievable rate performance [4]. The optimal maximal achievable rate performance is achieved by using $\mathscr{F}^n$, which indicates the uniform distribution of x on the n-dimensional power shell [4]. An explanation therefore is that short blocklength codes should efficiently use the available power resource [4]. With an i.i.d. Gaussian input distribution, some codewords would not utilize the maximum available power budget P, which degrades the performance [4]. The dispersion for an

i.i.d. Gaussian input distribution, given by $V_{\mathrm{iid}} = \frac{\mathrm{SNR}}{1+\mathrm{SNR}} \log_2^2 e$, is therefore higher than the dispersion for a uniform distribution on the power shell [4].

Dispersion for the discrete-input-continuous-output Gaussian channel for CM

For the application of a finite constellation alphabet the input distribution is assumed to be an i.i.d. uniform distribution. For the same reasons as explained before the normalized mutual information random variable has to be taken. For CM and a blocklength n, it is given by [4, 33]

$$\frac{1}{n}\tilde{i}(x^n; Y^n) = \frac{1}{n}\sum_{t=1}^{n}\tilde{i}(x_t; Y_t) \tag{3.49}$$

$$= -\frac{1}{n}\sum_{t=1}^{n}\log_2\left(\sum_{l=1}^{M}Q_X(x(l))e^{\frac{\|Z_t\|^2-\|x_t+Z_t-x(l)\|^2}{2\sigma_z^2}}\right), \tag{3.50}$$

where the mutual information random variable is conditioned on the input sequence of length n, which fulfills the cost constrained given in Equation (3.24). By taking the variance of Equation (3.50), the channel dispersion is given by [4]

$$V^{\mathrm{CM}}(\mathrm{SNR}) := \sum_{i=1}^{M}Q_X(x(i))\mathbb{V}_Z\left[\log_2\left(\sum_{l=1}^{M}Q_X(x(l))e^{\frac{\|Z\|^2-\|x(i)+Z-x(l)\|}{2\sigma_z^2}}\right)\right]. \tag{3.51}$$

For MPSK with an i.i.d uniform input distribution as the capacity achieving input distribution, achieving the lowest dispersion, the following expression for the channel dispersion is obtained [4]

$$V_{\mathrm{PSK}}^{\mathrm{CM}}(\mathrm{SNR}) := \frac{1}{M}\sum_{i=1}^{M}\mathbb{V}_Z\left[\log_2\left(\sum_{l=1}^{M}e^{\frac{\|Z\|^2-\|x(i)+Z-x(l)\|}{2\sigma_z^2}}\right)\right]. \tag{3.52}$$

For MQAM a higher dispersion will occur. As already mentioned in Subchapter 3.2.1, it is highly complex to find the capacity achieving input distribution for MQAM [4]. Therefore, for MQAM also a uniform input distribution is assumed and the channel capacity is calculated by Equation (3.35). This is why an additional loss in coding rate
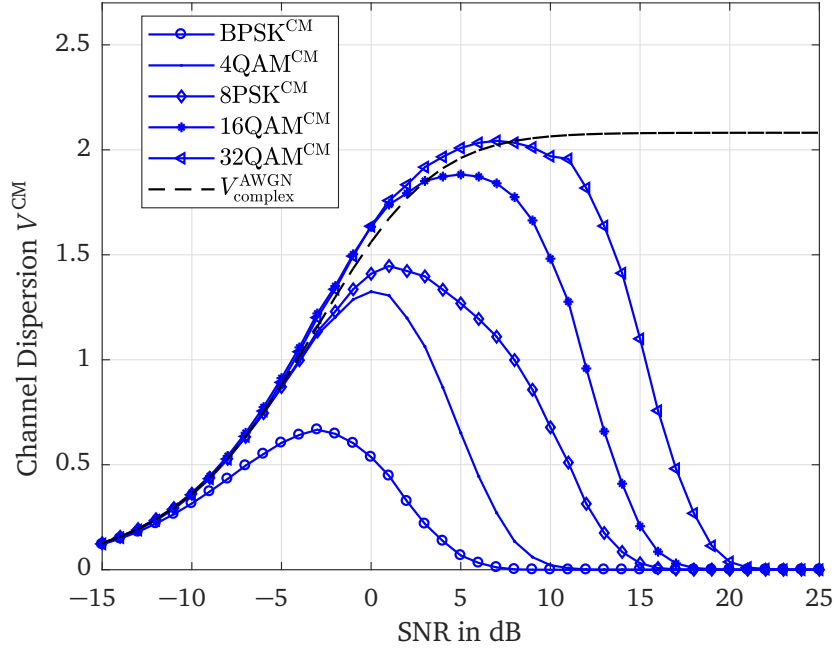
Figure 3.3: Dispersion for CM with finite constellation input alphabets over the SNR in dB compared to the dispersion caused by coding over the optimal power shell for continuous channel input. The dispersion is given in squared information units per channel use for a transmission over an AWGN channel. Figure according to [4].

incurs, which has to be accounted for by the channel dispersion. Therefore, the penalty for MQAM will be higher than the one for MPSK. Its dispersion is given by [4]

$$V_{\text{QAM}}^{\text{CM}}(\overline{\text{SNR}}) := V_{\text{PSK}}^{\text{CM}}(\overline{\text{SNR}}) + \mathbb{V}_X\left[\mathbb{E}\left[\log_2\left(\sum_{l=1}^{M} e^{\frac{\|\bar{z}\|^2 - \|x(i) + \bar{Z} - x(l)\|}{2\sigma_{\bar{z}}^2}}\right)\bigg|X\right]\right] \tag{3.53}$$

$$= \frac{1}{M}\sum_{i=1}^{M}\mathbb{E}_{\bar{Z}}\left[\left\{\log_2\left(\sum_{l=1}^{M} e^{\frac{\|\bar{z}\|^2 - \|x(i) + \bar{Z} - x(l)\|}{2\sigma_{\bar{z}}^2}}\right)\right\}^2\right] - \tag{3.54}$$

$$\left\{\frac{1}{M}\sum_{i=1}^{M}\mathbb{E}_{\bar{Z}}\left[\log_2\left(\sum_{l=1}^{M} e^{\frac{\|\bar{z}\|^2 - \|x(i) + \bar{Z} - x(l)\|}{2\sigma_{\bar{z}}^2}}\right)\right]\right\}^2. \tag{3.55}$$

The channel dispersion for MQAM considers $\overline{\text{SNR}} = \text{SNR} - \delta$ for $\delta > 0$, because of the same constraint-violation probability reasons as considered for capacity calculation in Equation (3.35). Accordingly, the corresponding noise random variable $\overline{Z}$ and noise variance $\sigma_{\bar{z}}^2$ have to be taken.

The channel dispersion for CM and finite constellation input alphabets for a transmission over a Gaussian channel is depicted in Figure 3.3. The results for 16QAM and for the continuous Gaussian input case verify the findings in [4, Figure 4.1]. If the continuous

Gaussian channel input is changed to discrete constellations, the following development can be observed. For very low SNR until $-5\,\mathrm{dB}$ the dispersion is not affected by constraining the channel input to discrete constellations [4]. However, for an SNR between $-5\,\mathrm{dB}$ and $7\,\mathrm{dB}$ for 16QAM and 32QAM the channel dispersion gets slightly larger. At high SNR for the use of discrete constellation the channel dispersion converges to zero, i.e., at high SNR there is no penalty induced by the application of finite blocklength coding and also uncoded modulation appears to be optimal [4].

Analogously to the the results in [4], the channel dispersion for BICM will be derived in the following.

Dispersion for the discrete-input-continuous-output Gaussian channel for BICM

According to Equation (3.37) and Equation (3.36), which show the capacity calculation for BICM, it can be inferred with the help of Equation (3.8), which shows the analogy to the calculation of the mutual information, that the mutual information random variable for BICM is of the form

$$i_{\mathrm{BICM}}(X,Y) = \log_2\left(\frac{\sum\limits_{x'\in\mathscr{X}_b^j}\exp(-|X-x'-Z|^2)}{\frac{1}{2}\sum\limits_{x'\in\mathscr{X}}\exp(-|X-x'-Z|^2)}\right). \tag{3.56}$$

Now, by using Equation (3.43), which indicates the calculation of the channel dispersion, and a channel input conditioned on input values, which satisfy the cost constraint, the dispersion for BICM is the sum of the individual dispersions given in each subchannel k, described by

$$V^{\mathrm{BICM}} = \sum_{j=1}^{k}\mathbb{V}[i(b_j,Y)], \tag{3.57}$$

with b_j being a realization of the random input variable B_j for the jth input channel. By the application of simplifications given in [65] the expression for $M\mathrm{PSK}$ is given by

$$V_{\mathrm{PSK}}^{\mathrm{BICM}} = \sum_{j=1}^{k}\frac{1}{M}\sum_{\substack{i=1\\x\in\mathscr{X}}}^{M}\mathbb{V}_Z\left[\log_2\left(\sum_{\substack{l=1\\x'\in\mathscr{X}}}^{M}e^{\frac{\|Z\|^2-\|x(i)+Z-x'(l)\|}{2\sigma_z^2}}\right)-\log_2\left(\sum_{\substack{l=1\\x'\in\mathscr{X}_b^j}}^{M}e^{\frac{\|Z\|^2-\|x(i)+Z-x'(l)\|}{2\sigma_z^2}}\right)\right]. \tag{3.58}$$
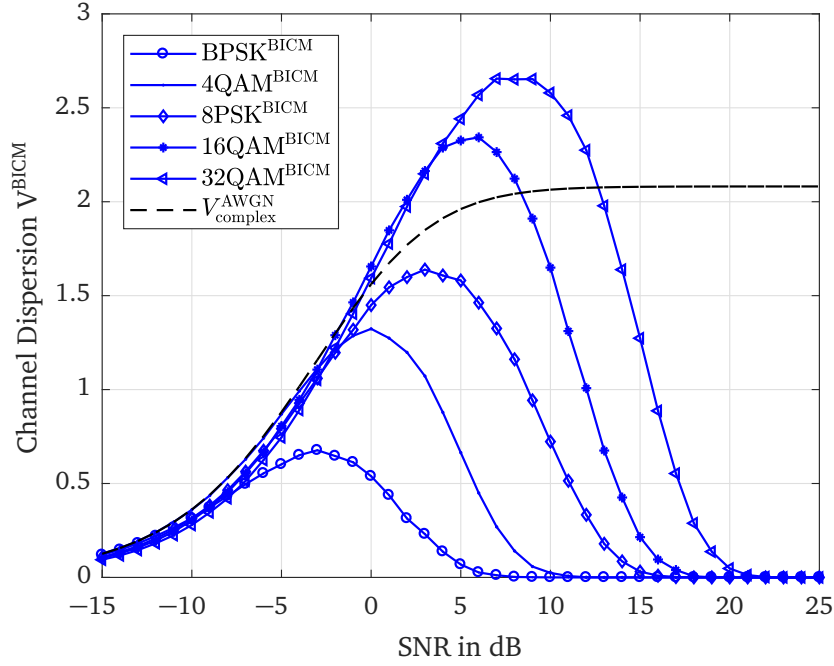
Figure 3.4: Dispersion for BICM with finite constellation input alphabets over the SNR in dB compared to the dispersion caused by coding over the optimal power shell for continuous channel input. The dispersion is given in squared information units per channeluse for a transmission over an AWGN channel.

The variance is taken over all signal constellation points in $\mathcal{X}_b^j$, over the bits b and noise Z. Accordingly, for MQAM following the explanation given for the CM case, the dispersion is obtained by

$$V_{\mathrm{QAM}}^{\mathrm{BICM}}(\overline{\mathrm{SNR}}) := V_{\mathrm{PSK}}^{\mathrm{BICM}}(\overline{\mathrm{SNR}}) + \mathbb{V}_X \Bigg[\mathbb{E} \Bigg[\log_2 \Bigg(\sum_{\substack{l=1 \\ x' \in \mathcal{X}}}^{M} e^{\frac{\|\bar{z}\|^2 - \|x(i) + \bar{z} - x'(l)\|}{2\sigma_{\bar{z}}^2}} \Bigg) \tag{3.59}$$

$$- \log_2 \Bigg(\sum_{\substack{l=1 \\ x' \in \mathcal{X}_b^j}}^{M} e^{\frac{\|\bar{z}\|^2 - \|x(i) + \bar{z} - x'(l)\|}{2\sigma_{\bar{z}}^2}} \Bigg) \Bigg| X \Bigg] \Bigg], \tag{3.60}$$

for $\overline{\mathrm{SNR}} = \mathrm{SNR} - \delta$ and $\delta > 0$, for the same assumptions and reasons as given for Equation (3.35).

The behavior of the channel dispersion for BICM is shown in Figure 3.4. It can be compared to the channel dispersion of CM given in Figure 3.3. For discrete constellations with low cardinality, i.e., BPSK and 4QAM there is no difference between the dispersion of CM and BICM. An explanation therefore is, that for these constellations interleaving

does not cause an additional dispersion because the number of parallel channels k is low and therefore the overall transmission system behaves like a CM scheme. However, there is a difference for the remaining discrete constellations. For low SNR until $-1\,\mathrm{dB}$ the dispersion is lower than for CM. On the other side it is larger for higher SNR. The more parallel channels are assumed, the higher the dispersion becomes in comparison to the results displayed in Figure 3.3. Like for CM, the dispersion converges to zero for very high SNR, indicating the SNR value from which uncoded modulation is also optimal.

3.2.2 Normal Approximation

The normal approximation given by Equation (3.20) can be expressed in a more precise way by using a second order approximation. For a transmission over DMC and Gaussian channels the second order approximation of the normal approximation is obtained by [7, 8, 19, 58]

$$\log_2 W^*(n, \epsilon) = nC - \sqrt{nV}Q^{-1}(\epsilon) + \mathcal{O}(\log_2 n). \tag{3.61}$$

The normal approximation is a function of high generality. For each channel model, the related dispersion V and capacity C have to be used to obtain the channel specific $\log_2 W^*(n, \epsilon)$. Moreover, Equation (3.61) can easily be reformulated to calculate the maximum achievable coding rate $R^*(n, \epsilon)$. Its definition is given in the following.

Definition 3.8. The maximum coding rate is the largest rate among all codes with blocklength n and error probability ϵ [7]. The maximum coding rate is given by the second order approximation, neglecting the third term of the following expression [7]

$$R^*(n, \epsilon) = C - \sqrt{\frac{V}{n}}Q^{-1}(\epsilon) + \mathcal{O}\left(\frac{\log_2 n}{n}\right). \tag{3.62}$$

For an average power constraint the third order approximation is known to be the following expression without the forth term [7]

$$R^*(n, \epsilon) = C - \sqrt{\frac{V}{n}}Q^{-1}(\epsilon) + \frac{3\log_2 n}{2n} + \mathcal{O}(1). \tag{3.63}$$

For equal-power and maximal-power it is given by leaving the forth term in the following expression [7]

$$R^*(n, \epsilon) = C - \sqrt{\frac{V}{n}}Q^{-1}(\epsilon) + \frac{\log_2(n)}{2n} + \mathcal{O}(1). \tag{3.64}$$

For small error probabilities $\epsilon \leq 0.5$ the second term is negative and causes a rate penalty or backoff from channel capacity due to the use of finite blocklength codes [4].

One of the main advantages of knowing the channel dispersion and applying the normal approximation is, that the minimal blocklength n^* required to achieve a given fraction η of capacity with a given error probability ϵ can easily be approximated by [7]

$$n^* \gtrsim \left(\frac{Q^{-1}(\epsilon)}{1 - \eta} \right)^2 \frac{V}{C^2}, \tag{3.65}$$

where $\frac{V}{C^2}$ is referred to as the coding horizon. It is a relevant quantity to characterize the necessary blocklength for achieving a certain fraction of the channel capacity [4, 7]. The larger the noise variance gets, the higher the coding horizon becomes. Therefore, the lower the SNR becomes, the larger blocklength is needed [7]. The explanation for this behavior is intuitive. To achieve a fraction of a low-capacity link it is necessary to code over a large blocklength, i.e., the delay to achieve a fraction η of the capacity becomes higher [7]. The development of the coding horizon over the SNR is depicted in Figure 3.5. The coding horizon for a continuous channel input is shown in black with circle markers. The performance for CM and higher order modulations is indicated by solid lines, while the performance for a BICM scheme is given in dashed lines. Additionally, those cases are indicated by the superscripts 'BICM' and 'CM'. For large noise values a high coding
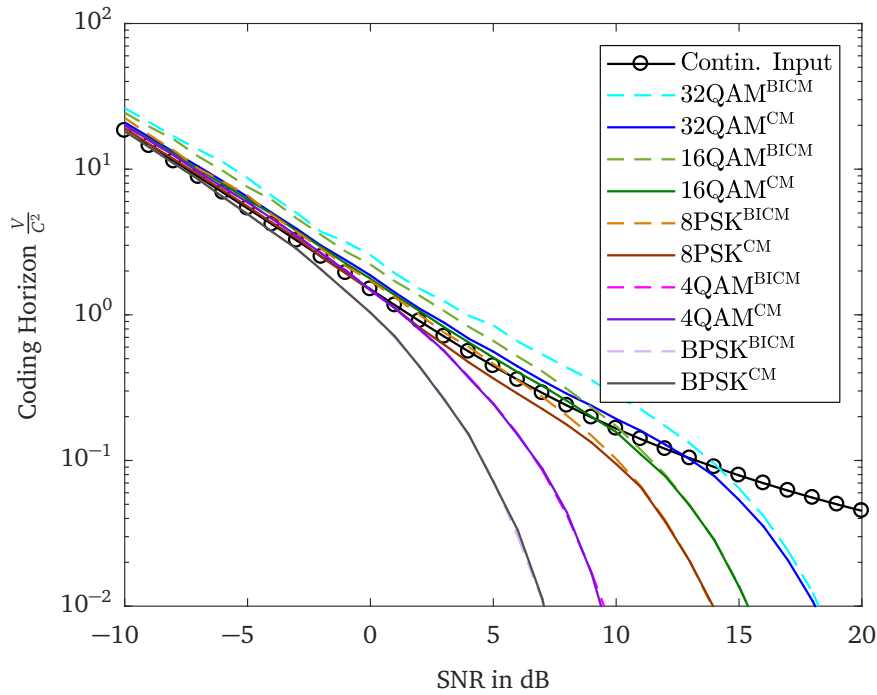
Figure 3.5: Coding horizon over the SNR for CM shown by solid lines and for BICM indicated by dashed lines. As a reference, the coding horizon for continuous channel input is shown in black with circle markers. Figure according to [4, Figure 4.4].

horizon is required. The higher the SNR becomes, the lower its value gets. For discrete channel input, the coding horizon decays quickly, as uncoded modulation becomes optimal for high SNR. The performance of BICM is worse for the three largest higher order modulations than the one of CM because as was already mentioned, its capacity is slightly lower (cf. Figure 2.2) and the dispersion higher (cf. Figure 3.4). For high SNR the performance converges to the same value. The performance is equally good for 4QAM and BPSK as there are no deviations for capacity (cf. Figure 2.2) or dispersion (cf. Figure 3.4).

Equation (3.65) provides a tight answer to the question asked in the beginning of Chapter 3:

What is the minimum blocklength n^*, which sustains a desired error probability ϵ and guarantees to achieve a fraction η of the channel capacity [55]?

Chapter 4

Evaluation and Analysis of a Single Carrier System

In this chapter, the theoretical bounds for the maximum achievable rate, derived for BICM in Chapter 3 for a transmission over the AWGN channel are established. Furthermore, they are compared to the simulation results obtained for a transmission over the equalized THz channel. For simulation the Single Carrier (SC) system introduced in Chapter 2.2 is taken.

This chapter is organized as follows. First, in Subchapter 4.1 the calculated theoretical bounds for the maximum achievable rate for all modulation schemes of interest are shown and the impact of various parameters on the performance is analyzed. Secondly, in Subchapter 4.2 the simulation results are shown and compared with these calculated theoretical bounds.

4.1 Calculation of Bounds for Maximum Achievable Rates

The theoretical calculations follow the concept in [4]. Therefore an average probability of error (cf. Equation (3.2)) and an average per code word power constraint (cf. Equation (3.24)) are assumed. The bounds for the maximum achievable rate are obtained by using the third order approximation given in Equation (3.64) [7].

The rest of this Subchapter is organized as follows. In Subchapter 4.1.1 the theoretical bounds for a BICM system, considering a transmission over the AWGN channel, are introduced and compared to the CM performance. Next, in Subchapter 4.1.2 the effects of various parameters on these bounds will be analyzed. For all following sample Figures the parameters $\text{SNR} = 20\,\text{dB}$, $n = 100$ and $\epsilon = 10^{-3}$ are assumed unless otherwise stated.

4.1.1 Transmission over the AWGN Channel

As an SC system with MMSE-LE is assumed for simulation, the equivalent channel model, shown in Figure 2.8 has an $\text{SNR}_{\text{MMSE-LE}}$ given by Equation (2.6). Its performance should be compared to the bounds obtained for an AWGN channel with the same overall SNR. Therefore, to calculate the maximum achievable rate by using the normal approximation Equation (3.64) operates with the obtained $\text{SNR}_{\text{MMSE-LE}}$ value, which is smaller than the input SNR_{in} of the transmission system (cf. Figure 2.7). For the calculation of the channel capacity Equation (3.34) and Equation (3.35) are taken for CM, whereas Equation (3.38) and Equation (3.39) are used for a transmission over a BICM system. The dispersion is obtained by taking Equation (3.52) and Equation (3.53) for CM, while Equation (3.58) and Equation (3.59) are used for BICM. Transmission is assumed over the AWGN channel.

The results for both transmission systems are shown in Figure 4.1. The maximum achievable rate is given over the SNR. The solid lines show the performance for CM, while the dashed lines indicate the theoretical bounds for BICM. Additionally, both cases are indicated by superscripts 'BICM' and 'CM'. Only the performance for 16QAM, 32QAM
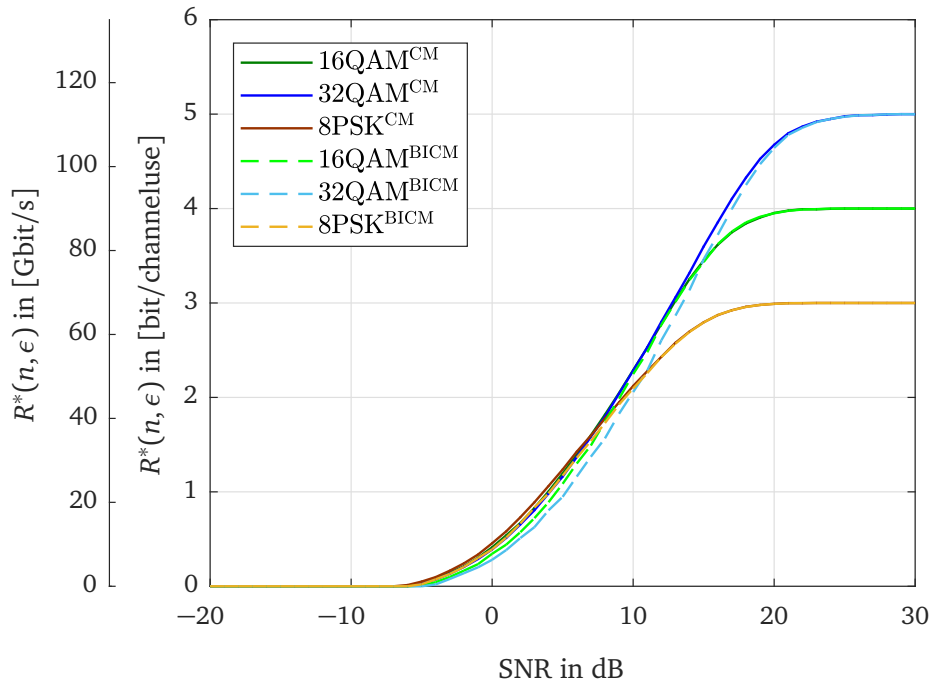
Figure 4.1: Theoretical bounds for CM compared to the theoretical bounds of BICM. Assumed paramters: $\text{SNR} = 20\,\text{dB}$, $n = 100$, $\epsilon = 10^{-3}$ and channel model: AWGN.
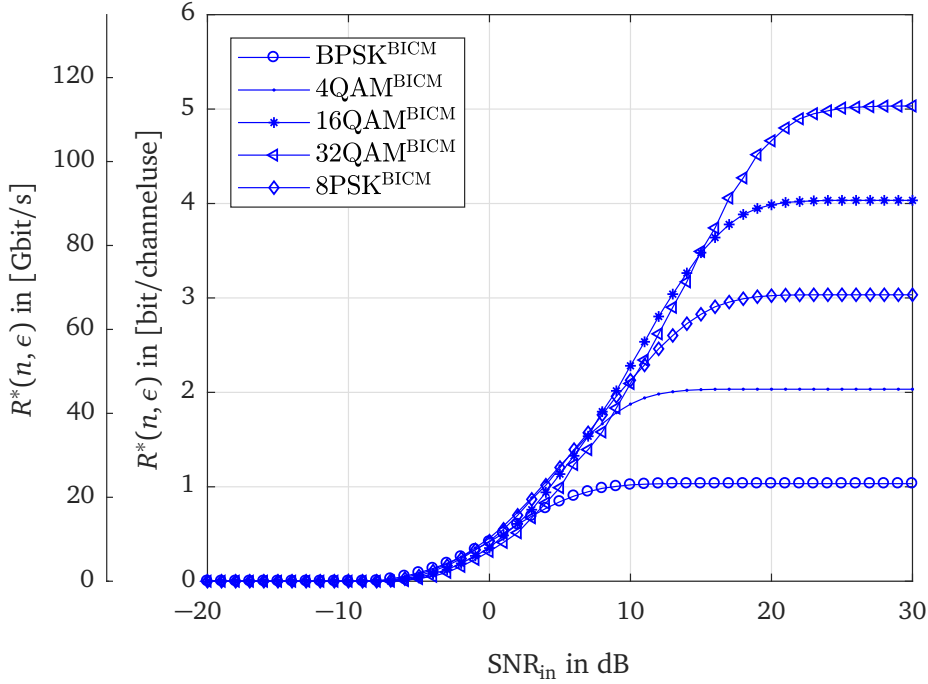
Figure 4.2: Theoretical bounds for a transmission over a BICM system and for all higher order modulations assumed in this thesis. Assumed parameters: $n = 100$, $\epsilon = 10^{-3}$ and channel model: AWGN.

and 8PSK is shown, since the performance for BPSK and 4QAM coincide for BICM and CM. One explanation therefore could be the low impact of interleaving on bits contained in symbols of such small constellations. However, this explanation cannot be applied for modulations of higher constellation sizes. As was already indicated in Figure 2.2, the capacity of BICM is lower for higher order modulations than for CM. Moreover, the channel dispersion for BICM for low to moderate SNR, shown in Figure 3.4, is higher than the channel dispersion for CM shown in Figure 3.3. These are all parameters, which influence the maximum achievable rate given by Equation (3.64). Therefore, for low to moderate SNR the deviation of the maximum achievable rate for BICM from CM is reasonable. For high SNR the maximum achievable rates of both coincides, because the dispersion approaches zero (cf. Figure 3.3 and Figure 3.4) and the maximal achievable rate achieves the channel capacity for discrete input with $\approx \log_2(M)$ in the limit. The result will be slightly higher, as the third term in Equation 3.64 does also influence the maximum achievable rate.

Figure 4.1 (and also further following Figures) additionally shows, the transmission rate in [Gbit/s]

$$R^*(n, \epsilon) \text{ in } [\text{Gbit/s}] = \frac{R^*(n, \epsilon) \text{ in } [\text{bit/channeluse}]}{10^9 \cdot T \text{ in } [s]},$$

with the symbol duration T taken from Table 2.1. According to Figure 4.1, a maximum transmission rate of about 110 Gbit/s can theoretically be achieved. This is a transmission rate recently achieved by hardware realizations, reported for instance in [18].

The finally obtained theoretical bounds for a transmission over the AWGN channel by using BICM with all higher order modulations considered in this thesis are demonstrated in Figure 4.2. They can be adjusted to each blocklength, SNR and error probability of interest and used to find the optimum modulation scheme achieving the maximum rate. An example is shown in Figure 4.3, where the same room scenario as in Chapter 2.1 is assumed (cf. Figure 2.1). To obtain the maximum achievable rate the $\text{SNR}_{\text{MMSE-LE}}$ after equalization of each depicted subband was taken by the normal approximation. The recommended higher order modulations for each Rx position in the room are indicated by
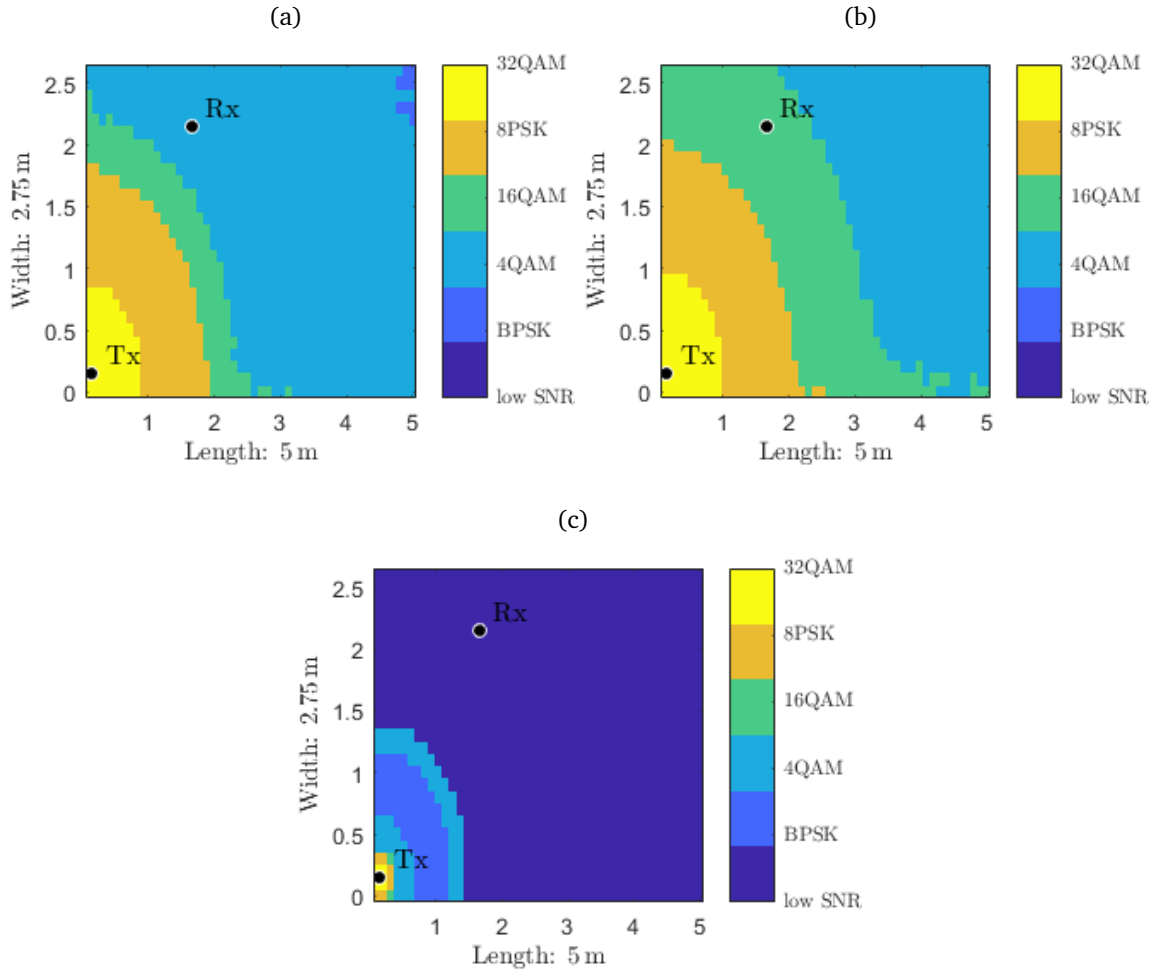
Figure 4.3: Recommended modulation schemes to achieve the theoretically highest rate for
(a) the first subband, $n = 100$ and $\epsilon = 10^{-3}$
(b) the first subband, $n = 1900$ and $\epsilon = 10^{-3}$
(c) the 32th subband, $n = 100$ and $\epsilon = 10^{-3}$.

different colors. Additionally, the considered Rx-Tx position is shown. Recommendations are given for the results obtained for the first subband and $n = 100$ (cf. Figure 4.3 (a)) and for the first subband and $n = 1900$ (cf. Figure 4.3 (b)). For the assumed Rx-Tx position in the first case 4QAM should be used to achieve the highest rate, while in the latter case 16QAM is recommended. A higher blocklength n can guarantee a more robust transmission as more error correction can be performed. Therefore, modulations with larger constellation sizes are recommended for higher n compared to transmissions with low n. Another effect is, that the higher the SNR gets, the more throughput can be achieved by using larger constellation sizes. The lower the SNR becomes, the more difficult the transmission gets. For a very low SNR $< -10\,\mathrm{dB}$ the recommendations become unreliable and the achievable rate gets very low. Therefore, no recommendation is possible in this case, which is indicated by a dark blue color. An example therefore is given in Figure 4.3 (c), where transmission over the critical 32nd subband of the THz channel is assumed. In the area between 0 and $-5\,\mathrm{dB}$ the recommendation becomes also slightly unreliable. This is why after a BPSK recommendation, in a distance of about $1.5\,\mathrm{m}$ from the Tx there is a recommendation for 4QAM again, due to numerical issues.

4.1.2 Parameter Analysis

In the following the performance of the normal approximation used to calculate the bounds for the maximum achievable rate is analyzed for various parameter settings.

In Figure 4.4 the effect of the blocklength n on the bounds is shown. The result for $n = 100$ is indicated by green dashed lines with markers and the superscript '100', while the result for $n = 1900$ is shown in solid blue lines with markers and the superscript '1900'. As can be seen, the maximum achievable rate increases for higher blocklength and small to moderate SNR. The reason therefore is, that more error correction can be performed by using larger blocklength and therefore, more useful throughput can be achieved. For high $\mathrm{SNR_{in}}$ due to the vanishing channel dispersion both approach the limit of the channel capacity for discrete channel input being $\approx \log_2(M)$ (cf. Subchapter 4.1.1).

Figure 4.5 illustrates the effect of a low error probability compared to a higher error probability. Solid blue lines with markers indicate the result for $\epsilon = 10^{-6}$, while green dashed lines with markers show the result for $\epsilon = 10^{-3}$. Additionally, this is indicated by the superscripts '10^{-6}' and '10^{-3}'. The lower the error probability is assumed, the harder it gets to achieve a certain maximal rate and the lower the maximum achievable rate becomes for low to moderate $\mathrm{SNR_{in}}$ values. For high $\mathrm{SNR_{in}}$ due to the vanishing channel dispersion the limit of the channel capacity for discrete channel input being $\approx \log_2(M)$ is achieved in both cases (cf. Subchapter 4.1.1).

Another interesting point is the influence of the third term of the third order approximation used to approximate the normal approximation given in Equation (3.64). In Figure 4.6 the theoretical performance is shown for $n = 100$. Solid blue lines with marker indicate the normal approximation given by Equation (3.64) considering the third term, while green dashed lines with marker illustrate the normal apprximation not considering the third term. Furthermore, the latter case is indicated by an additional apostrophe in the figure legend. The expression without the third term is equal to the second order approximation of the normal approximation given by Equation (3.62). It can be observed that if the third term is considered, also capacities over the limit of the maximum achievable rate given by $\log_2(M)$ can be achieved. However, this case is only true for non-zero error probability. The impact of the third term gets lower, the higher the blocklength becomes. This can be seen by comparing Figure 4.6 to Figure 4.7, where the same circumstance is demonstrated for a blocklength of $n = 1900$. In Figure 4.7 the third term barely influence the maximum achievable rate, as the blocklength is already very high. Therefore, the performance becomes similar for the second order approximation and the third order approximation
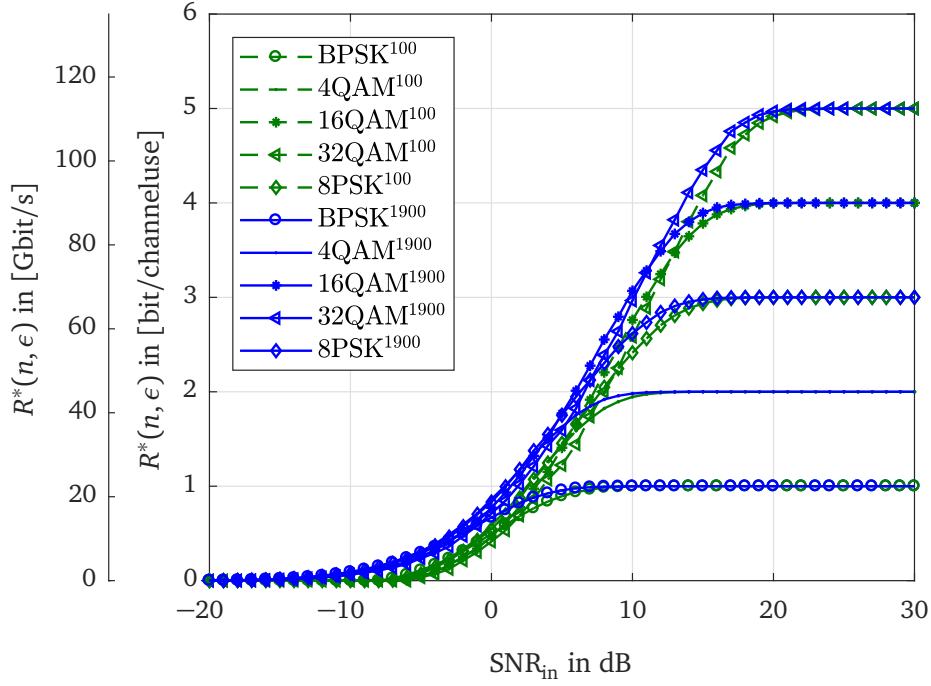
Figure 4.4: Theoretical bounds for BICM for green: $n = 100$ and blue: $n = 1900$. Assumed error probability: $\epsilon = 10^{-3}$ and channel model: AWGN.
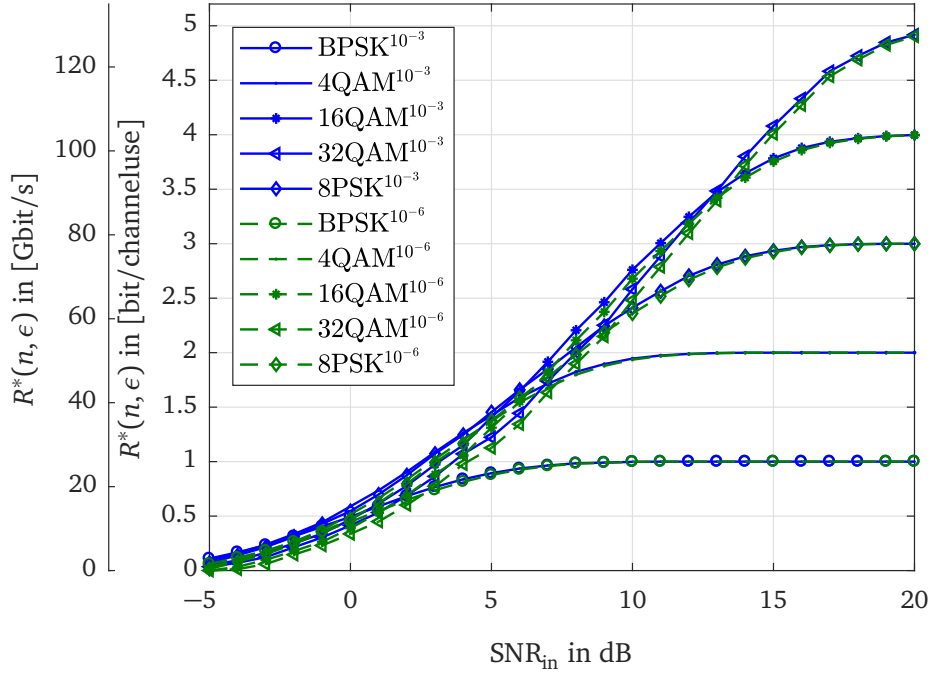

Figure 4.5: Theoretical bounds for BICM for green: $\epsilon = 10^{-6}$ and blue: $\epsilon = 10^{-3}$. Assumed error probability: dB, $n = 100$ and channel model: AWGN.
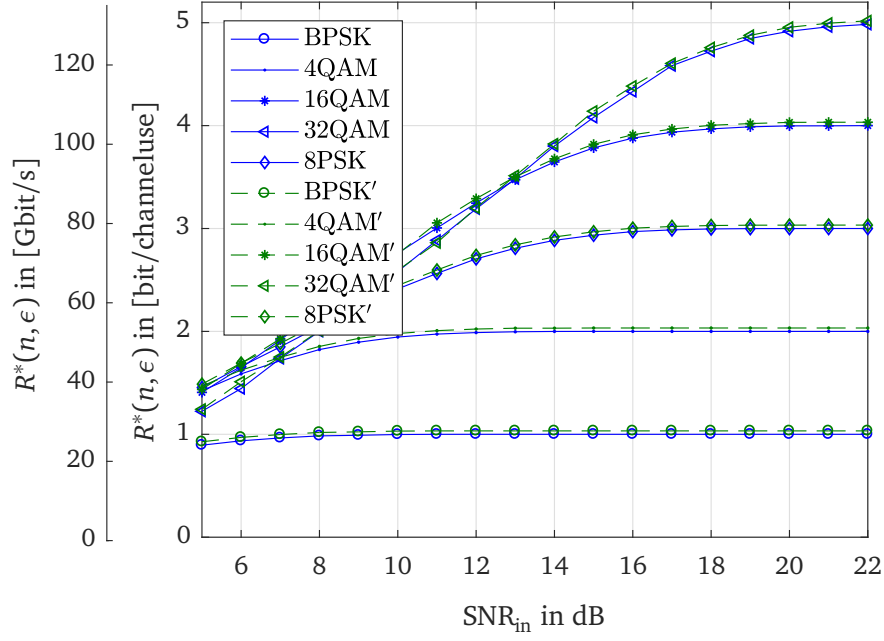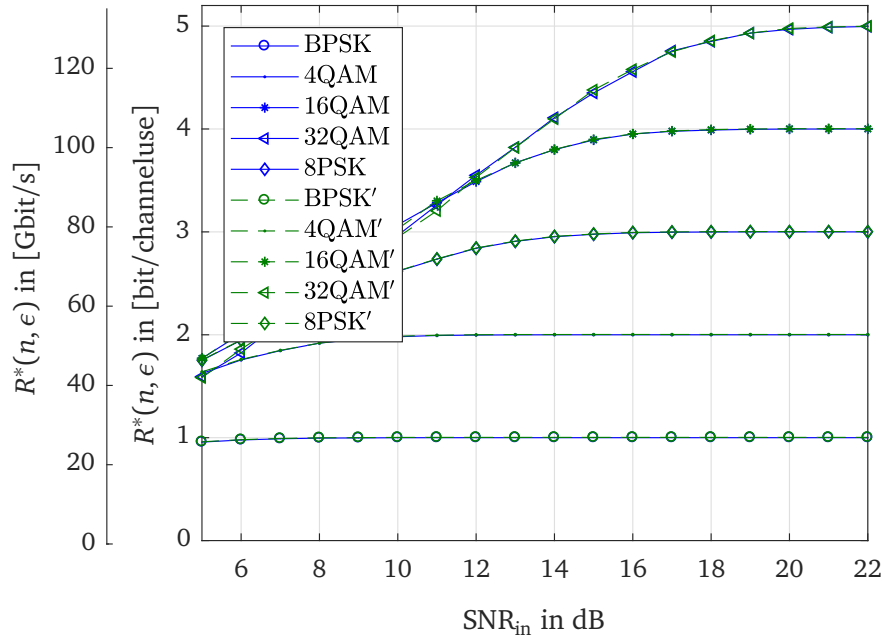
Figure 4.6: Theoretical bounds for BICM for green: with third term of third order approximation and blue: without third term of third order approximation. Assumed parameters: $n = 100$, $\epsilon = 10^{-3}$ and channel model: AWGN.
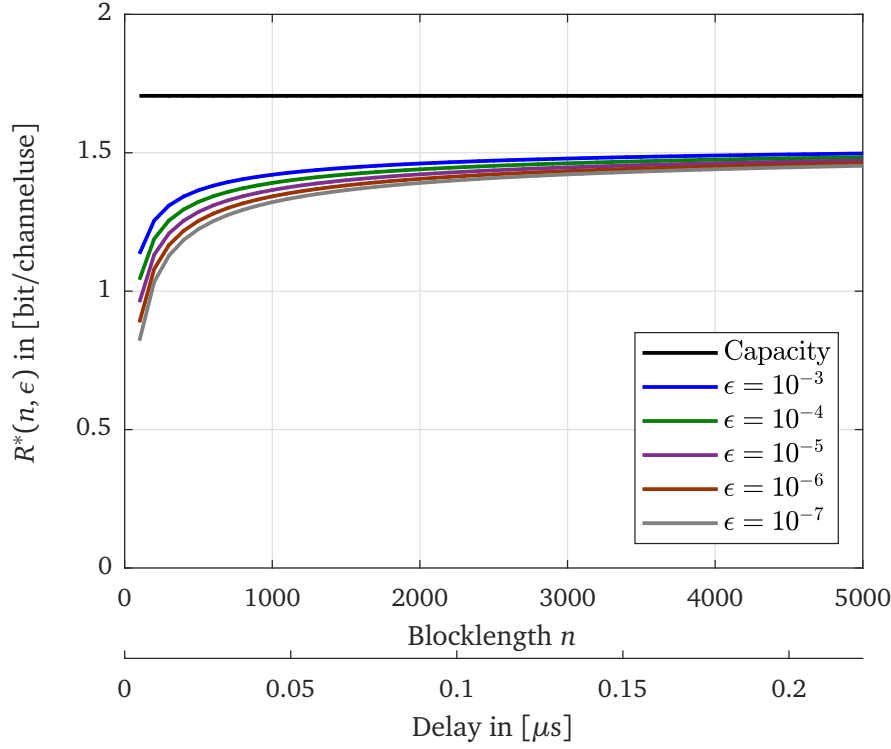

Figure 4.7: Theoretical bounds for BICM for green: with third term of third order approximation and blue: without third term of third order approximation. Assumed parameters: $n = 1900$, $\epsilon = 10^{-3}$ and channel model: AWGN.

Figure 4.8: Theoretical bounds for SNR $= 16$ dB and 16 QAM transmission. The maximum achievable rate is shown over the blocklength. The result is obtained for various values of ϵ. A transmission over the AWGN channel is assumed. Additionally, the delay in [μs] is shown, which is obtained by a transmission over the first subband of the THz channel.

4.2 Analysis of Simulation Results

After the development of the bounds for the maximum achievable rate was explained and after the influence of certain parameters was clarified, the simulation results can be analyzed and compared to the obtained theoretical results.

It was proven that the theoretically obtained $SNR_{MMSE-LE}$ (cf. Equation (2.6)) has only a deviation of about 10^{-3} from the simulative obtained $SNR_{MMSE-LE}^{sim}$ (cf. Equation (2.9)). This confirms the correctness and accordance of theory and simulation for the equalization part. The simulation performance is tested with and without interleaver. Firstly, results are obtained for a transmission over the equalized THz channel showing colored noise. Secondly, they are analyzed for a transmission over the AWGN channel. Both cases are analyzed for the same SNR_{in}. Furthermore, performances for hard-decision decoding and soft-decision decoding are compared.

One aim of this thesis was to analyze short delay transmission. By using THz transmission with a symbol duration of 0.04 ns given in Table 2.1, this can indeed be achieved. In Figure 4.8 the maximum achievable rates over the blocklength for 5 dB SNR and

16QAM transmission for different values of error probability ϵ are shown. The results are indicated by solid colored lines, while the channel capacity is shown as a reference in black. Additionally, the delay in [μs] is shown. It is obtained by $n \cdot T$. It can be observed that even for large blocklengths, the delay is in the order of a few [μs]. Therefore, a low delay transmission can be guaranteed.

This Subchapter is organized as follows. In Subchapter 4.2.1 each theoretically obtained bound for the maximum achievable rate is compared to the achievable rate achieved by simulation. Thereafter, in Subchapter 4.2.2 the final overall performance assuming all theoretical and simulated results is analyzed.

4.2.1 Performance of Higher Order Modulations

The following Figures 4.9 - 4.13 illustrate the simulation results by circles and their bounds by blue solid lines with different markers for a transmission with BPSK, 4QAM, 8PSK, 16QAM and 32QAM. For each case, the performance for a transmission over the equalized THz channel is show in (a) and a transmission over an AWGN channel is shown in (b). In each figure the maximum achievable rate $R^*(n, \epsilon)$ over the $\mathrm{SNR_{in}}$ is given. Additionally, the applied coding rate R_c for each simulation result is stated. The results are depicted for hard-decision decoding (small black filled circles), soft-decision decoding with interleaver (big black filled circles) and soft-decision decoding without interleaver (big black empty circles). Soft decision with interleaver is indicated by the superscript 'interleaver'.

One overall result is, that soft-decision decoding is always better than hard-decision decoding, as was expected based on the theoretical background stated in Chapter 2. Therefore, soft-decision decoding is preferred. Moreover, it can be observed that the deviation for all coding rates from the theoretical bounds becomes slightly larger the higher the SNR becomes. Furthermore, the effect of having an interleaver is almost negligible. For 4QAM and BPSK the simulation results for soft-decision decoding without interleaver coincide with the results for soft-decision decoding with interleaver (cf. Figure 4.9 (a) and Figure 4.10 (a)). For the other modulations with higher constellation size, the results show small irregular deviations, indicating numerical artifacts (cf. Figure 4.11 (a), Figure 4.12 (a) and Figure 4.13 (a)). One explanation for this behavior is given in the following. For simulations the equivalent channel model with colored noise according to Figure 2.8 is used. The interleaver size is as large as the blocklength, i.e., $n = 100$, which is short for perfectly resolving the colored noise. This might be one reason why the effect of having an interleaver is almost negligible. Furthermore, none of the modulation schemes achieves capacity. The results for a transmission over the AWGN channel shows the transmission case without colored noise. They are very closer to the theoretically

obtained bounds for the AWGN channel (cf. Figures 4.9 - 4.13 (b)). Therefore, these results confirm the correctness of the developed bounds for the AWGN channel. The loss that occurs for the simulation over the first subband of the THz channel is due to colored noise, and the fact that the interleaver size is to short.

For BPSK and 4QAM, assuming a transmission over the equalized THz channel and soft-decision decoding, the largest deviation from the obtained bound is about $2\,$dB for a code rate of $R_c = 0.88$ (cf. Figure 4.9 (a) and Figure 4.10 (a)).

The higher the constellation size of the modulation gets, the larger the deviation from the theoretical bound becomes. For 8PSK and for 16QAM, assuming a transmission over the equalized THz channel and soft-decision decoding, the largest deviation from the theoretical bound is about $2.5\,$dB for a code rate of $R_c = 0.88$ (cf. Figure 4.11 (a) and Figure 4.12 (a)).

The highest deviation from the theoretical bounds occurs for 32QAM transmission over the equalized THz channel assuming soft-decision decoding (cf. Figure 4.13 (a)). The deviation is about $3.3\,$dB for a code rate of $R_c = 0.88$.
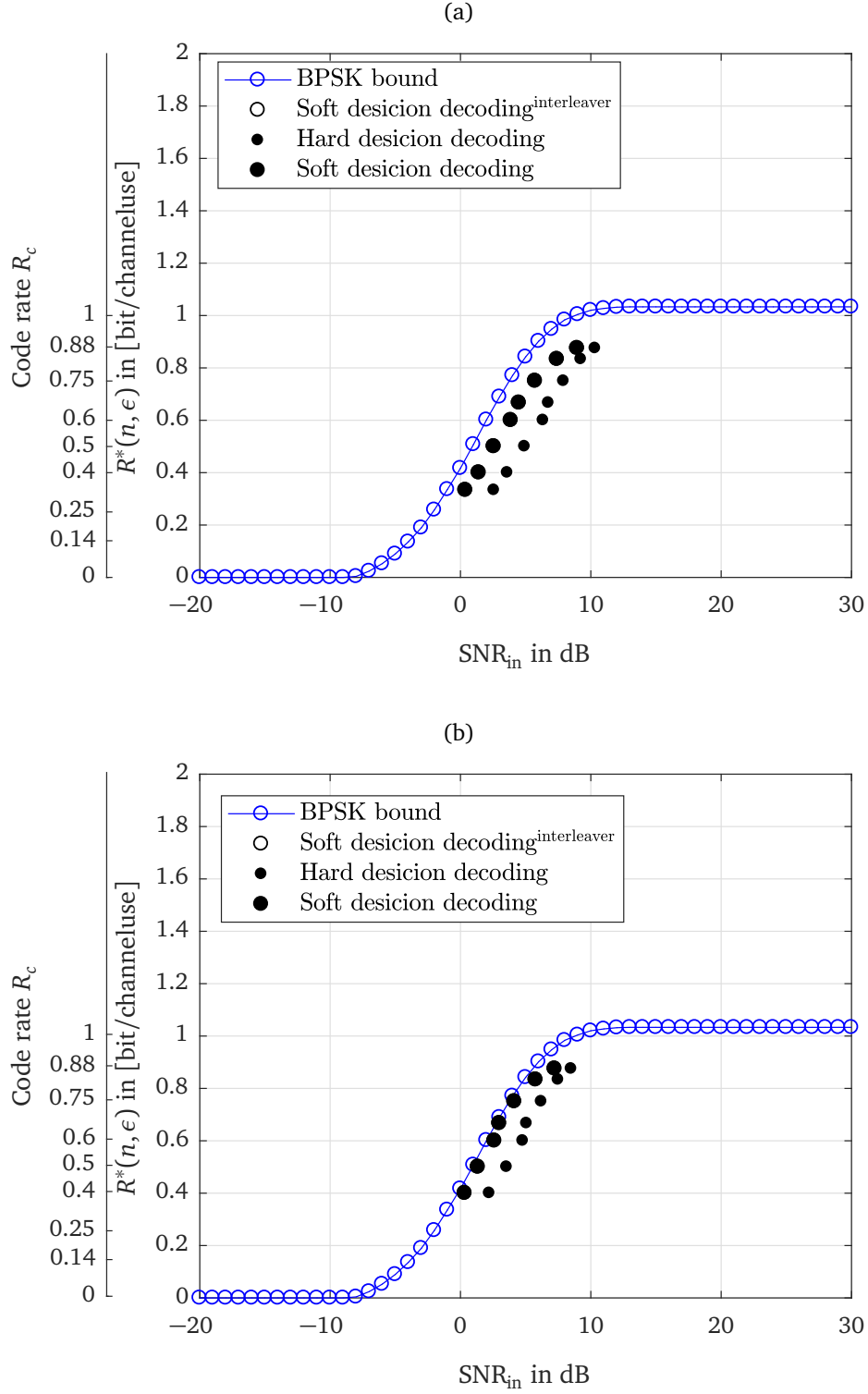
(a)

(b)

Figure 4.9: Simulation results for a transmission with BPSK compared to its theoretical bound. Simulation results are shown by circles, the bound is shown in blue. Assumed parameters for theoretical bound: $\epsilon = 10^{-3}$, $n = 100$ and for the simulations: channel model: (a) THz, first subband and (b) AWGN channel.
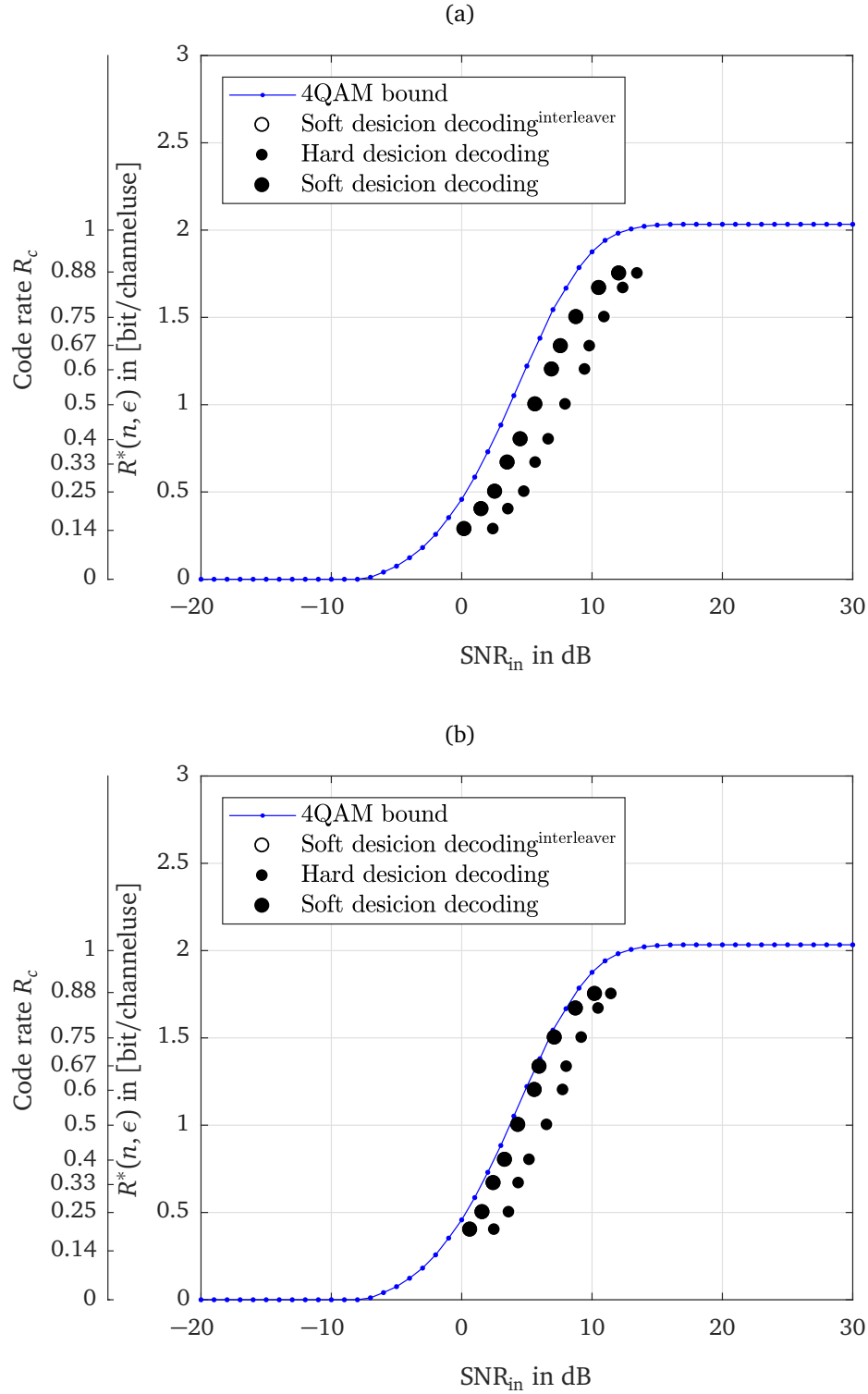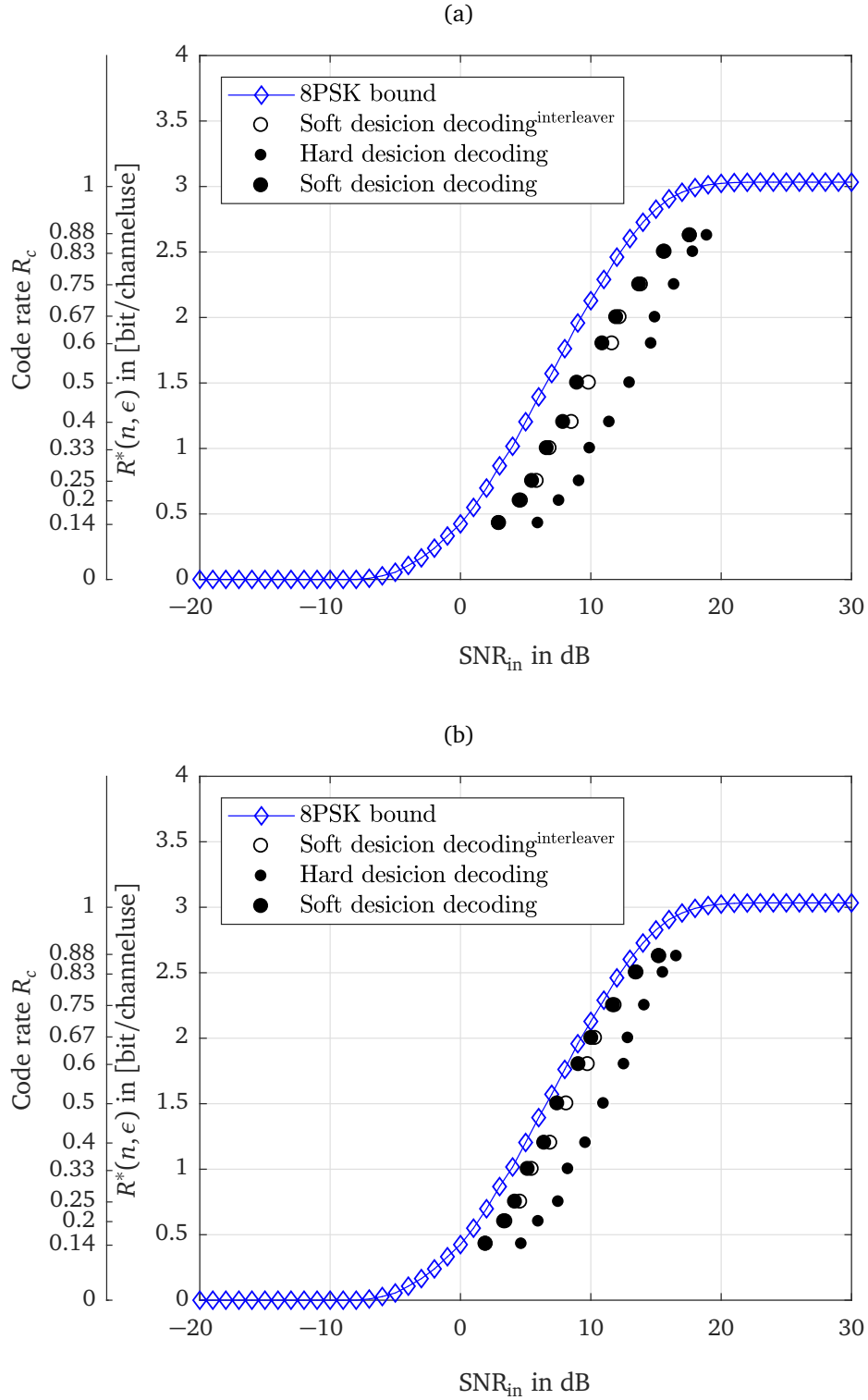
Figure 4.10: Simulation results for a transmission with 4QAM compared to its theoretical bound. Simulation results are shown by circles, the bound is shown in blue. Assumed parameters for theoretical bound: $\epsilon = 10^{-3}$, $n = 100$ and for the simulations: channel model: (a) THz, first subband and (b) AWGN channel.

Figure 4.11: Simulation results for a transmission with 8PSK compared to its theoretical bound. Simulation results are shown by circles, the bound is shown in blue. Assumed parameters for theoretical bound: $\epsilon = 10^{-3}$, $n = 100$ and for the simulations: channel model: (a) THz, first subband and (b) AWGN channel.
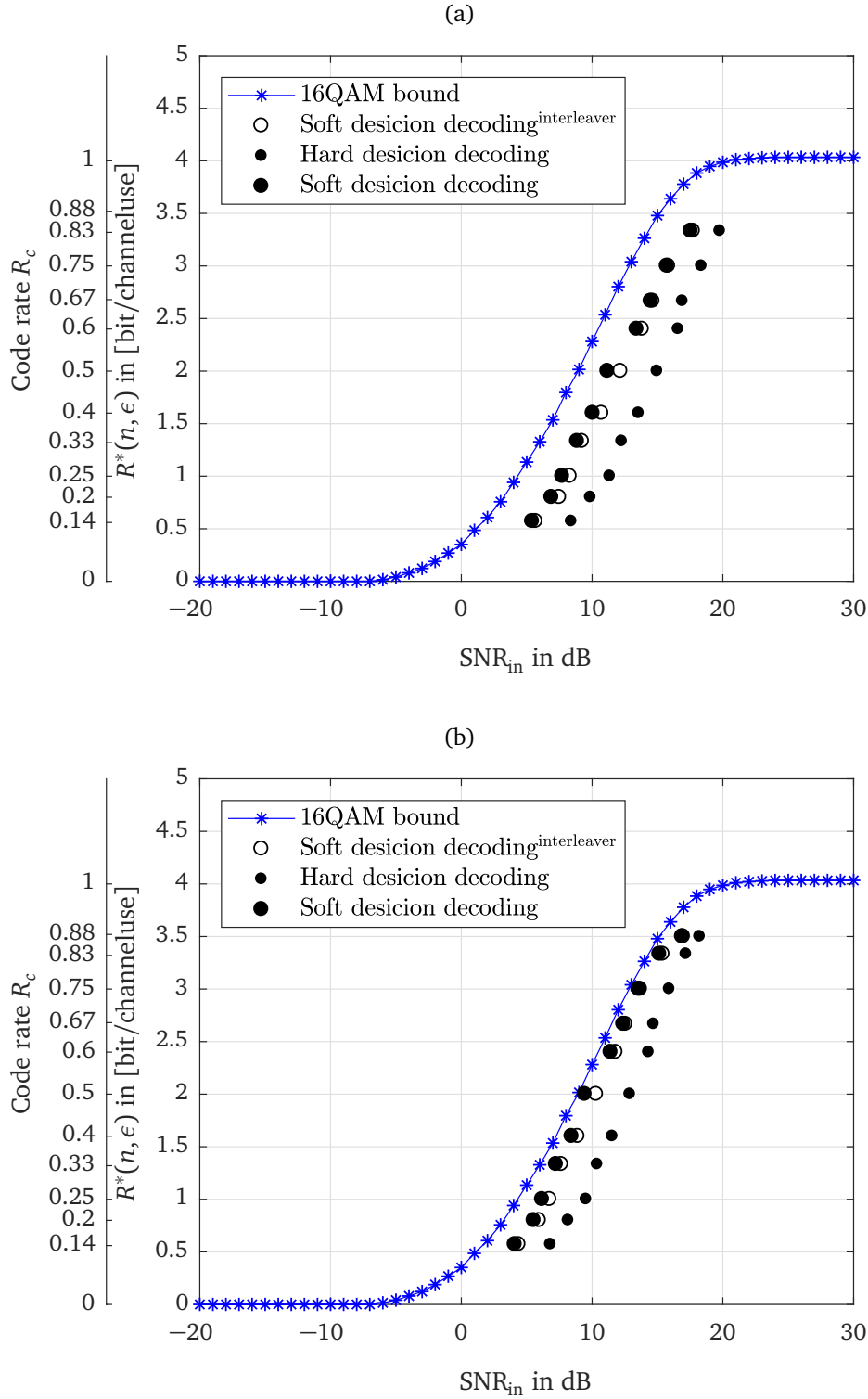
Figure 4.12: Simulation results for a transmission with 16QAM compared to its theoretical bound. Simulation results are shown by circles, the bound is shown in blue. Assumed parameters for theoretical bound: $\epsilon = 10^{-3}$, $n = 100$ and for the simulations: channel model: (a) THz, first subband and (b) AWGN channel.
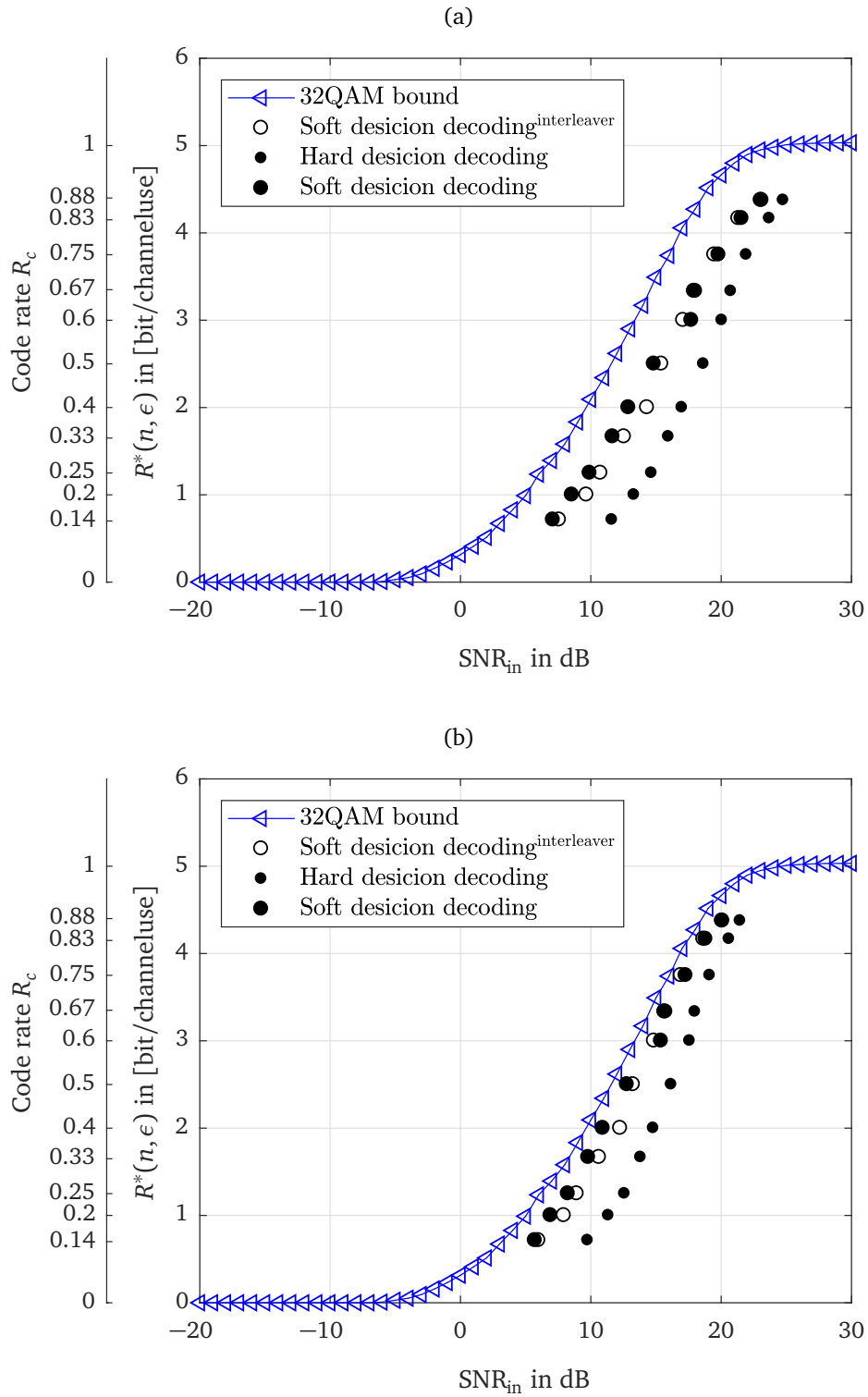
(a)

(b)

Figure 4.13: Simulation results for a transmission with 32QAM compared to its theoretical bound. Simulation results are shown by circles, the bound is shown in blue. Assumed parameters for theoretical bound: $\epsilon = 10^{-3}$, $n = 100$ and for the simulations: channel model: (a) THz, first subband and (b) AWGN channel.

4.2.2 Simulative Achievable Rates

The overall simulation performance is shown in Figure 4.14 for a blocklength (a) being $n = 100$ and (b) being $n = 1900$. The performances are shown for a system with interleaving. The bounds for the maximal achievable rate obtained by using the normal approximation are shown in gray solid lines with different markers for each constellation size. The simulative obtained results are indicated by blue solid lines with the same markers for each constellation size. A transmission over the first band of the THz channel is assumed. For $n = 100$ it can be observed that the simulation performance has a deviation of at most 3.3 dB from the theoretical bounds. The deviation gets less for a higher blocklength, it is 2.8 dB for $n = 1900$. The maximum achievable rate obtained by simulations is about 100 Gbps for the SNR_{in} being 22 dB, whereas the theoretical bound achieves about 110 Gbps for the same SNR_{in} value.
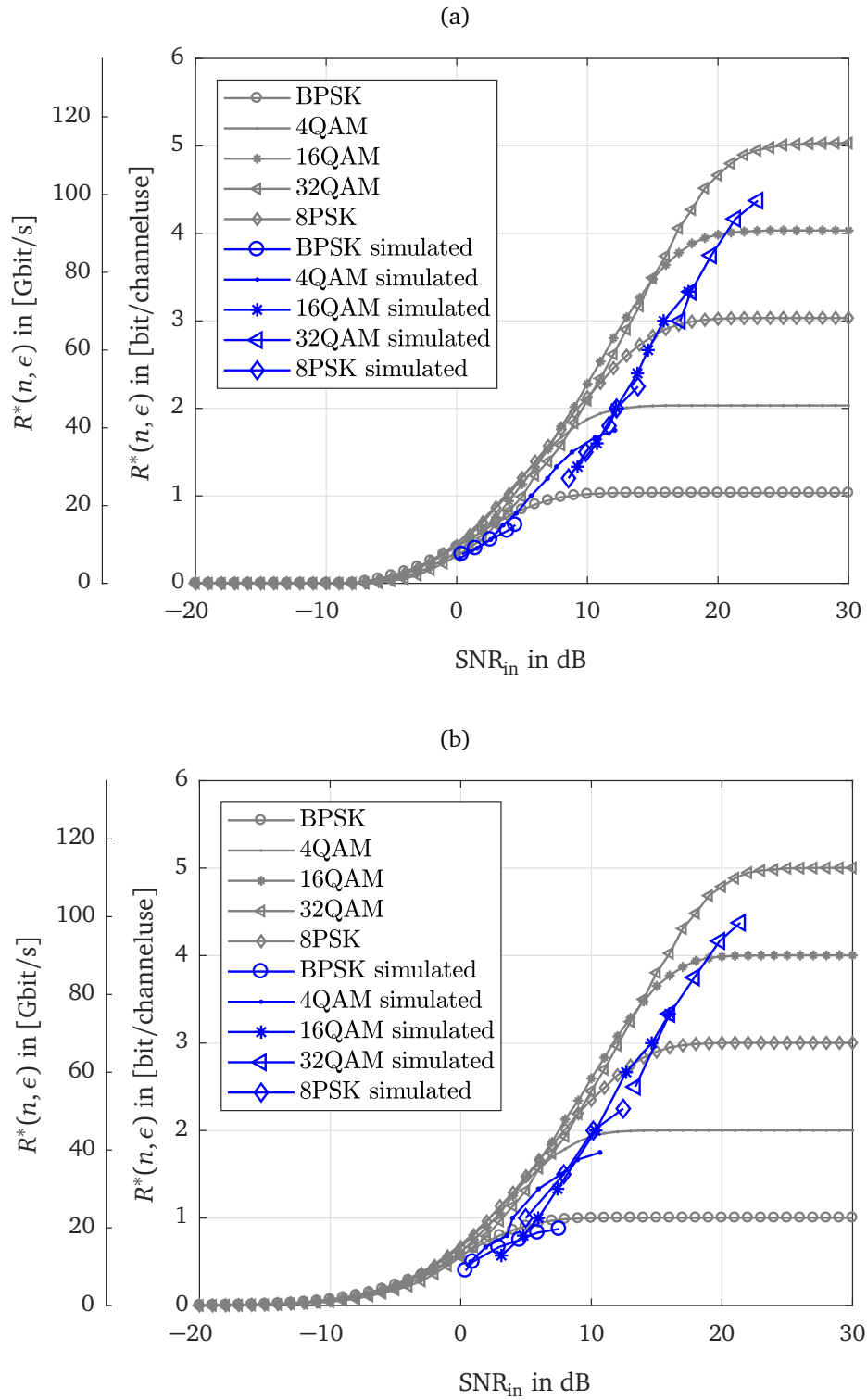
Figure 4.14: Simulation results for a transmission with higher order modulation over a BICM scheme compared to theoretical bounds. Simulation results are shown in blue, while the bound is shown in gray. Assumed parameters $\epsilon = 10^{-3}$, channel model: THz, first subband.
Results are shown for (a) $n = 100$ and (b) $n = 1900$.

Chapter 5

Theoretical Analysis of a Multi Carrier System

Orthogonal Frequency Devision Multiplexing (OFDM) is a Multi Carrier (MC) system, which compared to an SC transmission is able to weaken or completely avoid destructive transmission effects, like for instance, Intercarrier Interference (ICI) or ISI [67]. Therefore, this modulation scheme is interesting regarding the theoretical maximum achievable rate for a transmission over the frequency-selective THz channel. One question is, whether this scheme can compete with or even outperform SC systems. A comparison of OFDM MC transmission with SC transmission in the time-frequency domain is illustrated graphically in [67] and [68]. A short overview of the main advantages of OFDM is given in the following.

In OFDM a high-rate data stream gets converted into a number of low-rate streams by using orthogonal frequency multiplexing [67]. These low-rate streams are transmitted over parallel, narrowband channels [37, 67, 68]. Thereby, the symbol duration is increased to $T_{\mathrm{MC}} = K \cdot T$ for T being the SC symbol duration and K being the number of subcarriers used for OFDM transmission [37, 67]. A CIR $h(t)$ with multipath propagation has duration T_{channel} and by using an OFDM scheme the following property holds $T < T_{\mathrm{channel}} \ll T_{\mathrm{MC}}$. Hence, the CIR affects only parts of an OFDM symbol but it causes great ISI in the SC case, where multiple symbol intervals are affected [67]. Furthermore, in OFDM transmission, ISI and ICI can be completely avoided by using a guard interval [37, 67, 68, 69].

Additionally, viewed from a frequency perspective, narrowband signals are affected less by frequency-selective channels [67]. Frequency selectivity of the channel is caused by multipath propagation [67]. Some paths cause signal amplifications because of constructive superimpositions, others lead to signal loss because of destructive interference [67]. Frequency selective fading gets avoided by using narrowband subcarriers with a bandwidth of each subcarrier chosen as $B_s \ll B_{\mathrm{coh}}$ [67], where the variable B_{coh}

is the coherence bandwidth of the channel. It describes the bandwidth of the channel for which the channel frequency response $H(f)$ is assumed to be almost constant [67]. Therefore, flat fading can be guaranteed for each OFDM subchannel [67]. This reduces highly complex equalization techniques at the Rx [37, 67].

Moreover, OFDM transmission achieves a higher spectral efficiency as it uses parallel subchannels with overlapping spectra [67]. To avoid ICI, all subcarriers have to be orthogonal [37, 67, 68].

These advantages lead to the decision, that an OFDM scheme can be considered as an option for a transmission over the THz channel. For a better impression of its performance, the theoretical maximum achievable rate is compared to SC transmission systems.

This chapter is organized as follows. First, in Subchapter 5.1 the OFDM parameters for a transmission over the THz channel are defined. Secondly, in Subchapter 5.2 the theoretical bound is introduced. Finally, in Subchapter 5.3 the performance in terms of maximum achievable rate of OFDM transmission is compared to the maximum achievable rate of SC schemes, considering transmission systems with MMSE-LE, Zero Forcing Decision Feedback Equalization (ZF-DFE) and Minimum Mean Squared Error Decision Feedback Equalization (MMSE-DFE).

5.1 Definition of OFDM-Parameters

All OFDM parameters are defined based on [68] unless otherwise stated.

For the following, a transmission over the first subchannel of the THz channel is assumed. Its details are given in Table 2.1. The total bandwidth is $BW = 0.0281\,\text{THz}$ and the frequency range is from $0.1\,\text{THz} - 0.1281\,\text{THz}$.

To find the optimum OFDM parameters the Doppler frequency and the excess delay have to be analyzed. For the transmission scenario considered in this thesis stationary Rx and Tx are assumed (cf. Subchapter 2.1). Hence, the channel is time-invariant and there is no Doppler frequency to consider. However, the THz channel is a frequency-selective channel due to multipath propagation. Therefore, the excess delay $\Delta\tau$, for which the reception should be free of ISI, plays an important role. It is defined by the difference between the delay times of the longest and the shortest propagation path. From the work in [9] the power delay profile of the considered THz is known. The shortest radio path is $\tau_1 = 1.16\,\text{ns}$ and the longest path is $\tau_{\text{max}} = 19.23\,\text{ns}$. This leads to an excess delay of

$$\Delta\tau = 18.07\,\text{ns}. \tag{5.1}$$

The guard interval duration T_G is selected to be equal or larger than the excess delay, i.e.,

$$T_G \geq \Delta\tau = 18.07\,\text{ns}, \tag{5.2}$$

to guarantee that the guard interval can account for all ISI. It is realized as a cyclic prefix, i.e., the symbol signal waveform is extended periodically into the guard interval. This ensures that orthogonality of the subcarriers will be maintained over the symbol period and therefore, no ICI will occur [67, 69]. One drawback of the guard interval is, that it contains no information data. Therefore, it decreases the efficiency of the transmission system. Additionally, its usage increases the symbol duration, leading to

$$T_{\text{OFDM}} = T_G + T_{MC} \tag{5.3}$$

for $T_{MC} = K \cdot T$ being the duration of the actual information data. To absorb all ISI and to guarantee simultaneously the smallest efficiency degradation, $T_G = \Delta\tau$ is assumed.

For a transmission efficiency of around 80 % the following lower bound for the information symbol duration T_{MC} holds

$$\frac{T_{MC}}{T_{MC} + T_G} \geq 0.8 \tag{5.4}$$

$$T_{MC} \geq 4 \cdot T_G \tag{5.5}$$

$$T_{MC} \geq 72,28\,\text{ns}. \tag{5.6}$$

As there is no Doppler frequency to account for and the goal is to achieve a low delay transmission, the information symbol duration T_{MC} is set equal to the lower bound obtained in Equation (5.6), i.e.,

$$T_{MC} = 72.28\,\text{ns}. \tag{5.7}$$

Finally, the smallest subcarrier spacing Δf, which guarantees orthogonality, is given by

$$\Delta f = \frac{1}{T_{MC}} = 13.84\,\text{MHz}. \tag{5.8}$$

In a digital OFDM modulator, first, the input data is converted into parallel data streams. Each data stream is then mapped onto symbols of a discrete mapping alphabet. A transmission signal is generated by performing an Inverse Discrete Fourier Transformation (IDFT) of these data symbols. Thereby, frequency-domain samples, which are equally spaced according to Equation (5.8) ([69]), get transformed into time-domain samples. Finally, a parallel-to-serial conversion is performed, the guard interval is inserted and the

data is transmitted over the channel after a digital-to-analog conversion. The optimum IDFT length is obtained by

$$K \geq BW \cdot T_{MC} = 2031.07 \tag{5.9}$$

$$K = 2^{11} = 2048. \tag{5.10}$$

In practical cases the IDFT is realized as an Inverse Fast Fourier Transformation (IFFT) and K is chosen as the lowest power of two fulfilling Inequality (5.9), therefore Equation (5.10) follows. The number of used subcarriers is given by

$$N_u = \frac{BW}{\Delta f} = 2029. \tag{5.11}$$

Unused subcarriers $K - N_u$ are filled with zeros, i.e., zero-padding is applied.

The OFDM demodulator performs the inverse tasks of the OFDM modulator. As it is not part of this thesis the concept of an OFDM modulator and of an OFDM demodulator will not be described closer. The interested reader is referred to [37], [67] or [68].

Similar to SC systems coding can be employed in OFDM systems to improve its performance in fading channels, resulting in Coded Orthogonal Frequency Devision Multiplexing (COFDM) [37]. The main difference to SC systems is, that in an OFDM scheme data can be transmitted at different frequencies and at different times [37]. Therefore, a coding scheme for an OFDM system can be designed with mappers and interleavers which are able to assign the different coded bits in the time-frequency domain appropriately, depending on the channel characteristics [37]. For highly frequency-selective channels it is recommended in [37] to code only across K available frequencies, without interleaving or coding along the time axis [37]. This option has the following two advantages [37]. First, this scheme also works in static channels and second, lower latency of the transmission and decoding process can be achieved without interleaving [37]. In the current transmission scenario, Tx and Rx are assumed to be stationary, i.e., the channel is time-invariant. However, it is highly frequency-selective because of multipath propagation [37]. Therefore, only coding across the available subcarriers will be considered.

5.2 Calculation of Bounds for Maximum Achievable Rate

The theory for the calculation of theoretical bounds for the maximum achievable rate of an COFDM system is according to [24] and [70] unless otherwise stated.

As was mentioned before, coding over K subcarriers is considered. Therefore, the codeword x^n is assumed to be partitioned into K parallel channels so that K blocks of equal length $p = \frac{n}{K}$ are obtained, i.e. $x_k^p = x_1^p, ..., x_K^p$. Therefore, the blocklength n has to be an integer multiple of K.

Codewords are assumed to have constant power in each block and $x^n \in \mathscr{X}^n$ for

$$\mathscr{X}^n = \{x^n = [x_1^p, ..., x_K^p] \big| \|x_k^p\|^2 = \frac{n}{K} P_k\}, \quad \text{for } k = 1, ...K, \tag{5.12}$$

i.e., the theoretical bound for the maximum achievable rate is calculated for a specific power vector. A power constraint of the form

$$\sum_{k=1}^{K} P_k = P_{\text{tot}} \tag{5.13}$$

can be incorporated. It can be realized by the use of standard constrained optimization techniques.

During transmission, each block sees a different AWGN channel. The AWGN channel experienced by the kth block is of the form $y_k^p = x_k^p + z_k^p$, with z_k^p being additive white Gaussian noise with zero mean and noise variance $\sigma_{z_k}^2$, with independent noise entries in each subchannel k, resulting in K parallel Gaussian channels.

The capacity C_{real} for a transmission with real channel input over K parallel AWGN channels is calculated by

$$C_{\text{real}} = \frac{1}{K} \sum_{k=1}^{K} \frac{1}{2} \log_2(1 + \text{SNR}_k) \tag{5.14}$$

for SNR_k being the SNR of subchannel k. Furthermore, the channel dispersion V_{real} is obtained by

$$V_{\text{real}} = \frac{1}{K} \sum_{k=1}^{K} \frac{\text{SNR}_k(2 + \text{SNR}_k)}{2(1 + \text{SNR}_k)^2}. \tag{5.15}$$

Accordingly, both parameters can be calculated for a transmission with complex channel inputs. For the capacity C_{complex}, the following holds

$$C_{\text{complex}} = \frac{1}{K} \sum_{k=1}^{K} \log_2(1 + \text{SNR}_k) \tag{5.16}$$

with the corresponding channel dispersion V_{complex} given by

$$V_{\text{complex}} = \frac{1}{K} \sum_{k=1}^{K} \frac{\text{SNR}_k(2 + \text{SNR}_k)}{(1 + \text{SNR}_k)^2}. \tag{5.17}$$

The capacity can be achieved for an i.i.d. Gaussian channel input. Depending on whether real or complex transmission is assumed, Equation (5.14) and Equation (5.15) or Equation (5.16) and Equation (5.17) are to be used to calculate the maximum achievable rate, given by

$$R^*(n, \epsilon) = C - \sqrt{\frac{V}{n}} \log_2(e) \cdot Q^{-1}(\epsilon) + \frac{\log_2(n)}{2n}, \qquad (5.18)$$

which is obtained by a third order approximation of the normal approximation given by Equation (3.20) (cf. Subchapter 3.2.2).

5.3 Comparison to Single Carrier Systems

In the following the performance of COFDM transmission is compared to SC schemes. The MC system uses the discrete channel model according to Figure 2.5. For transmission complex Gaussian inputs are assumed fulfilling an equal power constraint. Hence, in the COFDM case, the maximum achievable rate gets calculated by inserting the results of Equation (5.16) and Equation (5.17) in Equation (5.18). The SC case uses Equation (3.64) for the calculation of the maximum achievable rate and Equation (3.26) and Equation (3.48) for the calculation of the capacity and channel dispersion. If a different power constraint is assumed, Equations (5.14) - (5.18) can be adjusted accordingly, more information is given in [24]. The SNR of each subcarrier SNR_k is determined by [37, 71]

$$\text{SNR}_k = \frac{|H(k\frac{BW}{K})|^2 \cdot P_k}{\sigma_{z_k}^2}, \qquad (5.19)$$

where $H(f)$ is the Discrete Fourier Transformation (DFT) of the channel $h[\kappa_n]$ scaled by $\sqrt{K}$ [71]. $|H(k\frac{BW}{K})|^2$ denotes the channel attenuation at frequency $f = k\frac{BW}{K}$ [37]. The noise entries are assumed to be independent in each subcarrier for the same value of noise variance, i.e., $\sigma_{z_k}^2 = \sigma_z^2$. The CIR can assumed to be almost constant in each subchannel. Therefore, each subchannel is considered as an AWGN channel. For a comparison with an SC transmission using a Decision Feedback Equalizer (DFE) a whitened matched filter is assumed at the Rx input, which leads to the same noise variance of both schemes for an equivalent overall channel. If a comparison with an SC transmission using liner equalization is considered, the same SNR_{in} is assumed in both cases.

The minimum DFT length for the THz channel is $K = 2048$ obtained by using Equation (5.10). According to Subchapter 5.2 the blocklength n for the MC system has to be an integer multiple of K. Hence, the smallest blocklength possible for this DFT size is $n = 2048$. This leads to the assumption that the COFDM system in its actual appearance is not suited for a transmission over the THz channel with short blocklength of about

$n = 100$. Further modifications of the system design are needed. For reasons of simplicity and to enable a comparison with SC systems a highly ineffective transmission scheme is assumed and lower DFT sizes are also accepted. The smallest DFT length that can be compared to SC systems with a blocklength of about $n = 100$ is $K = 128$. Additionally, a guard interval of $T_G = \Delta\tau$ is assumed to ensure that no ISI and ICI will occur. The efficiency of this system is only about 20 % (cf. Equation (5.4)). However, based on these assumptions the performance in terms of achievable rates for short blocklengths of about $n = 100$ can be compared to SC transmission systems.

This Subchapter is organized as follows. Firstly, in Subchapter 5.3.1 COFDM is compared in terms of maximum achievable rate to an SC system which uses MMSE-LE. Secondly, in Subchapter 5.3.2 its performance is compared to an SC scheme using ZF-DFE. Thereafter, in Subchapter 5.3.3 a comparison is made to an SC system with MMSE-DFE. Finally, in Subchapter 5.3.4 all SC schemes are jointly compared to COFDM.

5.3.1 COFDM vs. MMSE-LE

The principle of MMSE-LE was already thoroughly described in Subchapter 2.2.3. The performance in terms of maximum achievable rate of COFDM and of an SC system using MMSE-LE is shown in Figure 5.1 for a transmission with an input SNR of $\text{SNR}_{\text{in}} = 0\,\text{dB}$
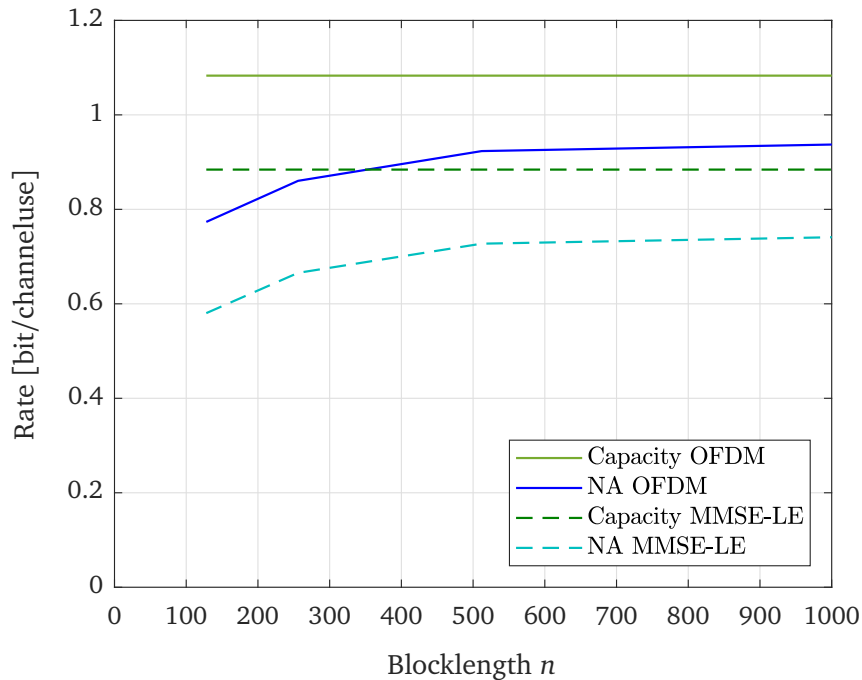

Figure 5.1: The channel capacity and the maximum achievable rate by using the normal approximation (NA) over the blocklength n are shown. Solid lines: COFDM system. Dashed lines: SC with MMSE-LE. This result is obtained for $\epsilon = 10^{-3}$ and $\text{SNR}_{\text{in}} = 0\,\text{dB}$.
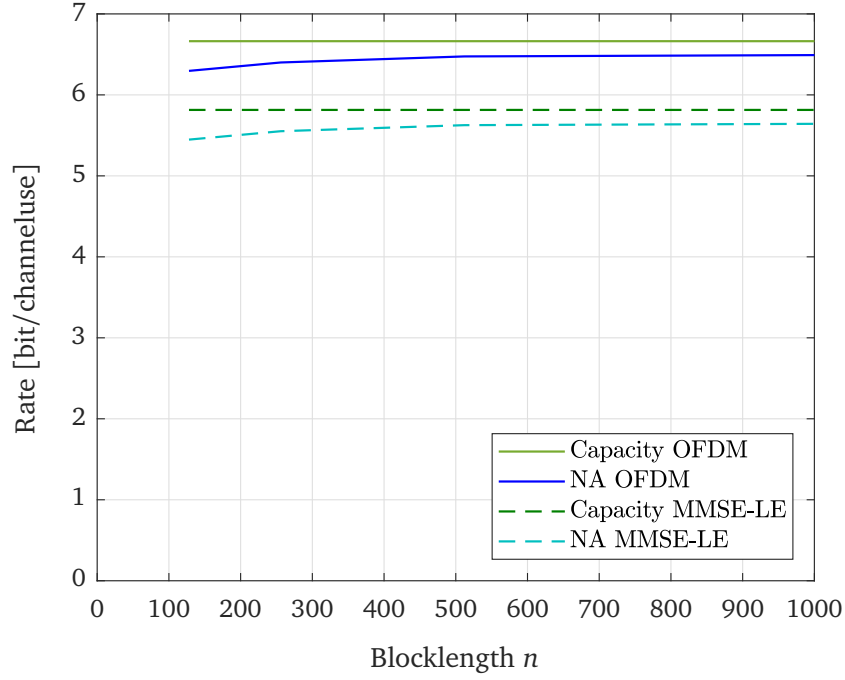
Figure 5.2: The channel capacity and the maximum achievable rate by using the normal approximation (NA) over the blocklength n are shown. Solid lines: COFDM system. Dashed lines: SC with MMSE-LE. This result is obtained for $\epsilon = 10^{-3}$ and $\mathrm{SNR_{in}} = 20\,\mathrm{dB}$.

and in Figure 5.2 for a transmission with $\mathrm{SNR_{in}} = 20\,\mathrm{dB}$. The performance of COFDM is indicated by solid lines, while the SC performance is shown in dashed lines. Both figures illustrate the channel capacity in green colors and the maximum achievable rate in blue colors. The performance of COFDM is always superior over the whole range of n to the performance of an SC system with MMSE-LE. Linear equalization is a suboptimal scheme for the equalization of severely distorting channels as it leads to noise enhancement and therefore to a high noise variance at the equalizer output [50]. Therefore, as already described in Subchapter 2.2.3, $\mathrm{SNR_{MMSE-LE}} < \mathrm{SNR_{in}}$ with the output SNR after equalization $\mathrm{SNR_{MMSE-LE}}$ given by Equation (2.6) and $\mathrm{SNR_{in}}$ given by Equation (2.8). In contrast to the SC case, the COFDM scheme operates at different SNR_k for each subcarrier, given by Equation (5.19). Thereby, it also considers the channel coefficient for each subcarrier, indicated by $|H(k\frac{BW}{K})|^2$. This reason lead to a higher overall SNR for the MC scheme than the output SNR available after equalization in the SC case. The SNR is an important value, which influences the capacity and channel dispersion contained in the normal approximation (cf. Equation (5.18)). Both values are significantly lower for the SC case. Therefore, COFDM outperforms an SC system for both high and low $\mathrm{SNR_{in}}$.

Additionally, Figure 5.3 is given to provide a deeper insight into the development of the maximum achievable rate over the $\mathrm{SNR_{in}}$. The performance of COFDM is shown by dark
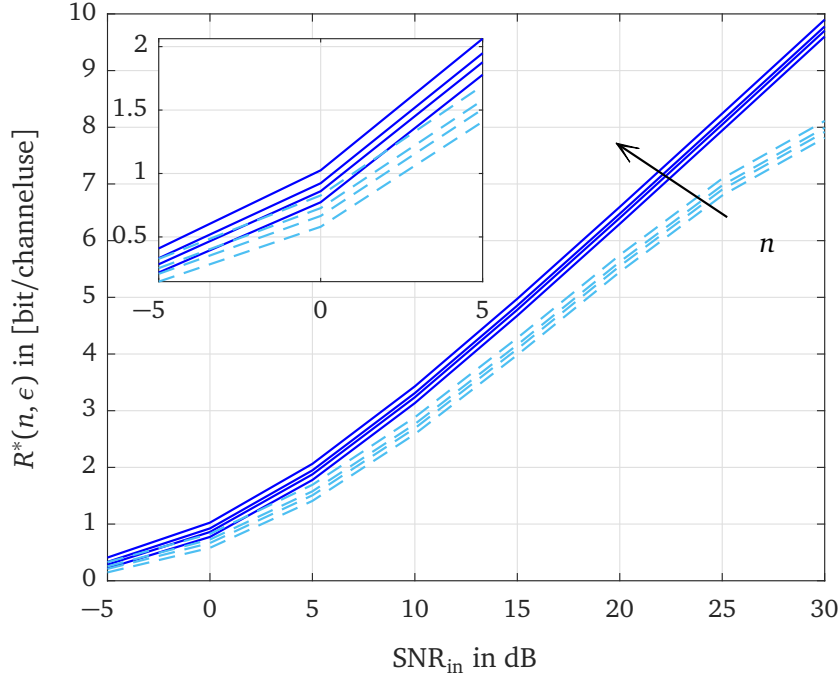
Figure 5.3: Maximum achievable rate over the input SNR. The result is shown for a COFDM system by solid lines and for MMSE-LE by dashed lines. Assumed parameters: $\epsilon = 10^{-3}$ and $n = 128, 256, 512, 4096$. The impact of increasing n is indicated by an arrow.

blue solid lines, while the maximum achievable rate for the SC scheme is indicated by light blue dashed lines. The results are shown for $n = 128, 256, 512, 4096$ and $\epsilon = 10^{-3}$. The effect of higher n is indicated by an arrow. The figure illustrates that an SC scheme with MMSE-LE will never approach the COFDM performance, not even in an asymptotic case for $n = 4096$. The gap between SC and COFDM increases for high SNR_{in}. This is caused by the MMSE-LE filter performance. The chosen filter length of $q_f = 1000$ (cf. Chapter 2.2.3) leads to a reasonable $\text{SNR}_{\text{MMSE-LE}}$ performance up to $\text{SNR}_{\text{in}} = 20\,\text{dB}$ (cf. Figure 2.7). For a better performance for higher SNR_{in} the filter length would have to be increased further.

5.3.2 COFDM vs. ZF-DFE

To avoid severe noise enhancement and to reduce noise variance a DFE is used [50]. A DFE uses knowledge about correctly detected bits in conjunction with knowledge about the CIR to compute the the impact of each bit, i.e., the ISI on subsequent samples of the received signal [37]. The ISI caused by each bit can then be subtracted from these later samples [37]. A DFE consists of a forward filter, which is a conventional linear filter and aims to suppress the precursor ISI, and of a feedback filter [37, 50]. As soon as the Rx has decided on a received symbol, its impact on all future samples (postcursor ISI) can

be computed, and via the feedback be subtracted from the received signal [37]. There is no noise enhancement, because a slicer eliminates the noise before the feedback filter applies on the signal [50].

From a frequency domain perspective, the goal of ZF equalization is to enforce a completely flat transfer function for the combination of the channel and the equalizer [37].

The equivalent channel model before equalization is given in Figure 2.5, where the CIR is causal and additive white Gaussian noise is added. For DFE the optimum filters get calculated by spectral factorization, which obtains a minimum phase expression of the channel and guarantees that a minimum variance of the prediction error σ_e^2 can be achieved. The currently considered discrete-time THz channel is already minimum phase and has a reference tap of one. Therefore, ZF-DFE transforms the discrete-time THz channel and the Rx input filter in an equivalent AWGN channel with $\text{SNR} = \frac{\sigma_x^2}{\sigma_e^2}$ for $\sigma_x^2 = 1$ and σ_e^2 being the minimum prediction error obtained by spectral factorization, i.e., for the considered channel model, the following holds: $\sigma_e^2 = \frac{\sigma_z^2}{|h[0]|^2} = \sigma_z^2$. Hence, for the output $\text{SNR}_{\text{ZF-DFE}}$ it can be concluded

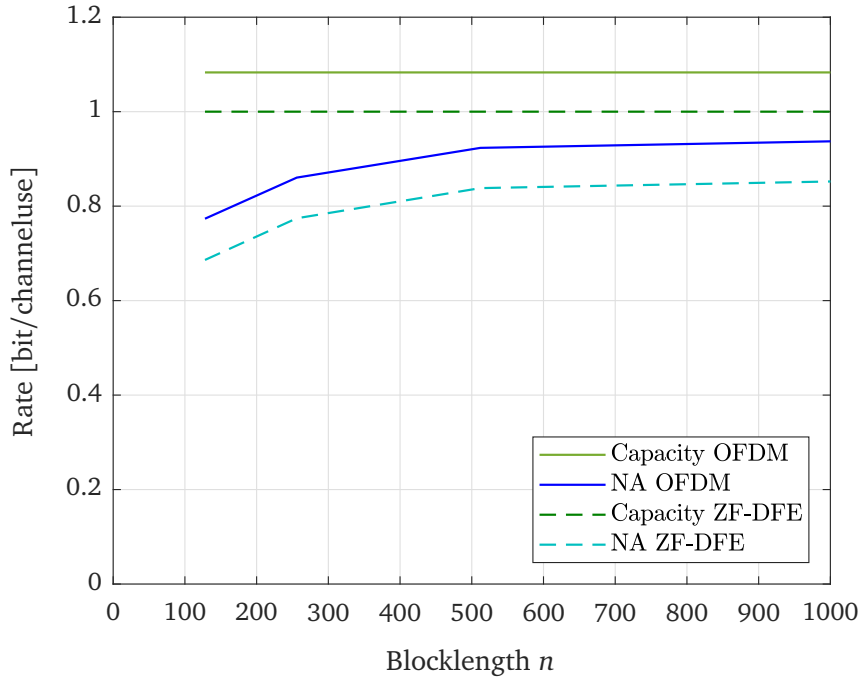$$\text{SNR}_{\text{ZF-DFE}} = \frac{1}{\sigma_z^2}. \tag{5.20}$$

Figure 5.4: The channel capacity and the maximum achievable rate by using the normal approximation (NA) over the blocklength n are shown. Solid lines: COFDM system. Dashed lines: SC with ZF-DFE. This result is obtained for $\epsilon = 10^{-3}$ and $\text{SNR}_{\text{in}} = 0\,\text{dB}$.
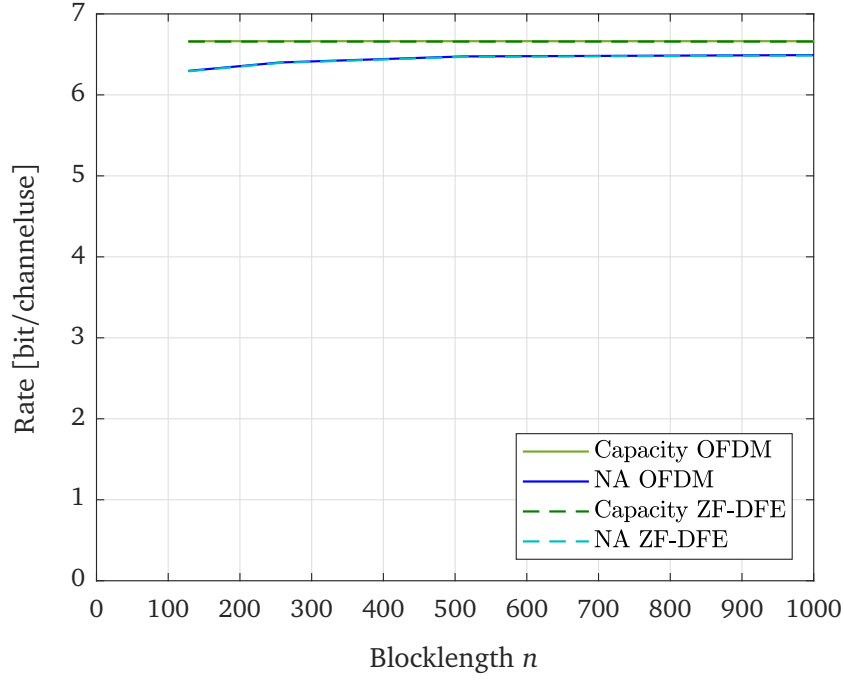
Figure 5.5: The channel capacity and the maximum achievable rate by using the normal approximation (NA) over the blocklength n are shown. Solid lines: COFDM system. Dashed lines: SC with ZF-DFE. This result is obtained for $\epsilon = 10^{-3}$ and $\mathrm{SNR_{in}} = 20\,\mathrm{dB}$.

A performance comparison with COFDM in terms of maximum achievable rate is shown in Figure 5.4 for $\mathrm{SNR_{in}} = 0\,\mathrm{dB}$ and in Figure 5.5 for $\mathrm{SNR_{in}} = 20\,\mathrm{dB}$. The performance of COFDM is indicated by solid lines, while the SC performance is shown in dashed lines. Both figures illustrate the channel capacity in green colors and the maximum achievable rate in blue colors. For the lower $\mathrm{SNR_{in}}$ of $0\,\mathrm{dB}$ the performance of COFDM compared to the SC system is better (cf. Figure 5.4). The lower the noise variance gets, the closer the maximum achievable rate for the SC system gets to the COFDM performance. This can be explained by comparing the calculation of the capacity and dispersion for OFDM (cf. Equation (5.16) and cf. Equation (5.17)) and SC (cf. Equation (3.26) and Equation (3.48)) transmission. For low noise variance, the $\mathrm{SNR_k}$ for COFDM obtained by Equation (5.19) and the calculation of $\mathrm{SNR_{ZF-DFE}}$ in Equation (5.20) coincides in the limit, and therefore the capacity and the dispersion achieves the same value. For high noise variances COFDM is better, because for the calculation of each $\mathrm{SNR_k}$ it also takes into account the channel coefficient $|H(k\frac{BW}{K})|^2$ for each subchannel, while ZF-DFE considers only the first channel tap $|h[0]|$. Capacity and channel dispersion influence the value of the maximum achievable rate (cf. Equation (5.18)).

To get a better understanding about the development of the maximum achievable rate for increasing $\mathrm{SNR_{in}}$ values Figure 5.6 shows $R^*(n, \epsilon)$ over $\mathrm{SNR_{in}}$. The performance
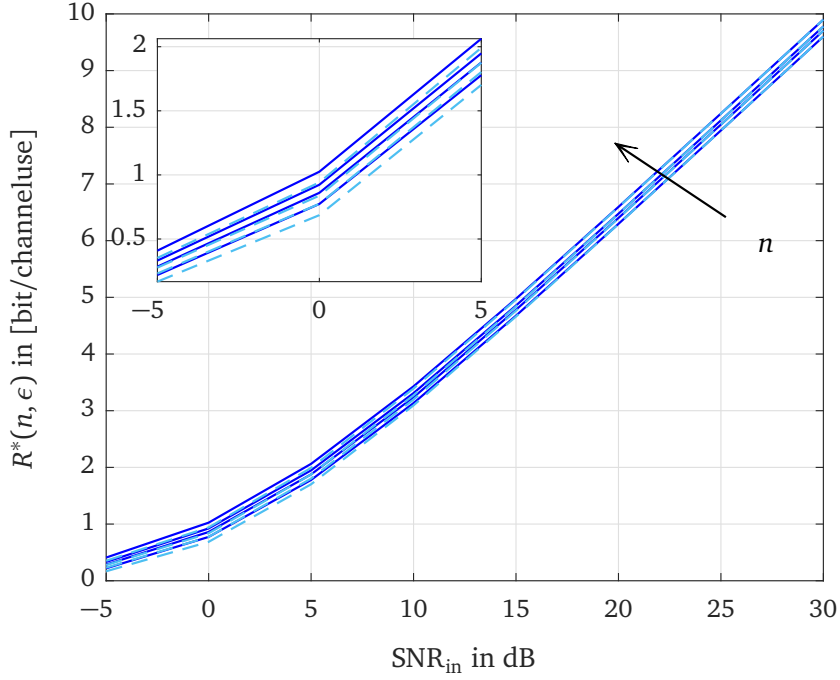
Figure 5.6: Maximum achievable rate over the input SNR. The result is shown for a COFDM system by solid lines and for ZF-DFE by dashed lines. Assumed parameters: $\epsilon = 10^{-3}$ and $n = 128, 256, 512, 4096$. The impact of increasing n is indicated by an arrow.

of COFDM is shown by dark blue solid lines, while the maximum achievable rate for the SC scheme is indicated by light blue dashed lines. The results are illustrated for $n = 128, 256, 512, 4096$ and $\epsilon = 10^{-3}$. The effect of increasing n is indicated by an arrow. The figure illustrates that an SC scheme with ZF-DFE will approach the performance of COFDM for high SNR_{in} values. The larger the blocklength n is chosen, the earlier the COFDM performance is approached. For low SNR_{in} values between $-5\,\text{dB}$ and $5\,\text{dB}$, COFDM is always better than the SC approach. The performance of the SC system never outperforms the COFDM scheme.

5.3.3 COFDM vs. MMSE-DFE

MMSE-DFE aims to minimize the MSE by balancing between noise enhancement and residual ISI [37]. This is the same goal as for the MMSE-LE [37]. However, noise enhancement is different in the DFE case, therefore the coefficients for the forward filter are different [37]. In the DFE case, postcursor ISI does not contribute to noise enhancement, and the aim is to minimize the sum of noise and (average) precursor ISI [37]. The MMSE criterion is more efficient than the ZF criterion, which leads to $\text{SNR}_{\text{MMSE-DFE}} > \text{SNR}_{\text{ZF-DFE}}$ [37, 50]. As in the ZF-DFE case, spectral factorization is applied to find the minimum error variance σ_e^2 which is smaller than for ZF-DFE. Hence,

Table 5.1: The output $SNR_{MMSE-DFE}$ in dB for a certain SNR_{in} in dB.

SNR_{in} in dB	-5	0	5	10	15	20	25	30
$SNR_{MMSE-DFE}$ in dB	-4.32	0.48	5.27	10.12	15.05	20.02	25	30

MMSE-DFE transforms the THz channel with the Rx input filter into an equivalent AWGN channel with noise variance $\sigma_z^2 = \sigma_e^2$ being smaller than in the ZF-DFE case.

For a comparison with the COFDM system the following parameters are assumed. For demonstration purposes and for the use of a reasonable filter length only the first 200 taps of the THz channel are considered. The feedforward filter is of order $q_f^{DFE} = 70$, the feedback filter is set to $q_b^{DFE} = 200$ and $k_0^{DFE} = q_f^{DFE}$. The output $SNR_{MMSE-DFE}$ in dB for a certain SNR_{in} in dB is shown in Table 5.1.

The performance in terms of maximum achievable rate for an SC system with MMSE-DFE and for the OFDM scheme is shown in Figure 5.7 for $SNR_{in} = 0$ dB. The result for COFDM is indicated by solid lines, while the SC performance is shown in dashed lines. The figure illustrates the channel capacity in green colors and the maximum achievable rate in blue colors. Already for a low SNR_{in} the maximum achievable rate of the SC and MC scheme is approximately equivalent, even for a short blocklength. The largest deviation is in the order of 10^{-2}.
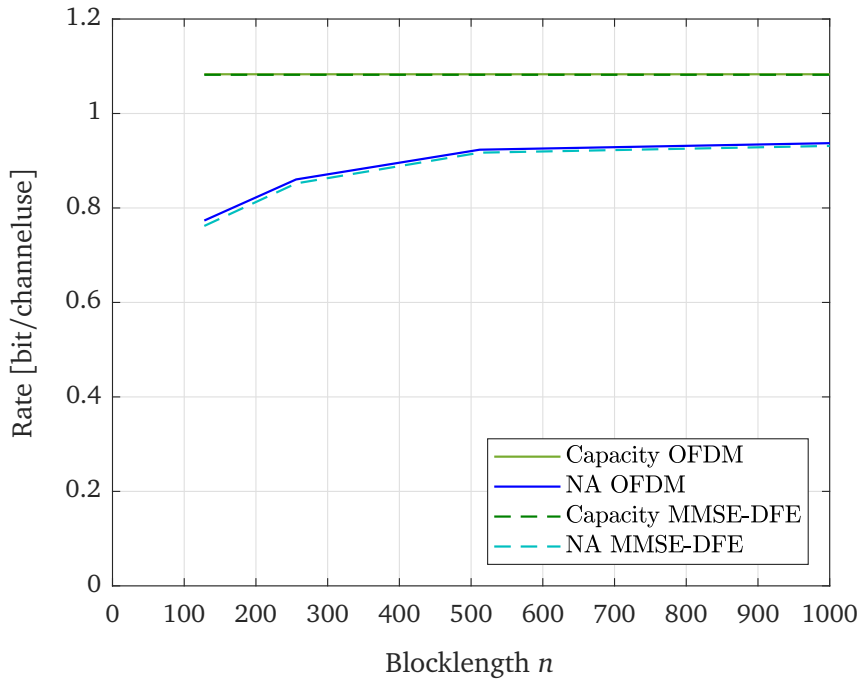

Figure 5.7: The channel capacity and the maximum achievable rate by using the normal approximation (NA) over the blocklength n are shown. Solid lines: COFDM system. Dashed lines: SC with MMSE-DFE. This result is obtained for $\epsilon = 10^{-3}$ and $SNR_{in} = 0$ dB.
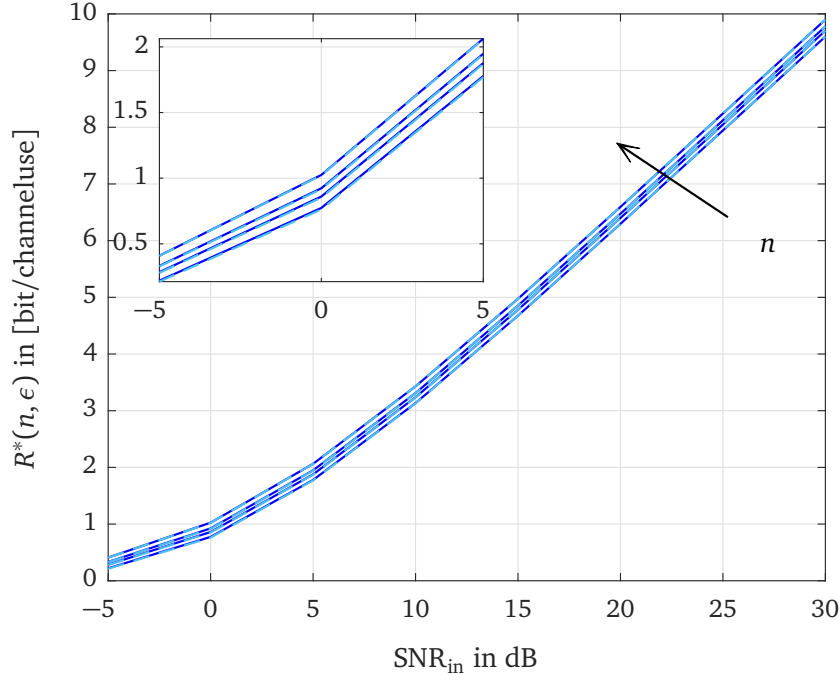
Figure 5.8: Maximum achievable rate over the input SNR. The result is shown for a COFDM system by solid dark blue lines and for MMSE-DFE by dashed light blue lines. Assumed parameters: $\epsilon = 10^{-3}$ and $n = 128, 256, 512, 4096$. The impact of increasing n is indicated by an arrow.

To get a better impression about the relation between the maximum achievable rate for COFDM and the maximum achievable rate for the SC approach, the development of the maximum achievable rate over the SNR_{in} is demonstrated in Figure 5.8. The performance of COFDM is shown in dark blue, while the maximum achievable rate for the SC scheme is indicated by a light blue color. The results are shown for $n = 128, 256, 512, 4096$ and $\epsilon = 10^{-3}$. The effect of increasing n is indicated by an arrow. This figure verifies that the performance in terms of maximum achievable rate of a system using MMSE-DFE is as good as the performance of a COFDM transmission scheme. Similar results are already obtained for a very short blocklength as short as $n = 128$ or $n = 256$.

5.3.4 Overall Result

A comparison of the maximum achievable rate of COFDM with the maximum achievable rate of all SC options presented before is illustrated in Figure 5.9. The maximum achievable rate is plotted over the SNR_{in}. The result for a COFDM system is shown by solid dark blue lines and for SC systems by dashed lines. MMSE-LE is indicated by a purple color. The results for ZF-DFE are demonstrated in black. MMSE-DFE is shown in a light blue color. The maximum achievable rate is calculated for $\epsilon = 10^{-3}$ and $n = 128, 256, 512$. The impact of increasing n is indicated by an arrow. The
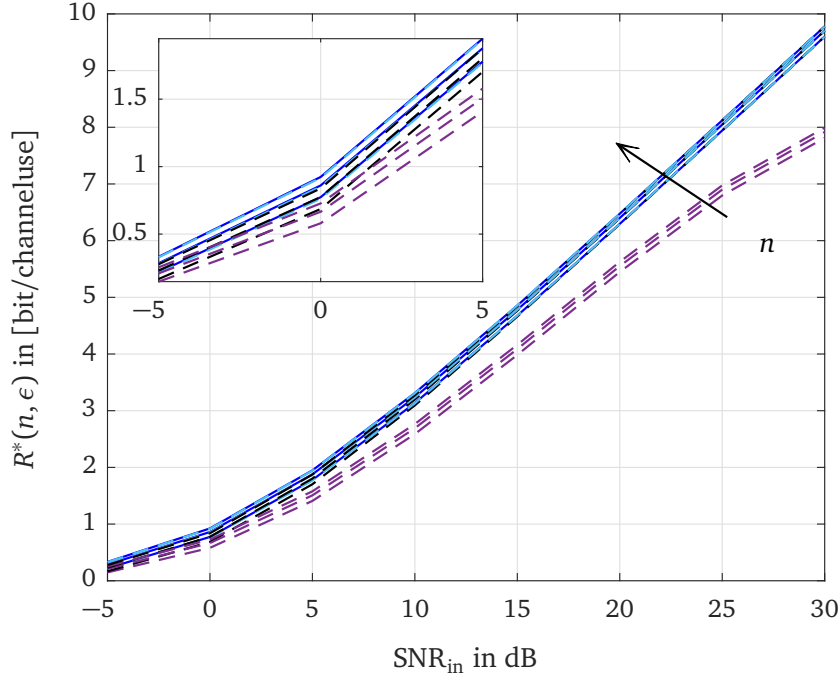
Figure 5.9: Maximum achievable rate over the input SNR_{in}. The result for a COFDM system is shown by solid dark blue lines and for SC systems by dashed lines. MMSE-LE is indicated by a purple color. The results for ZF-DFE are demonstrated in black. MMSE-DFE is shown in a light blue color. Assumed parameters: $\epsilon = 10^{-3}$ and $n = 128, 256, 512$. The impact of increasing n is indicated by an arrow.

worst performance is obtained by MMSE-LE. ZF-DFE achieves a performance as good as COFDM for asymptotically large SNR_{in} values. The best performance for operating at short blocklength n is obtained by COFDM and MMSE-DFE. Therefore, one of these two options should be considered for a transmission over the THz channel.

However, both options have some drawbacks. One disadvantage of DFE is error propagation due to feedback of erroneous decisions [37, 50]. Furthermore, a straightforward combination with channel coding is not possible, because DFE requires immediate decisions on the data symbols for the feedback, while channel coding is based on long blocks of symbols, and decisions on all symbols of a block are made simultaneously [50]. However, this problem can be solved by the application of precoding. More information can be found in [50].

An OFDM scheme is sensitive to frequency offset and suffers from high Peak to Average Power Ratio (PAPR) which occurs because the peak amplitude of the emitted signal can be considerably higher than the average amplitude [37]. This effect gets problematic, if some amplitudes reach the nonlinear region in power amplifiers [37, 72]. PAPR reduction techniques can be used to overcome the high PAPR problem. More information is given in [37]. To be more robust to the frequency offset, the design of the OFDM parameters

can be adjusted accordingly [68]. By doing so, some frequency offset could be accepted for OFDM transmission [68]. More information is given in [68].

The final decision for an SC scheme with MMSE-DFE or for a COFDM scheme depends on system requirements and acceptable implementation effort.

Chapter 6

Conclusion

In this concluding chapter a brief summary of the main results is given and possibilities for future work that would further improve the developed approach are discussed.

Summary

One goal of this work was to find bounds for the maximum achievable rate according to the finite blocklength approach of PPV. These bounds should be applicable for a transmission over the THz channel using higher order modulations and furthermore, they should be verified by simulations applying channel coding for various coding rates. Theoretical and simulative results should be analyzed regarding various performance criteria to be able to give design guidelines for coding schemes with very low latency.

In Chapter 2 the implemented system model used for simulations was described. A BICM system was considered for an SC point-to-point transmission according to the work of [27]. As the THz channel is highly frequency-selective, MMSE-LE was incorporated into the system model. The result is an overall channel with colored noise and some residual ISI for low SNR_{in}. For high SNR_{in} the residual ISI becomes almost negligible. For decoding hard- and soft-decision concepts were implemented. Furthermore, transmission with higher order modulations considering BPSK, 4QAM, 16QAM, 32QAM and 8PSK and coding with different coding rates being $\frac{1}{7}, \frac{1}{5}, \frac{1}{4}, \frac{1}{3}, \frac{1}{2}, \frac{2}{5}, \frac{2}{3}, \frac{3}{4}, \frac{5}{6}$ and $\frac{7}{8}$ was realized.

The theory behind the finite blocklength approach according to the work of PPV and behind the normal approximation, which is used to approximate the bounds for the maximum achievable rates, was introduced in Chapter 3. One necessary channel specific parameter which is indispensable for the analysis of the normal approximation is the *channel dispersion*. In this context the work of [4] was explained, where the maximum achievable rate including the channel dispersion is obtained for a transmission using a CM system and higher order modulations. This approach was adapted to the implemented BICM scheme and an expression for the BICM channel dispersion was presented.

In Chapter 4 the developed bounds for the established BICM system were presented and compared to CM. The maximum achievable rate of a BICM system is slightly lower than the one of a CM scheme. Theory-based recommendations for the modulation schemes which are suited best to achieve the maximum rate for the considered transmission scenario were given. Furthermore, a parameter analysis was presented for the normal approximation. The maximum achievable rates depend on the blocklength, the error probability and on the third term of the third order approximation. The higher the first two mentioned parameters are chosen, the higher the maximum achievable rate becomes. Moreover, it was shown that with a transmission over the THz channel a low delay transmission in the order of just some tenth of a microseconds is realizable. Finally, the simulative results were shown to approach the theoretically obtained bounds up to 3.3 dB for 32QAM and up to $2 - 2.5$ dB for the other modulation schemes. Soft decision decoding was proven to be better than hard-decision decoding. The maximum achievable rate obtained by using the normal approximation is 110 Gbps. Simulative results achieve a maximum value of about 100 Gbps for the same SNR_{in}.

An OFDM transmission scheme is another option for a transmission over frequency-selective channels. Therefore, in Chapter 5 the finite blocklength regime was extended to MC transmission. Firstly, suitable OFDM parameters were obtained. Secondly, the theoretical approach of [24] was introduced. It was used to derive the bounds for the maximum achievable rate for an COFDM transmission over the THz channel. Finally, these theoretical bounds were compared to the bounds for SC approaches considering MMSE-LE, ZF-DFE and MMSE-DFE. Therefore, in addition to the SC results using MMSE-LE given in Chapter 4, bounds for an SC using ZF-DFE and MMSE-DFE were presented. The following results using Gaussian channel inputs were obtained. An SC system with MMSE-LE performs worse than the OFDM system. An SC system with ZF-DFE performs worse for low SNR_{in} values, but achieves the OFDM performance in the limit of high SNR_{in} values. An SC system with MMSE-DFE performs as good as the OFDM system. No SC approach outperforms the OFDM scheme.

Discussion and Future Work

The implemented SC system was able to verify the obtained bounds for the maximum achievable rate up to $2 - 3.3$ dB, which is a satisfying result. However, it could be further improved. The loss in capacity and therefore in the maximum achievable rate of BICM systems compared to CM systems can be overcome by extending the BICM scheme to a scheme with iterative decoding called BICM-ID. It can be used to account for the performance loss compared to CM [36].

In this work convolutional codes with an i.i.d. uniform distribution of the symbols were implemented. However, it was mentioned in [4] that constant composition codes are able to achieve a better performance without harming the maximum power constraint. They could be considered in future work. The bounds would have to be adjusted accordingly, neglecting the subtraction of δ for MQAM schemes.

In this thesis theoretical bounds were obtained for a discrete channel input and a transmission over an AWGN channel. In future work the approach mentioned in [20] to find the dispersion for Gaussian channels with colored noise and continuous channel input could be taken to develop an upper bound for a transmission over the THz channel. The simulation results for discrete channel input obtained in this work are expected to be close to this bound for low to moderate SNR.

In this work the theoretical bounds for an OFDM transmission with Gaussian channel inputs were obtained. Of further interest are the theoretical bounds for the maximum achievable rate for an OFDM system with discrete channel input and a transmission over the THz channel. Moreover, in future work all theoretical results obtained for OFDM need to be verified by simulations.

Appendix A

Electronic Appendix

Folder	Content
1_Max_Achiev_Rate_SC	Code to obtain the bounds for the maximum achievable rate for SC systems.
2_Max_Achiev_Rate_MC	Code to obtain the bounds for the maximum achievable rate for MC systems.
3_Code_for_Simulation_SC	Code used for simulations.
4_Analysis_of_Simulation_SC	Code to analyze simulation results.
5_Capacity_plots	Some auxiliary Matlab scripts to plot capacity over SNR.
Masters_Thesis	Master's thesis in pdf.

Bibliography

[1] I. Akyildiz, J. Jornet, and C. Han. Terahertz band: Next frontier for wireless communications. *Physical Communication*, 12:16–32, 2014.

[2] N. Heuveldop. Ericsson mobility report, June 2017.

[3] Cisco Systems Inc. Cisco visual networking index: global mobile data traffic forecast update, 2016 - 2021 White Paper, February 2017.

[4] E. MolavianJazi. *A unified approach to Gaussian channels with finite blocklength*. PhD thesis, 2014.

[5] B. Friedrichs. *Kanalcodierung: Grundlagen und Anwendungen in modernen Kommunikationssystemen*. Springer-Verlag, 1996.

[6] C. E. Shannon and W. Weaver. *The mathematical theory of communication*. University of Illinois press, 1998.

[7] Y. Polyanskiy, H. V. Poor, and S. Verdú. Channel coding rate in the finite blocklength regime. *IEEE Transactions on Information Theory*, 56(5):2307–2359, 2010.

[8] V. Strassen. Asymptotic estimates in Shannon's information theory. In *Proceedings of 3rd Trans. Prague Conf. Inf. Theory*, pages 689–723, 2009.

[9] A. Moldovan, M. A. Ruder, I. F. Akyildiz, and W. H. Gerstacker. LOS and NLOS channel modeling for Terahertz wireless communication with scattered rays. *Globecom 2014 Workshop - Mobile Communications in Higher Frequency Bands*, pages 388 – 392, 2014.

[10] A. Moldovan, S. Kisseleff, I. F. Akyildiz, and W. H. Gerstacker. Data rate maximization for Terahertz communication systems using finite alphabets. In *Proceedings of IEEE International Conference on Communications (ICC)*, pages 1–7, 2016.

[11] J. Jornet and I. Akyildiz. Channel modeling and capacity analysis for electromagnetic wireless nanonetworks in the Terahertz band. *IEEE Transactions on Wireless Communications*, 10(10):3211–3221, 2011.

[12] S. U. Hwu, C. T. Jih, et al. Terahertz (THz) wireless systems for space applications. In *Proceedings of Sensors Applications Symposium (SAS)*, pages 171–175. IEEE, 2013.

[13] H. Han, J. Yuan, and J. Tong. Design of THz space application system. *Journal of Computer and Communications*, 3(03):61, 2015.

[14] D. Yuan-Ming, G. Shan, S. Xin, and W. Hao. Analysis of inter-satellite Terahertz communication link. *Advances in Computer Science Research*, 44, 2016. 3rd International Conference on Wireless Communication and Sensor Network.

[15] T. Nagatsuma, G. Ducournau, and C. C. Renaud. Advances in Terahertz communications accelerated by photonics. *Nature Photonics*, 10(6):371, 2016.

[16] H. Shams, T. Shao, M. Fice, P. Anandarajah, C. Renaud, F. Van Dijk, L. P. Barry, and A. J. Seeds. 100 Gb/s multicarrier THz wireless transmission system with high frequency stability based on a gain-switched laser comb source. *IEEE Photonics Journal*, 7(3):1–11, 2015.

[17] M. F. Hermelo, P. B. Shih, M. Steeg, A. Ngoma, and A. Stöhr. Spectral efficient 64-QAM-OFDM THz communication link. *Optics Express*, 25(16):19360–19370, 2017.

[18] L. Lopacinski, M. Brzozowski, and R. Kraemer. Data link layer considerations for future 100 Gbps Terahertz band transceivers. *Wireless Communications and Mobile Computing*, 2017.

[19] M. Hayashi. Information spectrum approach to second-order coding rate in channel coding. *IEEE Transactions on Information Theory*, 55(11):4947–4966, 2009.

[20] Y. Polyanskiy, H. V. Poor, and S. Verdú. Dispersion of Gaussian channels. In *Proceedings of International Symposium on Information Theory (ISIT)*, pages 2204–2208. IEEE, 2009.

[21] V. Kostina and S. Verdú. Channels with cost constraints: strong converse and dispersion. *IEEE Transactions on Information Theory*, 61(5):2415–2429, 2015.

[22] Y. Polyanskiy, H. V. Poor, and S. Verdú. Dispersion of the Gilbert-Elliott channel. *IEEE Transactions on Information Theory*, 57(4):1829–1848, 2011.

[23] A. Ingber and M. Feder. Parallel bit interleaved coded modulation. In *Proceedings of the 48th Annual Allerton Conference on Communications*, pages 215–222. IEEE, 2010.

[24] T. Erseghe. Coding in the finite-blocklength regime: bounds based on Laplace integrals and their asymptotic approximations. *IEEE Transactions on Information Theory*, 62(12):6854–6883, 2016.

[25] S. Yan, B. He, Y. Cong, and X. Zhou. Covert communication with finite blocklength in AWGN channels. In *Proceedings of International Conference on Communications (ICC)*, pages 1–6. IEEE, 2017.

[26] K. G. Shenoy and V. Sharma. Finite blocklength analysis of energy harvesting channels. *arXiv preprint:1612.06844*, 2016.

[27] G. Caire, G. Taricco, and E. Biglieri. Bit-interleaved coded modulation. *IEEE transactions on information theory*, 44(3):927–946, 1998.

[28] Allied Business Intelligence Inc. ABI research anticipates in-building mobile data traffic to grow by more than 600% by 2020, January 2016. https://www.abiresearch.com/press/abi-research-anticipates-building-mobile-data-traf/. Accessed: October, 2017.

[29] Global Mobile Suppliers Association. Small cell network white paper, November 2016.

[30] CommScope Solutions Germany GmbH. Wireless in buildings: what building professionals think, 2016.

[31] S. X. Ng, T. H. Liew, L-L. Yang, and L. Hanzo. Comparative study of TCM, TTCM, BICM and BICM-ID schemes. 4:2450–2454, 2001.

[32] J. L. Massey. Coding and modulation in digital communications. In *Proceedings on 3rd International Zurich Seminar on Digital Communications, Zurich, Switzerland*, 1974.

[33] G. Ungerboeck. Channel coding with multilevel/phase signals. *IEEE Transactions on Information Theory*, 28(1):55–67, 1982.

[34] A. Alvarado, L. Szczecinski, and E. Agrell. On BICM receivers for TCM transmission. *IEEE Transactions on Communications*, 59(10):2692–2702, 2011.

[35] E. Zehavi. 8-PSK trellis codes for a Rayleigh channel. *Transactions on Communications*, 40(5):873–884, 1992.

[36] A.G. i Fàbregas, A. Martinez, G. Caire, et al. Bit-interleaved coded modulation. *Foundations and Trends in Communications and Information Theory*, 5(1–2):1–153, 2008.

[37] A. F. Molisch. *Wireless communications*, volume 34. John Wiley & Sons, 2012.

[38] A. Burr. *Modulation and coding: for wireless communications*. Pearson Education, 2001.

[39] C. Stierstorfer. *A Bit-level-lased approach to coded multicarrier transmmission*. PhD thesis, FAU Erlangen-Nürnberg, SS 2009.

[40] C. Stierstorfer and R. Fischer. Mappings for BICM in UWB scenarios. In *Proceedings of 7th International ITG Conference on Source and Channel Coding (SCC)*, pages 1–6. VDE, 2008.

[41] J. Huber and R. Schober. Digitale Übertragung. SS 2014.

[42] T. Hehn and J. B. Huber. LDPC codes and convolutional codes with equal structural delay: A comparison. *IEEE Transactions on Communications*, 57(6), 2009.

[43] C. Li. Chapter10 Convolutional Codes. Wireless Information Transmission System Lab, National Sun Yat-sen University.

[44] J. M. Cioffi. EE379B: Digital Communications - Coding.

[45] C. Stierstorfer, R. Fischer, and J. Huber. Grundlagen der Kanalcodierung. 2013.

[46] S. Bawane and V. Gohokar. Simulation of convolutional encoder. *International Journal of Research in Engineering and Technology (IJRET), India*, 3(3):557–561, 2014.

[47] The MathWorks Inc. Punctured convolutional coding, 2017. https://de.mathworks.com/help/comm/ug/punctured-convolutional-coding-1.html. Accessed: January, 2017.

[48] J. Bisla, N. Dhillon, and K. Sharma. Performance evaluation of punctured convolutional codes for OFDM-WiMAX system. *International Journal of Electronics and Electrical Engineering*, 2(3):142–148, 2014.

[49] L. Szczecinski and A. Alvarado. *Bit-interleaved coded modulation: fundamentals, analysis and design*. John Wiley & Sons, 2015.

[50] W. Gerstacker. Equalization and adaptive systems for digital communications. WS 2015/2016.

[51] K. Du and M. Swamy. *Wireless communication systems: from RF subsystems to 4G enabling technologies*. Cambridge University Press, 2010.

[52] K. Muranov. Survey of MMSE channel equalizers. *University of Illinois Chicago, USA, Tech. Rep*, 2010.

[53] R. Y. Yen. Unbiased MMSE vs. biased MMSE equalizers. 12(1):45–56, 2009.

[54] W. Yang, Y. S. Cho, W. G. Jeon, J. W. Lee, J. Kim, J. Paik, M. Lee, K. I. Lee, K. W. Park, and K. S. Woo. *Matlab/Simulink for digital communication*. Hongrung Publishing Comany, 2013.

[55] Y. Polyanskiy. *Channel coding: non-asymptotic fundamental limits*. PhD thesis, 2010.

[56] J. Nicholas. Laneman. On the distribution of mutual information. In *Proceedings of Information Theory and Applications Workshop*, 2006.

[57] S. Dolinar, D. Divsalar, and F. Pollara. Code performance as a function of block size. *TMO progress report*, 42(133), 1998.

[58] Y. Polyanskiy. 6.441 Information Theory. Spring 2016. https://ocw.mit.edu, Accessed: January, 2018.

[59] J. Huber and R. Fischer. Informationstheorie und deren Anwendungen zur Nachrichtenübertragung. SS 2015.

[60] W. Yang, G. Durisi, T. Koch, and Y. Polyanskiy. Block-fading channels at finite blocklength. In *Proceedings of the 10th International Symposium on Wireless Communication Systems*, pages 1–4. VDE, 2013.

[61] Y. Huang and P. Moulin. Finite blocklength coding for multiple access channels. In *Proceedings of International Symposium on Information Theory Proceedings (ISIT)*, pages 831–835. IEEE, 2012.

[62] T. Erseghe. On the evaluation of the Polyanskiy-Poor–Verdú converse bound for finite block-length coding in AWGN. *IEEE Transactions on Information Theory*, 61(12):6578–6590, 2015.

[63] S. Ikeda, K. Hayashi, and T. Tanaka. Capacity and modulations with peak power constraint. *arXiv preprint:1005.3889*, 2010.

[64] E. MolavianJazi and J. N. Laneman. Coded modulation for Gaussian channels: dispersion-and entropy-limited regimes. In *Proceedings of Wireless Communications and Networking Conference (WCNC)*, pages 528–533. IEEE, 2015.

[65] A. Martinez, A. G. i Fabregas, G. Caire, and F. Willems. Bit-interleaved coded modulation in the wideband regime. *IEEE Transactions on Information Theory*, 54(12):5447–5455, 2008.

[66] R. Kumar. Summary channel coding rate in the finite blocklength regime - Polyanskiy et al., 2011. https://www.semanticscholar.org/paper/Summary. Accessed: January, 2018.

[67] K.-D. Kammeyer. *Nachrichtenübertragung*. Vieweg and Teubner, 2008.

[68] R. Müller and W. Koch. Fundamentals of mobile communications. WS 2014/2015.

[69] W. Xiaodong and V. Poor. *Wireless communication systems: advanced techniques for signal reception*. Pearson Education India, 2004.

[70] University of Padua DEI-Gruppo Telecomunicazioni. Finite blocklength regime, 2017. http://dgt.dei.unipd.it/pages/read/92/. Accessed: February, 2018.

[71] Tse D. and Viswanath P. *Fundamentals of wireless communication*. Cambridge University Press, 2005.

[72] D. R. Wasserman, A. U. Ahmed, and D. W. Chi. BER performance of polar coded OFDM in multipath fading. *arXiv preprint:1610.00057*, 2016.